POROVISCOELASTIC DYNAMIC FINITE ELEMENT MODEL OF BIOLOGICAL TISSUE

by

Zhaochun Yang

BS, Beihang University, PR China, 1991

MS, University of Petroleum, PR China, 1994

Submitted to the Graduate Faculty of

the School of Engineering in partial fulfillment

of the requirements for the degree of

Doctor of Philosophy

University of Pittsburgh

2004

UNIVERSITY OF PITTSBURGH

SCHOOL OF ENGINEERING

This dissertation was presented

by

Zhaochun Yang

It was defended on

December 2, 2004

and approved by

Dr. Lars G.Gilbertson, Associate Professor, Department of Bioengineering

Dr. William S.Slaughter, Associate Professor, Department of Mechanical Engineering

Dr. Jeenshang Lin, Associate Professor, Department of Civil and Environmental engineering

Dissertation Director: Dr. Patrick Smonlinski, Associate Professor, Department of Mechanical Engineering

POROVISCOELASTIC DYNAMIC FINITE ELEMENT MODEL OF BIOLOGICAL TISSUE

Zhaochun Yang, PhD

University of Pittsburgh, 2004

Clinical evidences have demonstrated the important contribution of biomechanical factors to the behavior of soft tissues. Finite element analysis is used to study the mechanical behavior of biological tissue because it can provide numerical solutions to problems that are intractable to analytic solutions. This dissertation develops a finite element method that includes poro-viscoelastic material behavior, finite deformations, inertia and mechano-electrochemical effects for the modeling of biological tissue.

The finite strains and inertial effects are introduced into the poroelastic model of biological tissues. Thus, the weak forms for the porous - electric-chemical model are developed by treating cation and anion as variables. Newmark-β method, the backward method, and Newton's method are incorporated into the implicit nonlinear solutions with the nearly incompressible and fully incompressible cases considered.

This methodology and codes developed for the study have been verified with one – dimensional analytical solutions. Moreover, this study, using two dimensional examples, clearly demonstrates the importance of the finite deformation, the viscoelasticity of the material, and the electric-chemic effect. Finally, a preliminary work on the effect of impact loads on brain has show the capability of the present work in capturing sophisticated response behavior of the brain.

TABLE OF CONTENTS

LIST OF TABLES

LIST OF FIGURES

NOMENCLATURE

A_i	amplitude
B_f	coupling coefficient in the chemical potential
c^F	fixed charge density
C	concentration of the third phase
C	viscous damping matrix
D	"drained" material stiffness matrix
$\mathbf{D}_v$	matrix of material constants, which is grouped with the material constants
E	Cauchy –Green strain tensor
$\hat{\mathbf{E}}$	current strain
$\mathbf{E}^e$	elastic strain
$\mathbf{E}^v$	viscoelastic strain
$f_{\alpha\beta}$	frictional coefficients per unit tissue volume between α and β components
F	deformation gradient
F_c	Faraday constant
$\mathbf{F}^e$	local instantaneous elastic deformation gradient
$\mathbf{F}^v$	local viscous deformation gradient
$\overline{\mathbf{F}}$	applied force vector

$\hat{\mathbf{F}}$ current deformation gradient

$\hat{\mathbf{F}}^{e}$ current elastic deformation gradient

$\hat{\mathbf{F}}^{v}$ current visco deformation gradient

$I_0(z)$ modified Bessel function of zero order

$\mathbf{J}^{+}$ positive ion flux relative to the solid phase

$\mathbf{J}^{-}$ negative ion flux relative to the solid phase

J_{e} volume of the element

J_v relax memory function

k, $\hat{k}$ permeability in Eulerian and Lagrangrian form

K_s "true" bulk moduli for the solid

K_f "true" bulk moduli for the fluid

$\mathbf{K}$ stiffness matrix

$\Delta\mathbf{L}^{v}$ viscoelastic increment

m total mass

m^{s} solid mass

m^{f} fluid mass

m^{c} amount of charge

m^{c^F} amount of fixed charge

$\mathbf{m}$ vector form of Kronecker delta

$\mathbf{m'}$ modified vector form of Kronecker delta

$\mathbf{M}$ mass matrix

M^{+} molecular weight of cation

M^- molecular weight of anion

n porosity

n_{eq} total number of displacement equations after boundary conditions have been imposed

n_c total number of incompressibility constraints

N_i shape or basis functions

P fluid pressure

p^c pressure due to the chemical potential

R universal gas constant

R_s isotropic resistivity

$\mathbf{S}^e$ elastic stress

$\mathbf{S}^v$ viscoelastic stress

T absolute temperature

T_c chemical expansion stress

t_i pressure at the boundary

u_i nodal values of the unknown function to be determined

u displacement of solid

$\bar{\mathbf{u}}$ displacement of solid of the nodes

$\dot{\mathbf{u}}$ velocity of solid

$\ddot{\mathbf{u}}$ acceleration of solid

$\mathbf{v}^\alpha$ velocity of α component

V total volume

V^s solid volume

V^f fluid volume

V_R volume in the reference position

$\mathbf{w}$ relative displacement of fluid

$\overline{\mathbf{w}}$ relative displacement of fluid of the nodes

$\dot{\mathbf{w}}$ relative velocity of fluid

$\ddot{\mathbf{w}}$ relative acceleration of fluid

$\hat{\mathbf{w}}$ relative displacement of fluid in Lagrangian form

$\dot{\hat{\mathbf{w}}}$ relative velocity of fluid in Lagrangian form

$\ddot{\hat{\mathbf{w}}}$ relative acceleration of fluid in Lagrangian form

$\mathbf{X}^n$ displacement vector at time nΔt

$\dot{\mathbf{X}}^n$ velocity vector at time nΔt

$\ddot{\mathbf{X}}^n$ acceleration vector at time nΔt

δX_j infinitesimal value to perturb the value of node j

γ^+ activity coefficients of cation

γ^- activity coefficients of anion

ε strain

ζ variation of water content

ϕ osmotic coefficient

λ, μ Lame's Constants

$\hat{\mu}^+$ electrochemical potentials for cation

$\hat{\mu}^-$ electrochemical potentials for anion

$\overline{\hat{\mu}}^+$ electrochemical potentials for cation of the nodes

$\overline{\hat{\mu}}^{-}$ electrochemical potentials for anion of the nodes

μ_0^w initial chemical water potential

μ_0^+ reference positive chemical potential

μ_0^- reference negative chemical potential

ρ^α mass density of α component

σ stress

σ total stress

σ' effective stress

τ_i relaxation time

υ poisson's ratio

∇ gradient operator in the original configuration

ACKNOWLEDGMENTS

I am deeply indebted to my advisor, Dr. Patrick Smonlinski for his guidance, support, collaboration and encouragement throughout my education and research. I also would like to gratefully thank Dr. Lars G.Gilbertson for his guidance and support. I deeply appreciate Dr. Qingming Wang, who is generous to give me great help. I am equally indebted to my advisory committee members Dr. William S.Slaughter and Dr. Jeenshang Lin for their providing invaluable suggestions towards this research.

Thanks go to several others who have contributed, both technically and through friendship: Fayan Xu, Tao Zhang, Qingming Chen, Deyu Li, Yixing Lu, Peng Yuan, and Zhiwei Shan. Great appreciation is also expressed to my sisters and brother for their great care of my study. I deeply thank for the help from my parents which I never forget in my life.

Lastly, a very special thanks to the person who most made the Ph.D. process endurable: my wife, Peng Tang

1.0 INTRODUCTION

Biological tissue is a group of cells that perform a similar function [1]. There are four basic types of tissue in the human body: epithelium, connective tissue, muscle tissue, nervous tissue [1]. Here we introduce a typical nervous tissue, disc, to represent the biological tissue.

1.1 CLINICAL DISC PROBLEM

About 26 million Americans between the ages of 20 and 64 are affected by frequent low back pain [1], which is one of the major causes of worker's disability and costs roughly $50-100 billion each year [2]. Consequently, more attention is being paid to prevent and treat this disease. Most of the lower back problems are concerned with intervertebral disc (IVD).

Although work has been done by a large number of researchers, the mechanisms that lead to low back pain still are not clear. However, many findings indicate that biomechanical factors are connected with disc aging, degeneration, and prolapse, the major causes of back pain and allied symptoms [4-8]. The motion segment, functional spinal unit, regarded as "the smallest segment of the spine that exhibits biomechanical characteristics similar to that of the entire spine" [9], has been the focus of much spine biomechanics research. Numerous experiments and

numerical studies have been done in this field. Further study of IVD (intervertebral disc) function could afford a better understanding of abnormal as well as normal spine function.

1.2 PREVIOUS DISC MODELS AND THEIR LIMITATIONS

Finite element analysis (FEA) has been applied in orthopedic biomechanics and spine biomechanics research since 1983. Belytschko et al. [10] were probably the first to set up a body-disc-body FE model. Later, this model was developed [11] to investigate the nonlinear behavior of the disc under axial load with the annulus fibrous treated as nonlinear elastic material. Further, a similar FE model [12, 13] was set up to do a parametric study of the effect of disc geometry and (isotropic) material property parameters under compressive loading and under complex loading. In the study of disc material properties, nine elastic constants to define the material properties of the annulus were identified in [14] when the annulus was taken to be orthotropic.

Because fibers are embedded in the disc annulus, Shirazi-Adl [15, 16] treated the disc annulus as a composite of fibers and ground substance with the annular fibers modeled as tension-only. The ground substance was considered as a homogeneous isotropic material, and the nucleus as an incompressible material. This is a typical current model of the disc.

Many experimental observations suggest that it would be more realistic to consider biological tissue as a biphasic model. For example, when the disc is compressed, fluid flows out from either whole disc [17-19] or disc slices [19-22]. Similar behaviors also occur with articular cartilage, a closely related tissue [23-26]. Therefore, the biological tissues should be considered as multiphase system.

1.3 GENERAL REVIEW OF MULTI-PHASE MODELS

During the last decade, two theories of multi-phase behavior have been developed to study the soft tissue. They are biphasic theory [25] and poroelastic theory [39, 40]. Both theories and their development are reviewed as follows.

1.3.1 Biphasic Theory

Mow et.al. [25] first presented the biphasic theory where the material was modeled as a mixture of two distinct phases: an incompressible, porous solid phase to describe the collagen-proteoglycan matrix and an incompressible fluid phase to represent the interstitial fluid. The constitutive equations, continuity equations and momentum equations were derived. This theory was applied to study biphasic creep and biphasic stress relaxation.

Spilker et al.[26] proposed a finite element formulation of the linear biphasic model for articular cartilage and other hydrated soft tissues where the fluid phase and solid phase are considered as incompressible. The Galerkin weighted residual method is applied to the momentum equation and mechanical boundary conditions of both the solid phase and the fluid phase. The penalty method is utilized to deal with the problem of the intrinsically incompressible binary mixture. The u (the solid phase displacement) –v (fluid phase velocity) form is adopted to express the weak form of the weighted residual statements for the solid and fluid phases. Suh [66] went further to consider the solid phase as hyperelastic, and define the stress-strain relations in terms of the free energy function. Levenston et al. [32] derived a three-field mixed (u-p-w) finite

element formulations capable of describing both geometric and material nonlinearities based on three variational principles that make use of alternate penalized forms of the internal energy.

It was demonstrated that the viscoelastic behavior of the tissue is not only due to the diffusive interaction between the solid matrix and the interstitial fluid (flow-dependent), but also to the intrinsic viscoelasticity of the solid (flow –independent) [27], therefore, many models were developed to describe it. Mak [28] made an integral-type linear viscoelastic model to represent the intrinsic viscoelaticity of the solid matrix [29]. Based on this work, Suh et al.[30,31] combined a viscoelastic solid phase and a mixed –penalty based finite element formulation to model cartilage in confined and unconfined compression. Also, Huang [58] incorporated biphasic theory [25], and a biphasic-conewise linear elastic model [60] with the biphasic poroviscoelastic model [28] into a single model to analyze the response of cartilage to standard testing configurations. Wolfgang [59] developed a model to combine a descriptive representation of the linear viscoelasticity law for the organic solid matrix with biphasic theory.

Since significant deformations resulting from loading and inherent swelling mechanisms in the soft tissues have been described [19, 22, 33-35], Lai et al. [36] developed a triphasic model to consider the effects of swelling and transport in continuum descriptions of soft tissue mechanics.

1.3.2 Triphasic Theory

Triphasic theory [36] views the soft tissue as a mixture of three phases: an incompressible solid phase, an incompressible fluid phase and an ion phase of two species (cations and anions) of a single salt. This theory is the combination of the physical-chemical theory for ionic and

polyionic solutions with the biphasic theory for cartilage. The momentum equations involve chemical potentials whose gradients are the driving forces for movements of ions. These chemical potentials are determined by fluid pressure, salt concentration, solid matrix dilatation, and fixed charge density.

Gu [67] extended triphasic theory to model the mechano-electrochemical behaviors of charged – hydrated soft tissues containing multi-electrolytes. There are n+2 phases such as 1 charged solid phase, 1 non charged solvent phase, and n ion species. The corresponding continuity equations, momentum equations, and constitutive equations were derived. Sun et al. [72] gave the corresponding finite element formulation for Gu [67] theory. Similarly, Huyghe et al. [37] derived a chemo-eletro-mechanical formulation of quasi-static finite deformation of swelling incompressible porous media from mixture theory, in which four phases are defined: solid, fluid, anions and cations. Based on the assumption of incompressible and isothermal deformation, balance laws are derived for each phase and for the mixture as a whole. These equations are solved by the finite element method using a weighted residual approach [68]. This model was applied to study the intervertebral disc tissue [38].

1.3.3 Poroelastic Model

B.R. Simon [39, 40] considered the soft tissues in the spinal motion segment as poroelastic materials which were treated as a fluid phase flowing through the pores of a deformable porous solid skeleton or solid phase. A u (displacement of solid phase)-w (displacement of fluid phase) formulation was utilized where the fluid motion is relative to the deforming solid phase. The field equations given by Biot [41] include an overall dynamic equilibrium equation and a

generalized Darcy law for the dynamic equilibrium for the fluid motion. Later, Simon [61] extended this work to large strains. He gave both Eulerian and Lagrangian forms of the governing equations.

On the basis of Simon's work [39, 40], Laible [42] modified the constitutive law and added initial stresses to include the effects of swelling caused by osmotic pressure. The results in this paper demonstrated the dramatic effect of swelling on the load carrying mechanisms in the disc.

1.3.4 Poroelastic Transport-Swelling (PETS) Model

In 1996, B.R.Simon et al. [43] extended poroelastic model to poroelastic transport –swelling (PETS) model which includes chemical effects, therefore, the governing equations of PETS have the terms of chemical potential inside and include the diffusion equation of ions as well.

The latest development in this area is a 3-dimensional formulation for a poroelastic and chemical electric (PEACE) model [44]. Based on the work of Sun [67] and Simon [39, 40], this model adopted the field variables of solid displacement u, relative fluid velocity w, electric potential and Cl concentrations c^- and Na concentrations c^+ to investigate the influence of fixed charge density magnitude and distribution on a slice of disc material. The results show that the mechanical, chemical, and electrical behaviors were all strongly influenced by the amount as well as the distribution of fixed charges in the matrix.

1.3.5 Comparison of PETS and Triphasic Theory

The PETS model takes the solid skeleton as the problem domain. The derivation of the governing equation of the fluid was based on empirical evidence that the fluid flow in porous media obeys a conduction-type law (Darcy's law), where the flow is proportional to the pressure gradient. Besides, the motion of the ions is described by the diffusion equation.

On the contrary, in Triphasic model, the solid and fluid phases are considered separate overlapping continua. The individual phases, and the mixture as a whole, have separate balance equations. According to principle of mixture, these equations should all have similar forms. For the ion phase, it is controlled by the electroneutrality condition and ion diffusion – convection equation.

However, Levenston [32] and Simon [43] established the equivalence of both theories.

1.4 LIMITATIONS OF EXISTING MODELS

The features of the existing models are listed in Table 1.1. This table clearly shows that these models incorporate increasing more features of actual biological tissue. However, except for the model of Simon [39, 40], the methods are quasi-static which means the inertia is ignored. Actually, the inertia terms can be significant when the external forces vary rapidly. This table also shows that most of the models are limited in small strain case except the model of Spilker[26] and Levenston[32], but in fact, because of the low stiffness of biological tissue [39,

Table 1.1 Basic features of previous models

References	Theory	Deformation	Solid Elastic	Solid Viscous	Fluid	Chemical Behavior	Inertial
Mow[25]	Biphasic	Small	Linear	No	Incompressible	No	Quasi-static
Spilker[26,66]	Biphasic	Large	Nonlinear	No	Incompressible	No	Quasi-static
Levenston[32]	u-p-w	Large	Nonlinear	No	Incompressible	No	Quasi-static
Suh[30,31]	Biphasic	Small	Linear	Visco	Incompressible	No	Quasi-static
Huang[58]	Biphasic	Small	Linear	Visco	Incompressible	No	Quasi-static
Wolfgang[59]	Biphasic	Small	Linear	Visco	Incompressible	No	Quasi-static
Lai[36]	Triphasic	Small	Linear	No	Incompressible	+,-ions	Quasi-static
Sun[72]	Chemo-Electric-Mechanical	Small	Linear	No	Incompressible	+,-ions	Quasi-static
Huyghe[37,38]	Chemo-Electric-Mechanical	Small	Linear	No	Incompressible	+,-ions	Quasi-static
B.R.Simon[39,40]	Poroelastic	Small	Linear	No	Incompressible	No	Dynamic
Laible[42]	Poroelastic	Small	Linear	No	Incompressible	Ion	Quasi-static
B.R.Simon[43]	PETS (Poroelastic)	Small	Linear	No	Incompressible	Ion	Quasi-static
C.I.James[44]	PEACE (Poroelastic)	Small	Linear	No	Incompressible	+,-ions	Quasi-static
Yang	PETS	Large	Linear	Visco	Incompressible	+,-Ions	Dynamic

40], many physiological cases involve large deformation. The constituents of biological tissue such as collagen fibrils and proteoglycan gel are highly viscoelastic, independent of fluid flow, but only the models of Suh [30, 31], Huang [58], and Wolfgang [59] considered this point, however, these models are limited in small strain. Additionally, some models considered the chemical and electrical effects, others not.

1.5 OBJECTIVES

From the above discussion, we can see that there is no model which includes large deformation, material viscoelasticity and inertial effects, and these are important features of the mechanical behavior of the biological tissue. In order to understand the mechanical behavior of the spine, we must distinguish the role of the interaction of the fluid and the solid and the role of the viscoelasticity of the materials. We also need to know the effect of large deformation and inertia because they exist in the biological tissue. Therefore the objective of this thesis research is to develop poro-viscoelastic, finite deformation, dynamic finite element model, including the mechano-electrochemical effects.

The paper is organized as follows:

- The background including the biomechanics of the disc is introduced in Chapter 2.
- The model formulation of the poroelastic theory is given in Chapter 3 along with a description of the material properties.
- Chapter 4 presents the numerical implement of the model.
- Some verifications of the program are done in chapter 5.

• Parametric studies of a 2-D model are accomplished in chapter 6.

• Conclusions and future research are included in chapter 7.

2. 0 BACKGROUND

2.1 NORMAL ANATOMY AND BIOMECHANICS

The intervertebral disc is the primary focus of this study and is used to represent the biological tissue. The intervertebral disc is composed of three distinct parts: the nucleus pulposus, the annular fibrosus, and the cartilaginous end-plate (Figure 2.1). The nucleus pulposus is a viscous, mucoprotein gel located in the center of the disc [45, 46]. It consists of plentiful sulfated glycosaminoglcans in a loose network of type II collagen. The water in nucleus varies with age. At birth, it has the maximum, approximately 90%, then decreases to 80% in the young adult and continues to decline with age. The annulus fibrosus is the outer boundary of the disc, which becomes differentiated from the periphery of the nucleus. The interface between the nucleus and the annulus is progressively more indefinite with age. Coarse type I collagen fibers in the annulus are oriented obliquely and arranged in lamellae which connect the adjacent vertebral bodies. The fibers are in the same direction within a given lamella but opposite to those in adjacent lamellae. The collagen content of the disc steadily increases along the radial direction from the center to outside, where collagen reaches 70% or more of the dry weight. Type I and II collagen are located radially in opposing concentration gradients. The cartilaginous end-plates are composed of layers of hyaline cartilage which cover the adjacent vertebral bodies over the nucleus and inner annulus. Nutrients transport into the disc along the channels within end-plates.

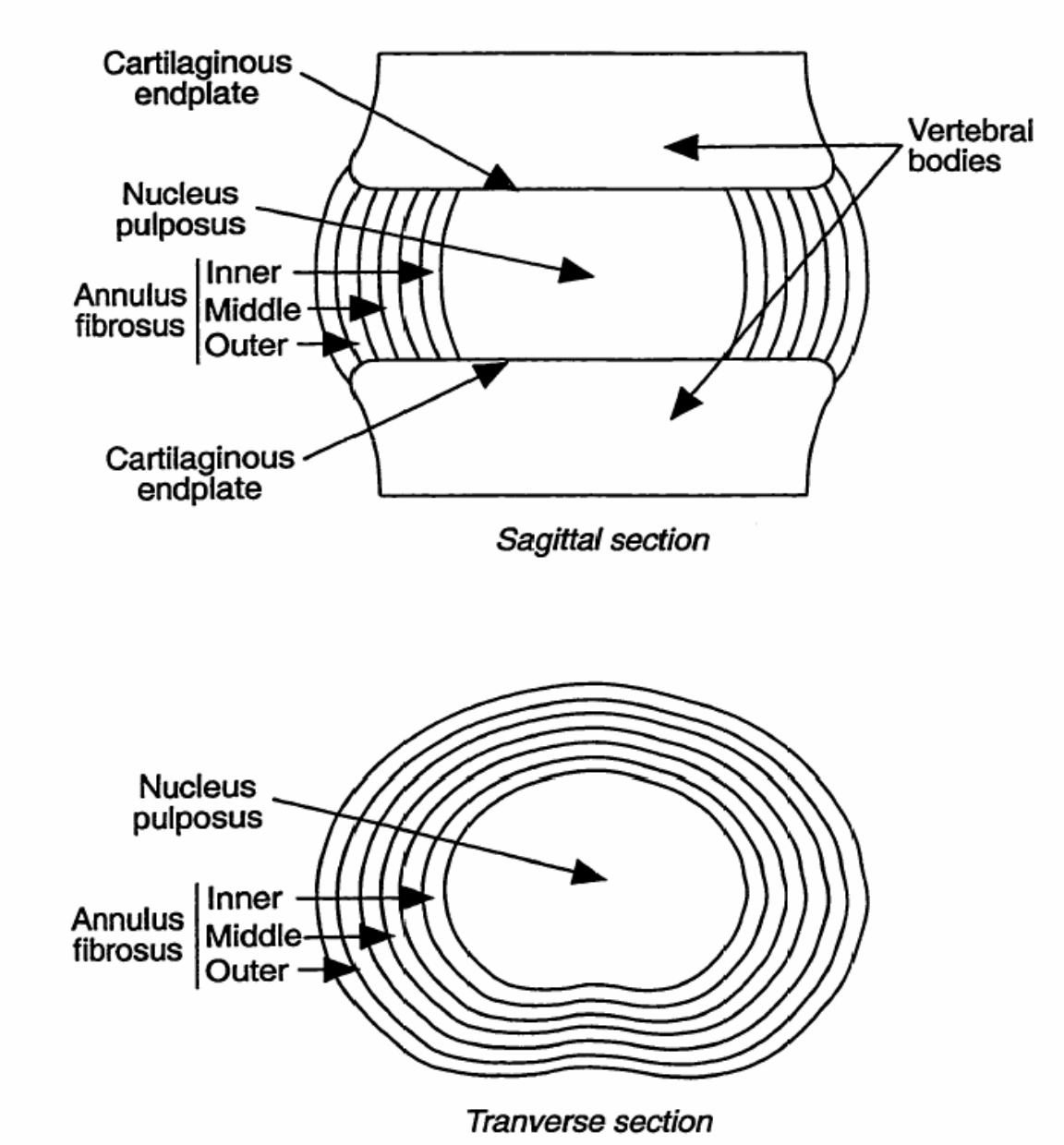

Figure 2.1 Schematic of human lumber intervertebral disc [38]

The structural properties of disc are related to its chemical effect inside. A ‘swelling pressure’ exists in nucleus to enable the disc to support spinal compressive loads. The pressurized nucleus also creates tensile pre-stress within the annulus and ligamentious structures surrounding the disc. It is found that the ±60º orientation of the collagen fibers, relative to the longitudinal axis of the spine is optimal to support the tensile stresses developed within a pressurized cylinder [47]. This state of pre-stress provides an innate mechanical stability to the disc.

When a stress is placed on the spine is greater than the nuclear swelling pressure, water is extruded from the disc, principally through the semipermeable cartilaginous end-plates. Therefore, significant disc water loss can occur [48]. Adams’ [50] experiments on cadaveric spines found that under sustained loading, intervertebral disc lose height, bulge, and become stiffer in compression and more flexible in bending. Loss of nuclear water also has some effects on the load distribution internal to the disc. McNally and Adams [51] found that in the healthy disc under compressive loading, compressive stress occurs mainly within the nucleus pulposus, with the annulus acting primarily in tension. After three hours of compressive loading, a significant change occurred in the pressure distribution, with the highest compressive stress occurring in the posterior annulus. There were similar pressure distributions noted in degenerated and denucleated discs [52, 53].

2.2 REQUIREMENTS OF THE BIOLOGICAL TISSUE MODEL

From the components and biomechanics of biological tissue, we can see that there are four phases: solid, fluid, positive and negative ions. As to these phases, there are different requirements.

For the solid, it should satisfy the static equilibrium equation, like biphasic [25] and triphasic theory [36], or the governing equation of motion like poroelastic [39,40] and PETS model [43]. The selection of the material property develops from linear isotropic in model of Mow [25], Lai [36], Simon [39, 40] to nonlinear elastic in model of Levenston [32] and Spilker [26] or viscoelasticity in models of Suh [30, 31], Huang [58], and Wolfgang [59]. In addition, large strains were considered in models of Levenston [32] and Spilker [26], while the other models just were limited to small strains.

For the fluid phase, there is little difference in these models. They should satisfy the Darcy equation. However, in model of poroelasticity [39, 40] and PETS [43], the equation includes the inertia term.

For the electrochemical effect, every model that includes the effect of ions like PETS [43], Triphasic theory [36], and the Huyghe model [37, 38], has the diffusion equation and the electroneutrality condition to describe the motion of the mobile ions.

3.0 MODEL FORMULATION METHODS

Simon et al. [43, 61] presented a formulation for poroelastic transport – swelling (PETS) field problem in soft tissues. However, this model is linear, small-strain, and quasi-static response, which limits the modeled behavior of soft tissue. Therefore, in this chapter, the PETS theory of Simon will be extended to include finite strains and inertial effects.

3.1 POROELASTIC MODELS

3.1.1 Mass and density [43]

The soft tissues are composed of a fibrous tissue matrix enclosing interstitial fluid (water), in which the mobile species can move. Therefore, there are four phases in the soft tissue: solid, fluid, negative ions, and positive ions. In the poroelastic model for soft tissue, its structure is composed of deformable, porous elastic materials that are saturated with a mobile fluid. In addition, the concept of pores is a continuum view of the material. The ion phases also include in this model.

In the current configuration, the soft tissue is described theoretically as a continuum of an infinitesimal total volume of the bulk material, dV, that is located at a position x at time t. At the reference position $\boldsymbol{X}$ at t_R=0, the volume dV is initially dV_R. Based on the assumption that the volume and the mass of the mobile ion phases are negligible, the volume dV is the sum of solid (dV^s) and fluid (dV^f),

$$dV = dV^s + dV^f \tag{3.1}$$

And the total mass, namely dm, as

$$dm = dm^s + dm^f \tag{3.2}$$

Thus, the overall density of the material in dV is given by

$$\rho = \frac{dm}{dV} \tag{3.3}$$

The porosity of the material n is defined as the ratio of the volume of the pores to the total volume of the material, therefore, the porosity of the soft tissues viewed as saturated porous solids is

$$n = \frac{dV^f}{dV} \tag{3.4}$$

The density of the solid is commonly defined by

$$\rho^s = \frac{dm^s}{dV^s} \tag{3.5}$$

and the density of the fluid as

$$\rho^f = \frac{dm^f}{dV^f} \tag{3.6}$$

Substituting equations (3.2), (3, 5) and (3, 6) into (3.3), yields

$$\rho = (1-n)\rho^s + n\rho^f \tag{3.7}$$

In the soft tissue, deformation results from the inherent swelling mechanism caused by the charges in the soft tissue. These charges are the ion phases in the soft tissue. The concentration of the ion phase c is defined in terms of the amount of positive and negative ions per volume of the fluid as

$$c^{+} = \frac{dm^{c^{+}}}{dV^{f}} \tag{3.8}$$

$$c^{-} = \frac{dm^{c^{-}}}{dV^{f}} \tag{3.9}$$

Some charges in the soft tissue, namely fixed charges, are immobile and fasten to the porous solid. So, fixed charge density (FCD) is defined in terms of the amount of fixed charge $dm^{c^{F}}$ in dV^{f} as

$$c^{F} = \frac{dm^{c^{F}}}{dV^{f}} \tag{3.10}$$

The electroneutrality condition requires

$$c^{+} = c^{-} + c^{F} \tag{3.11}$$

3.1.2 Kinematics

In this problem, there are four primary field variables: the displacement of the porous solid, **u**; the displacement of the pore fluid relative to the deforming solid **w**; the concentration of the negative ion phase c^{-}; and the concentration of the positive ion phase c^{+}.

Consider a material point having a position vector ***X*** located in an initial coordinate system. At time t, the coordinate of the material point moves to a new location, which is denoted

as ***x***, Thus, mathematically, the motion can be expressed as a mapping, Θ, of the initial (material) coordinates ***X*** to the current (spatial) coordinates ***x***:

$$\mathbf{x} = \Theta(\mathbf{X}, t) \tag{3.12}$$

For the deformed material, the deformation information is available in the deformation gradient **F**, which is the key quantity in nonlinear elasticity, and is defined mathematically as follows:

$$\mathbf{F} \equiv \nabla \mathbf{x} = \mathbf{I} + \nabla \mathbf{u} \tag{3.13}$$

It is important to select the proper coordinate system in finite deformation analysis. There are two coordinate systems, one is in terms of the initial configuration (i.e. with respect to ***X***), called a material or Lagrangian description, another one is in a deformed state (i.e. with respect to ***x***), termed a spatial or Eulerian description.

3.1.2.1 Eulerian form The displacement of the saturated porous solid, u, is given by

$$\mathbf{u} = \mathbf{u(x,t)} = \mathbf{x} - \mathbf{X} \tag{3.14}$$

The corresponding velocity and acceleration are

$$\dot{\mathbf{u}} = \frac{D\mathbf{u}}{Dt} \tag{3.15}$$

$$\ddot{\mathbf{u}} = \frac{D\dot{\mathbf{u}}}{Dt} \tag{3.16}$$

The displacement of the pore fluid relative to the deforming solid, **w,** is

$$\mathbf{w} = \mathbf{w}(\mathbf{x}, t) = \mathbf{u}^f - \mathbf{u} \tag{3.17}$$

The relative velocity and acceleration of fluid are given by

$$\dot{\mathbf{w}} = \dot{\mathbf{u}}^f - \dot{\mathbf{u}} \tag{3.18}$$

$$\ddot{\mathbf{w}} = \ddot{\mathbf{u}}^f - \ddot{\mathbf{u}} \tag{3.19}$$

The concentrations c^+ and c^- are expressed as

$$c^+ = c^+(\mathbf{x},t) \tag{3.20}$$

$$c^- = c^-(\mathbf{x},t) \tag{3.21}$$

The motion of the ion phases are described as

$$\mathbf{u}^{c+} = \mathbf{u}^{c+}(\mathbf{x},t) \tag{3.22}$$

$$\mathbf{u}^{c-} = \mathbf{u}^{c-}(\mathbf{x},t) \tag{3.23}$$

The corresponding velocity is given by

$$\dot{\mathbf{u}}^{c+} = \dot{\mathbf{u}}^{c+}(\mathbf{x},t) \tag{3.24}$$

$$\dot{\mathbf{u}}^{c-} = \dot{\mathbf{u}}^{c-}(\mathbf{x},t) \tag{3.25}$$

Figure 3.1 illustrates the relationship between the absolute and relative displacements of the solid, fluid, negative ion phase and positive ion phase.

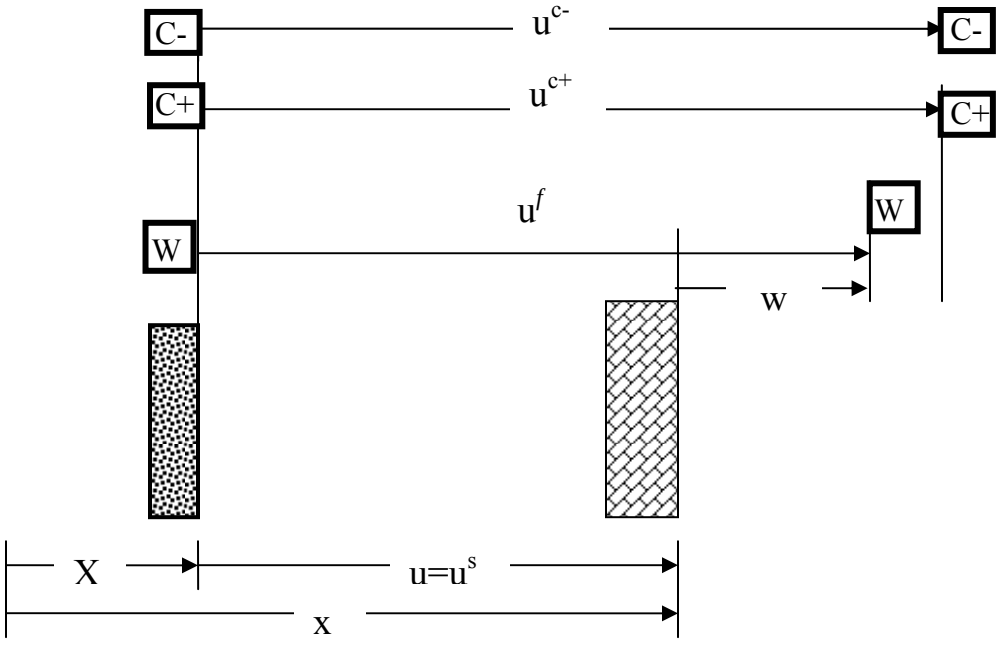

Fig.3.1 One-dimensional representation of kinematics, including motions relative to the deforming solid

3.1.2.2 Lagrangian form

3.1.2.2.1 Lagrangian form for the solid phase For an arbitrary material point of the solid phase initially located at **X** in the reference configuration and located at **x** in the current configuration, the displacement, velocity and acceleration are given by

$$\mathbf{u} = \mathbf{u}(\mathbf{X},\mathbf{t}) = \mathbf{x} - \mathbf{X} \tag{3.26}$$

$$\dot{\mathbf{u}} = \dot{\mathbf{u}}(\mathbf{X},\mathbf{t}) = \frac{d\mathbf{u}}{dt} \tag{3.27}$$

$$\ddot{\mathbf{u}} = \ddot{\mathbf{u}}(\mathbf{X},\mathbf{t}) = \frac{d\dot{\mathbf{u}}}{dt} \tag{3.28}$$

3.1.2.2.2 Lagrangian form for fluid phase Since the given fluid displacement is referred to the solid phase, with an assumption that an equal relative fluid mass flow rate occurs at the cross area, the relative fluid velocity the relationship of a relative fluid velocity between the Lagrangian form and Eulerian form is given in Appendix B as

$$\hat{\dot{\mathbf{w}}} = J\frac{\partial \mathbf{X}}{\partial \mathbf{x}}\dot{\mathbf{w}} \tag{3.29}$$

Similarly, in an average (in the bulk sense) view of $\hat{\ddot{\mathbf{w}}}$ and $\hat{\mathbf{w}}$, and assuming that the integration of $\hat{\ddot{\mathbf{w}}}$ and $\hat{\mathbf{w}}$ at the cross area is unchanged [Simon, 1992], the relative fluid displacements $\hat{\mathbf{w}}$ and acceleration $\hat{\ddot{\mathbf{w}}}$ are given as

$$\hat{\mathbf{w}} = J\frac{\partial \mathbf{X}}{\partial \mathbf{x}}\mathbf{w} \tag{3.30}$$

$$\hat{\ddot{\mathbf{w}}} = J \frac{\partial \mathbf{X}}{\partial \mathbf{x}} \ddot{\mathbf{w}} \tag{3.31}$$

3.1.2.2.3 Lagrangian form for ion phases For the ion phases, the motion and the velocity are given by

$$c^{+} = c^{+}(\mathbf{X}, t) \tag{3.32}$$

$$\mathbf{u}^{c+} = \mathbf{u}^{c+}(\mathbf{X}, t) \tag{3.33}$$

$$\dot{\mathbf{u}}^{c+} = \dot{\mathbf{u}}^{c+}(\mathbf{X}, t) \tag{3.34}$$

$$c^{-} = c^{-}(\mathbf{X}, t) \tag{3.35}$$

$$\mathbf{u}^{c-} = \mathbf{u}^{c-}(\mathbf{X}, t) \tag{3.36}$$

$$\dot{\mathbf{u}}^{c-} = \dot{\mathbf{u}}^{c-}(\mathbf{X}, t) \tag{3.37}$$

3.1.3 Momentum conservation laws (Eulerian Form)

There are four forces on solid phase: the frictional force between the solid and fluid $\mathbf{F}_{sf} (= R_s \dot{\mathbf{w}})$, body force, fluid pressure p, and pressure p^c which is function of concentration of ions c, chemical expansion stress T_c, and the deformation of fluid, so the momentum conservation laws for the porous solid in the absence of body force are [42, 43]

$$(1-n)\nabla p + R_s \dot{\mathbf{w}} - \nabla p^c + \mathbf{L}^T(\boldsymbol{\sigma}') = \rho_s (1-n)\ddot{\mathbf{u}} \tag{3.38}$$

where

$$\nabla^T = < \frac{\partial}{\partial x_1} \quad \frac{\partial}{\partial x_2} \quad \frac{\partial}{\partial x_3} > \tag{3.39}$$

$$\mathbf{L}^T = \begin{bmatrix} \frac{\partial}{\partial x_1} & 0 & 0 & \frac{\partial}{\partial x_2} & 0 & \frac{\partial}{\partial x_3} \\ 0 & \frac{\partial}{\partial x_2} & 0 & \frac{\partial}{\partial x_1} & \frac{\partial}{\partial x_3} & 0 \\ 0 & 0 & \frac{\partial}{\partial x_3} & 0 & \frac{\partial}{\partial x_2} & \frac{\partial}{\partial x_1} \end{bmatrix} \tag{3.40}$$

R_s = isotropic resistivity

p^c = pressure due to the chemical potential,

$$p^c = B_f \xi_w + T_c - \rho_f \mu_0^w + RT\phi(2c + c^F) \tag{3.41}$$

B_f = coupling coefficient in the chemical potential

ζ_w = variation of water content

μ_0^w = initial chemical water potential

T_c = chemical expansion stress

R = universal gas constant

T = absolute temperature

ϕ = osmotic coefficient

Because the pore fluid satisfies the Darcy equation, the momentum conservation laws for the pore fluid in the absence of body force have the form [43]

$$n\nabla p - R_s \dot{\mathbf{w}} + \nabla p^c = n\rho_f \ddot{\mathbf{u}}_f \tag{3.42}$$

Making use of equation (3.17), the above equation changes as

$$n\nabla p - R_s \dot{\mathbf{w}} + \nabla p^c = n\rho_f \ddot{\mathbf{u}} + n\rho_f \ddot{\mathbf{w}} \tag{3.43}$$

Thus, adding equations (3.7), (3.38) and (3.43), yields

$$\nabla p + \mathbf{L}^T(\boldsymbol{\sigma}') = \rho \ddot{\mathbf{u}} + n\rho_f \ddot{\mathbf{w}} \tag{3.44}$$

In the porous model, the total stress **σ** is composed of the effective stress **σ'** and the pore fluid pressure, p where p>0 for tension,

$$\boldsymbol{\sigma} = \boldsymbol{\sigma}' + \mathbf{m}p \tag{3.45}$$

where $\mathbf{m}^T = [\,1 \;\; 1 \;\; 1 \;\; 0 \;\; 0 \;\; 0\,]$ (3.46)

So, equation (3.44) becomes

$$\mathbf{L}^T\boldsymbol{\sigma} = \rho\ddot{\mathbf{u}} + n\rho_f\ddot{\mathbf{w}} \tag{3.47a}$$

Multiplying equation (3.43) by n^{-1} yields a generalized Darcy law,

$$\nabla p - \frac{n}{k}\dot{\mathbf{w}} + \frac{\nabla p^c}{n} = \rho_f\ddot{\mathbf{u}} + \rho_f\ddot{\mathbf{w}} \tag{3.47b}$$

where

$$k = \frac{1}{n^2 R_s} \tag{3.48}$$

Equations (3.47) are the governing equations of the soft tissue in Eulerian form in the absence of body forces.

3.1.4 Momentum conservation laws (Lagrangian Form)

Using equations (3.28), (3.29) and (3.31), equations (3.47) can be converted into the Lagrangian form,

$$\mathbf{L}_0^T(\mathbf{T}) = \rho\ddot{\mathbf{u}} + n\rho_f(J^{-1}\mathbf{F})\ddot{\dot{\mathbf{w}}} \tag{3.49a}$$

$$\mathbf{F}^{-1}\cdot\nabla_0 p + \mathbf{F}^{-1}\cdot\nabla_0\left(\frac{p^c}{n}\right) - \frac{n}{k}(J^{-1}\mathbf{F}^T)\dot{\mathbf{w}} = \rho_f\ddot{\mathbf{u}} + \rho_f(J^{-1}\mathbf{F}^T)\ddot{\dot{\mathbf{w}}} \tag{3.49b}$$

where

$$\mathbf{T} = \mathbf{F}^{-1}\cdot\boldsymbol{\sigma} \tag{3.50}$$

$$\nabla_0^T = < \frac{\partial}{\partial X_1} \quad \frac{\partial}{\partial X_2} \quad \frac{\partial}{\partial X_3} > \tag{3.51}$$

$$\mathbf{L}_0^T = \begin{bmatrix} \frac{\partial}{\partial X_1} & 0 & 0 & \frac{\partial}{\partial X_2} & 0 & \frac{\partial}{\partial X_3} \\ 0 & \frac{\partial}{\partial X_2} & 0 & \frac{\partial}{\partial X_1} & \frac{\partial}{\partial X_3} & 0 \\ 0 & 0 & \frac{\partial}{\partial X_3} & 0 & \frac{\partial}{\partial X_2} & \frac{\partial}{\partial X_1} \end{bmatrix} \tag{3.52}$$

Multiplying equation (3.49b) by $\mathbf{F}$ yields

$$\nabla_0 p + \nabla_0 (\frac{p^c}{n}) - \frac{n}{k} (J^{-1}\mathbf{F}\cdot\mathbf{F}^T)\dot{\hat{\mathbf{w}}} = \rho_f \mathbf{F}\cdot\ddot{\mathbf{u}} + \rho_f (J^{-1}\mathbf{F}\cdot\mathbf{F}^T)\cdot\ddot{\hat{\mathbf{w}}} \tag{3.53}$$

The permeability $\hat{\mathbf{k}}$ in Lagrangian form is defined by

$$\hat{\mathbf{k}} = kJ\mathbf{F}^{-T}\cdot\mathbf{F}^{-1} = \hat{k}\mathbf{I} \tag{3.54}$$

In this study, an average view of the permeability is taken, and $\hat{\mathrm{k}}$ is used to express the permeability of the porous material. Thus, equation (3.53) becomes

$$\nabla_0 (p + \frac{p^c}{n}) - \frac{n}{\hat{k}}\dot{\hat{\mathbf{w}}} = \rho_f \mathbf{F}\cdot\ddot{\mathbf{u}} + \rho_f (J^{-1}\mathbf{F}\cdot\mathbf{F}^T)\cdot\ddot{\hat{\mathbf{w}}} \tag{3.55}$$

3.1.5 Mass conservation laws (Lagrangian Form)

According to the mass conservation, the storage due to compressibility of the solid and of the fluid should be equal to the dilation of the fluid and of the solid, so in small deformation, the fluid pressure can be expressed as [57]

$$p = \alpha Q \mathbf{m}^T \mathbf{e} + Qn\zeta \tag{3.56}$$

where

$$\mathbf{e} = \mathbf{L}\mathbf{u} \tag{3.57}$$

$$\zeta = \nabla^T \mathbf{w} \tag{3.58}$$

$$\frac{1}{Q} = \frac{n}{K_f} + \frac{\alpha - n}{K_s} \tag{3.59}$$

$$\alpha = 1 - \frac{K}{K_s} \tag{3.60}$$

K = " apparent " bulk moduli for the solid [62]

K_s = "true" bulk moduli for the solid [62]

K_f = "true" bulk moduli for the fluid [62]

In case of large deformation, it can be converted to the Lagrangian Form as

$$p = Q\left[\alpha E'_{kk} + n\zeta\right] \tag{3.61}$$

where

$$\mathbf{E}' = J\mathbf{F}^{-T} \cdot \mathbf{E} \cdot \mathbf{F}^{-1} \tag{3.62}$$

The material of soft tissue is always considered as nearly incompressible or incompressible. In poroelastic theory, the soft tissue is considered as nearly incompressible, and in biphasic and triphasic theories, it is fully incompressible. In case of near incompressibility, the "true" Possion's ratio of solid phase is selected close to 0.5, which means K_s is relatively high. However, in case of full incompressibility, both the solid and fluid are fully incompressible, $K_s \to \infty$, and $K_f \to \infty, Q \to \infty$, which means the pressure can not be determined by $\mathbf{E}'$ and ζ directly. Thus, the incompressibility constraint can be applied to determine fluid pressure indirectly

$$\dot{E}''_{kk} + n\dot{\tilde{\zeta}} = 0 \tag{3.63}$$

where

$$\dot{\mathbf{E}}'' = J\mathbf{F}^{-T} \cdot \dot{\mathbf{E}} \cdot \mathbf{F}^{-1} \tag{3.64}$$

3.1.6 Mobile ions

In the triphasic theory [72], the gravitational and magnetic effects are neglected, and the gradients of chemical/electrochemical potentials $\nabla\hat{\mu}$ are the driving forces balanced by the frictional forces between phases such as the frictional force between the cation and solid phase $\mathbf{F}_{+s}(= f_{+s}(\mathbf{v}^s - \mathbf{v}^+))$. So the momentum equations are given as

Cation:

$$-\rho^+\nabla\hat{\mu}^+ + f_{+s}(\mathbf{v}^s - \mathbf{v}^+) + f_{+f}(\mathbf{v}^w - \mathbf{v}^+) + f_{+-}(\mathbf{v}^- - \mathbf{v}^+) = 0 \tag{3.65}$$

Anion:

$$-\rho^-\nabla\hat{\mu}^- + f_{-s}(\mathbf{v}^s - \mathbf{v}^-) + f_{-f}(\mathbf{v}^w - \mathbf{v}^-) + f_{-+}(\mathbf{v}^+ - \mathbf{v}^-) = 0 \tag{3.66}$$

Where

$f_{\alpha\beta}$ = frictional coefficients per unit tissue volume between α and β components, α, β $\in$ {solid (*s*),fluid (*f*), positive ion (+), negative ion (-)}

$\mathbf{v}^\alpha$ = velocity of α component

$\hat{\mu}^+$ = positive chemical potential

$\hat{\mu}^-$ = negative chemical potential

Since the permeability of the soft tissue is extremely low, about 10^{-14} m^4/Ns, it is reasonable to assume the soft tissue behaves like a pure solid [62], which means that the velocity of fluid is almost the same as that of solid. As a result, combining the second term and third term of equations (3.65) and (3.66), we have

Cation:

$$-\rho^{+}\nabla\hat{\mu}^{+} + f_{+sf}(\mathbf{v}^{s} - \mathbf{v}^{+}) + f_{+-}(\mathbf{v}^{-} - \mathbf{v}^{+}) = 0 \tag{3.67}$$

Anion:

$$-\rho^{-}\nabla\hat{\mu}^{-} + f_{-sf}(\mathbf{v}^{s} - \mathbf{v}^{-}) + f_{-+}(\mathbf{v}^{+} - \mathbf{v}^{-}) = 0 \tag{3.68}$$

Where

$$f_{+sf} = f_{+s} + f_{+f} \tag{3.69}$$

$$f_{-sf} = f_{-s} + f_{-f} \tag{3.70}$$

The constitutive equations for the negative and positive ions are given by [72]:

$$\hat{\mu}^{+} = \mu_{0}^{+} + \frac{RT}{M^{+}}\ln(\gamma^{+}c^{+}) + \frac{F_{c}\varphi}{M^{+}} \tag{3.71}$$

$$\hat{\mu}^{-} = \mu_{0}^{-} + \frac{RT}{M^{-}}\ln(\gamma^{-}c^{-}) - \frac{F_{c}\varphi}{M^{-}} \tag{3.72}$$

The ion fluxes relative to the solid phase are defined by [72]

$$\mathbf{J}^{+} = c^{+}(\mathbf{v}^{+} - \mathbf{v}^{s}) \tag{3.73}$$

$$\mathbf{J}^{-} = c^{-}(\mathbf{v}^{-} - \mathbf{v}^{s}) \tag{3.74}$$

Substituting (3.73) and (3.74) into equation (3.67), we have

$$-\rho^{+}\nabla\hat{\mu}^{+} + f_{+sf}(-\frac{\mathbf{J}^{+}}{c^{+}}) + f_{+-}(\frac{\mathbf{J}^{-}}{c^{-}} - \frac{\mathbf{J}^{+}}{c^{+}}) = 0 \tag{3.75}$$

$$\left(\frac{f_{+-}}{c^{-}}\right)\mathbf{J}^{-} - \left(\frac{f_{+sf} + f_{+-}}{c^{+}}\right)\mathbf{J}^{+} = \rho^{+}\nabla\hat{\mu}^{+} \tag{3.76}$$

Similarly, equation (3.68) becomes

$$\left(\frac{f_{-+}}{c^{+}}\right)\mathbf{J}^{+} - \left(\frac{f_{-sf} + f_{-+}}{c^{-}}\right)\mathbf{J}^{-} = \rho^{-}\nabla\hat{\mu}^{-} \tag{3.77}$$

So, from equations (3.76) and (3.77), $\mathbf{J}^{+}$ and $\mathbf{J}^{-}$ can be expressed as

$$\mathbf{J}^{+} = -\frac{\rho^{+}c^{+}\nabla\hat{\mu}^{+}(f_{-sf} + f_{-+}) + \rho^{-}c^{+}\nabla\hat{\mu}^{-}f_{+-}}{f_{+sf}f_{-sf} + f_{+sf}f_{-+} + f_{+-}f_{-sf}} \tag{3.78}$$

$$\mathbf{J}^{-} = -\frac{\rho^{-}c^{-}\nabla\hat{\mu}^{-}(f_{+sf} + f_{+-}) + \rho^{+}c^{-}\nabla\hat{\mu}^{+}f_{-+}}{f_{+sf}f_{-sf} + f_{+sf}f_{-+} + f_{+-}f_{-sf}} \tag{3.79}$$

or

$$\mathbf{J}^{+} = k_1^{+}c^{+}\nabla\hat{\mu}^{+} + k_2^{+}c^{+}\nabla\hat{\mu}^{-} \tag{3.80}$$

$$\mathbf{J}^{-} = k_1^{-}c^{-}\nabla\hat{\mu}^{-} + k_2^{-}c^{-}\nabla\hat{\mu}^{+} \tag{3.81}$$

where

$$k_1^{+} = -\frac{\rho^{+}(f_{-sf} + f_{-+})}{f_{+sf}f_{-sf} + f_{+sf}f_{-+} + f_{+-}f_{-sf}} \tag{3.82}$$

$$k_2^{+} = -\frac{\rho^{-}f_{+-}}{f_{+sf}f_{-sf} + f_{+sf}f_{-+} + f_{+-}f_{-sf}} \tag{3.83}$$

$$k_1^{-} = -\frac{\rho^{-}(f_{+sf} + f_{+-})}{f_{+sf}f_{-sf} + f_{+sf}f_{-+} + f_{+-}f_{-sf}} \tag{3.84}$$

$$k_2^{-} = -\frac{\rho^{+}f_{-+}}{f_{+sf}f_{-sf} + f_{+sf}f_{-+} + f_{+-}f_{-sf}} \tag{3.85}$$

The continuity equations for ions are

$$\frac{\partial c^{+}}{\partial t} + \nabla\cdot\mathbf{J}^{+} + \nabla\cdot(c^{+}\mathbf{v}^{s}) = 0 \tag{3.86}$$

$$\frac{\partial c^{-}}{\partial t} + \nabla\cdot\mathbf{J}^{-} + \nabla\cdot(c^{-}\mathbf{v}^{s}) = 0 \tag{3.87}$$

Equation (3.11) gives the electroneutrality condition for the global field, and for the local field it becomes

$$\nabla\cdot\mathbf{J}^{+} - \nabla\cdot\mathbf{J}^{-} = 0 \tag{3.88}$$

Combination of equations (3.86) and (3.87) gives

$$\frac{\partial c^k}{\partial t} + \nabla \cdot \mathbf{J}^+ + \nabla \cdot \mathbf{J}^- + \nabla \cdot (c^k \mathbf{v}^s) = 0 \tag{3.89}$$

where

$$c^k = c^+ + c^- \tag{3.90}$$

Equations (3.88) and (3.89) are the governing equations for the ions.

3.2 CONSTITUTIVE LAW

The effective stress **σ'** in equation (3.44) is the portion of the total stress in excess of the local pore fluid pressure [57], and is connected with the properties of the "drained" material. In this study, we consider the material as viscoelasticity due to the components of biological tissue such as collagen fibrils and proteoglycan gel are highly viscoelastic, independent of fluid flow. In order to deal with the viscoelasticity, a concept that the final stress state is only dependent on the elastic deformations is applied here, therefore it is necessary to define the local elastic deformation gradient and the local viscous deformation gradient of the finite strain.

3.2.1 Deformation gradient

In this study, this deformation process of soft tissue is considered to involve the local instantaneous elastic deformation and local viscous deformation [54]. As a result, the deformation gradient consists of two parts: elastic and viscous, which is expressed as follows

$$\mathbf{F} = \mathbf{F}^e \mathbf{F}^v \tag{3.91}$$

Fig. 3.2 shows the multiplicative decomposition of the deformation gradient **F**. First, $\mathbf{F}^{v}$ maps B_0 into B*, then $\mathbf{F}^{e}$ maps B* into the current configuration B. It should be noted that this transform isn't unique, because the intermediate configuration with arbitrary rigid body rotation does not affect the validity of equation (3.91). Consequently for a given total deformation gradient **F**, decomposition given in equation (3.91) should be not unique. Thus, it is assumed that rotation is absent in the permanent part of the deformation gradient $\mathbf{F}^{v}$ to remove nonuniqueness. This assumption provides a base of further study equation (4.96).

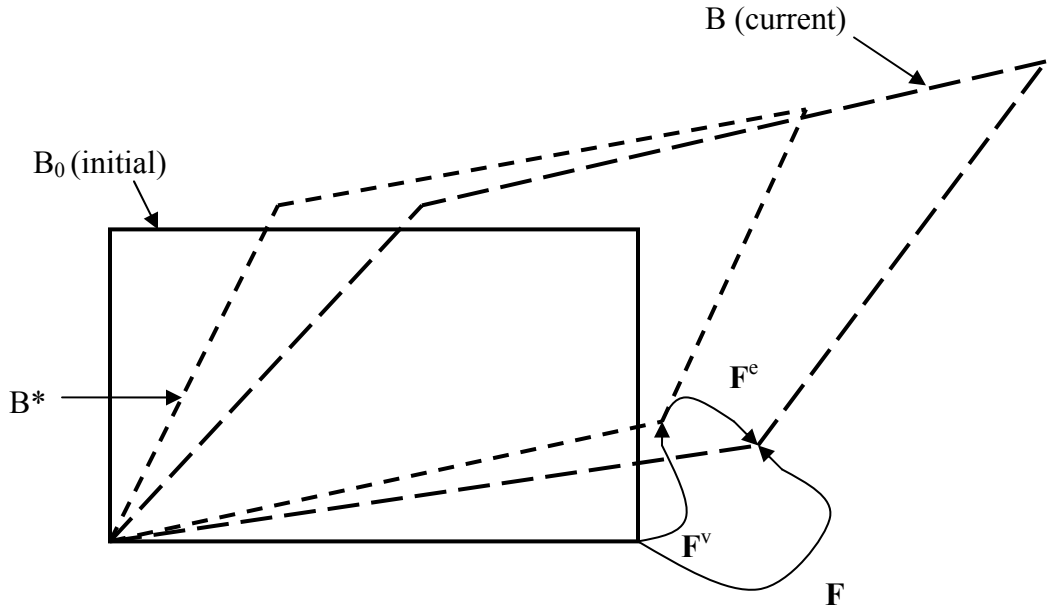

Fig.3.2 Configurations for describing the multiplicative decomposition of **F** [54]

3.2.2 Large strain

The Cauchy-Green strain tensor is defined as [54]

$$\mathbf{E} = \frac{1}{2}(\mathbf{F}^{\mathrm{T}}\mathbf{F} - \mathbf{I}) \tag{3.92}$$

Making use of equation (3.91), it can be written as

$$\mathbf{E} = \frac{1}{2}[(\mathbf{F}^{\mathrm{e}}\mathbf{F}^{\mathrm{v}})^{\mathrm{T}}(\mathbf{F}^{\mathrm{e}}\mathbf{F}^{\mathrm{v}}) - \mathbf{I}]$$

$$= \frac{1}{2}[(\mathbf{F}^{v})^{T}(\mathbf{F}^{e})^{T}\mathbf{F}^{e}\mathbf{F}^{v} - (\mathbf{F}^{v})^{T}(\mathbf{F}^{v}) + (\mathbf{F}^{v})^{T}(\mathbf{F}^{v}) - \mathbf{I}]$$

$$= (\mathbf{F}^{v})^{T}\{\frac{1}{2}[(\mathbf{F}^{e})^{T}\mathbf{F}^{e} - \mathbf{I}]\}\mathbf{F}^{v} + \frac{1}{2}[(\mathbf{F}^{v})^{T}\mathbf{F}^{v} - \mathbf{I}] \tag{3.93}$$

or

$$\mathbf{E} = (\mathbf{F}^{v})^{T}\mathbf{E}^{e}(\mathbf{F}^{v}) + \mathbf{E}^{v} \tag{3.94}$$

where $\mathbf{E}^{e}, \mathbf{E}^{v}$ are determined by:

$$\mathbf{E}^{e} = \frac{1}{2}[(\mathbf{F}^{e})^{T}\mathbf{F}^{e} - \mathbf{I}] \tag{3.95}$$

$$\mathbf{E}^{v} = \frac{1}{2}[(\mathbf{F}^{v})^{T}\mathbf{F}^{v} - \mathbf{I}] \tag{3.96}$$

3.2.3 Stress measures

The Cauchy stress tensor, or true stress, which is denoted by $\boldsymbol{\sigma}'$, is given in the current configuration B. Thus, the elastic stress and the viscoelastic stress are presented as follows [54].

The elastic stress related to the configuration B* is defined as:

$$\mathbf{S}^{e} = J(\mathbf{F}^{e})^{-1}\boldsymbol{\sigma}'(\mathbf{F}^{e})^{-T} \tag{3.97}$$

The viscoelastic stress related to the configuration B_0 is determined by:

$$\mathbf{S}^{v} = J(\mathbf{F}^{e}\mathbf{F}^{v})^{-1}\boldsymbol{\sigma}'(\mathbf{F}^{e}\mathbf{F}^{v})^{-T} = (\mathbf{F}^{v})^{-1}\mathbf{S}^{e}(\mathbf{F}^{v})^{-T} \tag{3.98}$$

The definition of those stress tensors and the strain tensors $\mathbf{E}^e$ and $\mathbf{E}^v$ shows clearly that the pair $\mathbf{S}^e$ and $\mathbf{E}^e$ is the Lagrangian pair with respect to the configuration B*, and the pair $\mathbf{S}^v$ and $\mathbf{E}^v$ is the pair related to the configuration B_0. Because elastic deformations are imposed on the configuration B*, it is reasonable to adopt $\mathbf{S}^e$ and $\mathbf{E}^e$ to describe purely elastic problem in the constitutive equations developed for the Lagrangian description, and $\mathbf{S}^v$ and $\mathbf{E}^v$ for Lagrangian description of viscoelasticity.

From equation (3.97), the effective stress $\boldsymbol{\sigma}'$ can be expressed as

$$\boldsymbol{\sigma}' = \frac{1}{J}(\mathbf{F}^e)\mathbf{S}^e(\mathbf{F}^e)^T \tag{3.99}$$

Thus, in order to calculate the effective stress $\boldsymbol{\sigma}'$, the constitutive equations between the stress and the strain must be set up.

3.2.4 Constitutive equations for viscoelastic materials

Roger [56] has done extensive work to describe the behavior of viscoelastic materials. In general, it is difficult to determine the large number of parameters in complex material models by experimental methods, thus, models with a small number of parameters have been used often in practice since they provide sufficient engineering accuracy in many applications.

3.2.4.1 Instantaneous linear elasticity For linear elastic problem, the relation between the stress and the strain is given as

$$\mathbf{S}^e = \mathbf{D} \cdot \mathbf{E}^e \tag{3.100}$$

where **D** has the isotropic form

$$\mathbf{D} = \begin{bmatrix} (\lambda+2\mu) & \lambda & \lambda & 0 & 0 & 0 \\ & \lambda+2\mu & \lambda & 0 & 0 & 0 \\ & & \lambda+2\mu & 0 & 0 & 0 \\ & & & \mu & 0 & 0 \\ & & & & \mu & 0 \\ \textit{symm.} & & & & & \mu \end{bmatrix} \tag{3.101}$$

3.2.4.2 Viscoelastic model [70] There are two ways to describe viscoelastic behavior of materials: the differential description and the hereditary integral description. Both approaches are equivalent in principle because the integral form is a solution of the differential equations used in the differential description of the problem. In practice for nonlinear problems, the integral formulation is much more common, so the integral formulation will be adopted in this study. The relaxation formulation is interpreted as follows.

For a body, at t=0, a stress σ_0 is applied suddenly, and the corresponding strain is produced,

$$\varepsilon = \sigma_0 J_v(t) \tag{3.102}$$

Later, σ undergoes change as an arbitrary function $\sigma(t)$. The corresponding strain at time t can be obtained by combination of the strain caused by all the steps that occurred at time $t' < t$ (Figure.3.3), that is,

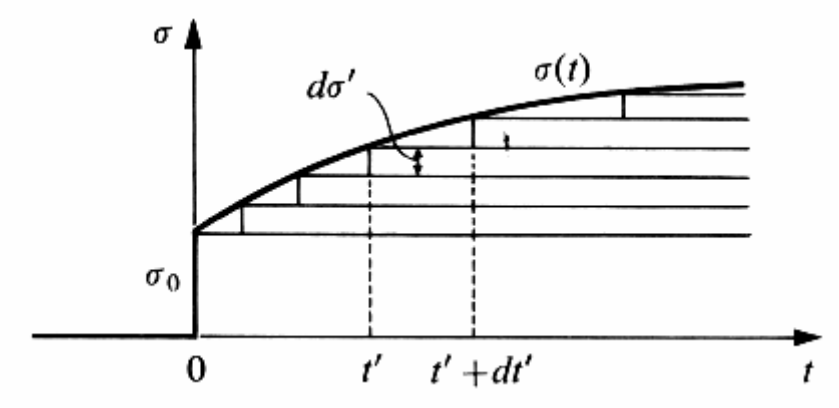

Fig.3.3 Derivation of the hereditary integral [70]

$$\varepsilon(t) = \sigma_0 J_v(t) + \int_0^t J_v(t-t') \frac{d\sigma'}{dt'} dt' \tag{3.103}$$

The above formula shows the strain at any given time is the function of the entire stress history $\sigma'(t')$, $t' < t$, which is quite different from what happens in an elastic material since the strain of an elastic material depends at any time solely on the stress acting at that time only.

The integral in (3.103) is called a hereditary integral. Another useful form can be obtained through integration by parts:

$$\varepsilon(t) = \sigma_0 J_v(t) + [J_v(t-t') \cdot \sigma(t')]_0^t - \int_0^t \sigma(t') \frac{dJ_v(t-t')}{dt'} dt' \tag{3.104}$$

It should be noted that all the zeros in these equations refer to 0^+. Thus, when the bracketed boundary term is evaluated, it combines with the first term.

Since

$$\frac{dJ_v(t-t')}{dt'} = \frac{-dJ_v(t-t')}{d(t-t')} \tag{3.105}$$

Equation (3.104) can be rewritten as

$$\varepsilon(t) = \sigma_0 J_v(0) + \int_0^t \sigma(t') \frac{dJ_v(t-t')}{d(t-t')} dt' \tag{3.106}$$

We can extend the above equation to general relaxation formulation, which can be used to describe a viscoelastic material. , and then J_v becomes the tensor $\mathbf{J_v}$. When $\mathbf{J_v}(0)=0$, one memory integral has the following form [55]:

$$\mathbf{E}^v(\tau) = \int_0^t \frac{\partial \mathbf{J}_v(t-\tau)}{\partial(t-\tau)} \mathbf{S}^v(\tau) d\tau \tag{3.107}$$

The nature of the relax memory matrix $\mathbf{J}_v(t)$ can be adequately described as

$$\mathbf{J}_v(\theta) = \mathbf{D}_v^{-1} \sum_{i=1}^{m} A_i (1 - e^{-\theta/\tau_i}) \tag{3.108}$$

where $\mathbf{D}_v^{-1}$ is a matrix of material constants. The number of terms m and the values of those constants depend on experimental data.

4.0 NUMERICAL IMPLEMENTATION

The mathematical model for the biological tissue has been described in the preceding chapters, including the porous model and the electro-chemical model. Equation (3.45) governs the porous model, and equation (3.81) and (3.82) controls the ion motion. Obviously, equation (3.45) couples the behavior of the solid and fluid, since the pressure is the function of the displacement of the solid and the fluid. Also, the coefficients in equations (3.81) and (3.82) are functions of unknown c^+ and c^-, and these equations are nonlinear. These complicated equations will be solved separately with two steps. First, equation (3.81) and (3.82) are solved to give the distribution of c^+ and c^- , and then with the known c^+ and c^- , equation (3.45) is computed to give the displacement of the solid and the fluid..

In this chapter, the numerical implementation is discussed, including linearization of solid stress equations. First, we start with the finite element form of the governing equations.

4.1 FINITE ELEMENT FORM OF THE POROUS MODEL

In the finite element method, the governing differential equations are always converted into their weak form. The weak form and the differential equation with the specified natural boundary

conditions are equivalent, but the weak form is an integral form that is easy to implement numerically. The standard Galerkin method is utilized to find the generalized weak form.

The porous model involves displacement of solid, displacement of fluid, pressure. Several finite element formulations were employed to solve it. In general, u-p formulation is common because of its computational efficiency [57]. However, its approximation of the fluid velocity field is poor, which is generally two orders lower than the solid displacement, and results in a discontinuous fluid flux at the element boundaries [73]. On the contrary, u-w-p formulation has no such problem, and was proved to be an effective form for the soft tissue problem [32, 65]. In addition, the near incompressibility and full incompressibility cases can be implemented easily with u-w-p formulation. Thus, u-w-p formulation is adopted in this study.

Since the soft tissue is considered as near incompressibility or full incompressibility with different governing equations to describe it, the weak form for the near incompressibility is given first, and then modified for full incompressibility.

4.1.1 Weak form for the near incompressibility

Equation (3.45a) governs the motion of the solid phase in the absence of gravity by

$$\frac{\partial T_{ji}}{\partial X_j} - \rho \ddot{u}_i - n\rho_f (J^{-1} \frac{\partial x_i}{\partial X_j}) \ddot{\hat{w}}_j = 0 \tag{4.1}$$

Multiply the above equation by the weight function H, and integrating over the domain of the problem, gives

$$\int_\Omega \mathrm{H} \left[\frac{\partial T_{ji}}{\partial X_j} - \rho \ddot{u}_i - n\rho_f (J^{-1} \frac{\partial x_i}{\partial X_j}) \ddot{\hat{w}}_j \right] d\Omega = 0 \tag{4.2}$$

Using integration by parts on the first term, the above equation is written as

$$\int_{\Omega} (\mathrm{H}T_{ji})_{,j}\, d\Omega - \int_{\Omega} \mathrm{H}_{,j} T_{ji}\, d\Omega - \int_{\Omega} \mathrm{H}\rho \ddot{u}_i\, d\Omega - \int_{\Omega} \mathrm{H} n \rho_f \left(J^{-1} \frac{\partial x_i}{\partial X_j} \right) \ddot{\hat{w}}_j\, d\Omega = 0 \tag{4.3}$$

and applying Green's theorem to the first term, yields

$$\int_{\partial\Omega} \mathrm{H}\bar{t}_i\, ds - \int_{\Omega} \mathrm{H}_{,j} T_{ji}\, d\Omega - \int_{\Omega} \mathrm{H}\rho \ddot{u}_i\, d\Omega - \int_{\Omega} \mathrm{H} n \rho_f \left(J^{-1} \frac{\partial x_i}{\partial X_j} \right) \ddot{\hat{w}}_j\, d\Omega = 0 \tag{4.4}$$

Choosing the shape functions and the weight functions as

$$\mathrm{H} = N^u_{Li} \tag{4.5a}$$

$$u_i = N^u_{Ki} \bar{u}_{Ki} \tag{4.5b}$$

$$\hat{w}_j = N^w_{Kj} \bar{w}_{Kj} \tag{4.5c}$$

and noting that the interpolation functions, N^u_{Ki} and N^w_{Kj}, are not time dependent, substituting equation (4.5) into equation (4.4) gives,

$$-\int_{\partial\Omega} N^u_{Li} \bar{t}_i\, ds + \int_{\Omega} N^u_{Li,j} T_{ji}\, d\Omega + \left(\int_{\Omega} \rho N^u_{Li} N^u_{Ki}\, d\Omega\right) \ddot{\bar{u}}_{Ki} + \left(\int_{\Omega} N^u_{Li} n \rho_f \left(J^{-1} \frac{\partial x_i}{\partial X_j} \right) N^w_{Kj}\, d\Omega\right) \ddot{\bar{w}}_{Kj} = 0 \tag{4.6}$$

Writing the above equation in matrix form, gives

$$\mathbf{M}_{ss} \ddot{\bar{\mathbf{u}}} + \mathbf{M}_{sf} \ddot{\bar{\mathbf{w}}} - \bar{\mathbf{f}}_u + \int_{\Omega} \mathbf{B}^T \mathbf{T}\, d\Omega = 0 \tag{4.7}$$

or

$$\mathbf{M}_{ss} \ddot{\bar{\mathbf{u}}} + \mathbf{M}_{sf} \ddot{\bar{\mathbf{w}}} = \bar{\mathbf{f}}_u - \int_{\Omega} \mathbf{B}^T \mathbf{T}\, d\Omega \tag{4.8}$$

where

$$(M_{ss})_{LK} = \int_{\Omega} \rho N^u_{Li} N^u_{Ki}\, d\Omega \tag{4.9}$$

$$(M_{sf})_{LK} = \int_{\Omega} N_{Li}^{u} n \rho_f \left(J^{-1} \frac{\partial x_i}{\partial X_j} \right) N_{Kj}^{w} d\Omega \tag{4.10}$$

$$(f_u)_L = \int_{\partial\Omega} N_{Li}^{u} \bar{t}_i ds \tag{4.11}$$

$$[\mathbf{B}]_{i,j}^{T} = N_{Li,j}^{T} \tag{4.12}$$

Equation (3.51) gives the governing equation for the fluid phase,

$$\frac{\partial (p + p^c / n)}{\partial X_i} - \frac{n}{\hat{k}} \dot{\hat{w}}_j - \rho_f \frac{\partial x_j}{\partial X_i} \ddot{u}_j - \rho_f (J^{-1} \frac{\partial x_k}{\partial X_i} \frac{\partial x_k}{\partial X_j}) \ddot{\hat{w}}_j = 0 \tag{4.13}$$

Multiplying the above equation by weight function Γ and integrating over the domain, gives

$$\int_{\Omega} \Gamma [\frac{\partial (p + p^c / n)}{\partial X_i} - \frac{n}{\hat{k}} \dot{\hat{w}}_j - \rho_f \frac{\partial x_j}{\partial X_i} \ddot{u}_j - \rho_f (J^{-1} \frac{\partial x_k}{\partial X_i} \frac{\partial x_k}{\partial X_j}) \ddot{\hat{w}}_j] d\Omega = 0 \tag{4.14}$$

Choosing weight function as $\Gamma = N_{Li}^{w}$ and substituting equation (4.5) into equation (4.14) yields

$$\int_{\Omega} N_{Li}^{w} N_{K,i} \, p_K d\Omega + \int_{\Omega} N_{Li}^{w} \frac{p^{c},_i}{n} d\Omega - \int_{\Omega} \frac{n}{\hat{k}} N_{Li}^{w} N_{Ki}^{w} d\Omega \dot{\bar{w}}_{Kj}$$

$$- \int_{\Omega} N_{Li}^{w} \rho_f \frac{\partial x_j}{\partial X_i} N_{Kj} d\Omega \ddot{\bar{u}}_{Kj} - \int_{\Omega} N_{Li}^{w} \frac{\rho_f}{J} \frac{\partial x_k}{\partial X_i} \frac{\partial x_k}{\partial X_j} N_{Ki}^{w} d\Omega \ddot{\bar{w}}_{Kj} = 0 \tag{4.15}$$

Writing equation (4.15) in matrix form, we get

$$\mathbf{M}_{fs} \ddot{\bar{\mathbf{u}}} + \mathbf{M}_{ff} \ddot{\bar{\mathbf{w}}} + \mathbf{M}_{d} \dot{\bar{\mathbf{w}}} = \bar{\mathbf{f}}_w \tag{4.16}$$

where

$$(M_{fs})_{LK} = \int_{\Omega} N_{Li}^{w} \rho_f \frac{\partial x_j}{\partial X_i} N_{Kj} d\Omega \tag{4.17}$$

$$(M_{ff})_{LK} = \int_{\Omega} N_{Li}^{w} \frac{\rho_f}{J} \frac{\partial x_k}{\partial X_i} \frac{\partial x_k}{\partial X_j} N_{Kj}^{w} d\Omega \tag{4.18}$$

$$(M_d)_{LK} = \int_{\Omega} \frac{n}{\hat{k}} N_{Li}^{w} N_{Kj}^{w} d\Omega \tag{4.19}$$

$$(\bar{f}_w)_L = \int_{\Omega} N_{Li}^{T} N_{K,i} \cdot p_K d\Omega + \int_{\Omega} N_{Li}^{w} \frac{p^{c},_i}{n} \cdot d\Omega \tag{4.20}$$

In case of the near compressibility, referred to equation (3.56), the pressure can be expressed as,

$$p = nQ\hat{w}_{i,i} + \alpha Q\left[J \frac{\partial X_r}{\partial x_k} E_{rs} \frac{\partial X_s}{\partial x_k} \right] \tag{4.21}$$

Multiplying the above equation by weight function Γ and integrating over the domain,

$$0 = \int_{\Omega} \Gamma(p - nQ\hat{w}_{i,i} - \alpha QJ\left[\frac{\partial X_r}{\partial x_k} E_{rs} \frac{\partial X_s}{\partial x_k} \right]) d\Omega \tag{4.22}$$

Selecting the weight function to be $\Gamma = N_L^p$, we get from the above equation

$$0 = \bar{\mathbf{f}}_p \tag{4.23}$$

where

$$(\bar{f}_p)_L = \int_{\Omega} N_L^p N_K^p d\Omega \cdot p_K - \int_{\Omega} (nQ\hat{w}_{i,i} + \alpha JQ\left[\frac{\partial X_r}{\partial x_k} E_{rs} \frac{\partial X_s}{\partial x_k} \right])_K N_L^p d\Omega \tag{4.24}$$

Combining equations (4.8), (4.16), and (4.23) into matrix form as follows:

$$\begin{bmatrix} \mathbf{M}_{ss} & \mathbf{M}_{sf} & 0 \\ \mathbf{M}_{fs} & \mathbf{M}_{ff} & 0 \\ 0 & 0 & 0 \end{bmatrix} \begin{Bmatrix} \ddot{\bar{\mathbf{u}}} \\ \ddot{\bar{\mathbf{w}}} \\ \ddot{\bar{\mathbf{p}}} \end{Bmatrix} + \begin{bmatrix} 0 & 0 & 0 \\ 0 & \mathbf{M}_d & 0 \\ 0 & 0 & 0 \end{bmatrix} \begin{Bmatrix} \dot{\bar{\mathbf{u}}} \\ \dot{\bar{\mathbf{w}}} \\ \dot{\bar{\mathbf{p}}} \end{Bmatrix} = \begin{Bmatrix} \bar{\mathbf{f}}_u - \int_{\Omega} \mathbf{B}^T \mathbf{T} d\Omega \\ \bar{\mathbf{f}}_w \\ \bar{\mathbf{f}}_p \end{Bmatrix} \tag{4.25}$$

or

$$\mathbf{M}\ddot{\mathbf{X}} + \mathbf{C}\dot{\mathbf{X}} = \overline{\mathbf{F}} \tag{4.26}$$

where

$$\mathbf{M} = \begin{bmatrix} \mathbf{M}_{ss} & \mathbf{M}_{sf} & 0 \\ \mathbf{M}_{fs} & \mathbf{M}_{ff} & 0 \\ 0 & 0 & 0 \end{bmatrix} \tag{4.27}$$

$$\mathbf{X} = \begin{Bmatrix} \mathbf{u} \\ \mathbf{w} \\ \mathbf{p} \end{Bmatrix} \tag{4.28}$$

$$\mathbf{C} = \begin{bmatrix} 0 & 0 & 0 \\ 0 & \mathbf{M}_{d} & 0 \\ 0 & 0 & 0 \end{bmatrix} \tag{4.29}$$

$$\overline{\mathbf{F}} = \begin{Bmatrix} \overline{\mathbf{f}}_{u} - \int_{\Omega} \mathbf{B}^{T}\mathbf{T}d\Omega \\ \overline{\mathbf{f}}_{w} \\ \overline{\mathbf{f}}_{p} \end{Bmatrix} \tag{4.30}$$

4.1.2 Weak form for the full incompressibility

Based on equation (3.57), the continuity equation becomes,

$$J\frac{\partial X_r}{\partial x_m}\dot{E}_{rs}\frac{\partial X_s}{\partial x_k} + n\dot{\tilde{\zeta}} = 0 \tag{4.31}$$

The weighted residual formulation for the above equation is

$$\int_{\Omega} \Gamma \cdot \left(J\frac{\partial X_r}{\partial x_m}\dot{E}_{rs}\frac{\partial X_s}{\partial x_k} + n\dot{\tilde{\zeta}} \right) d\Omega = 0 \tag{4.32}$$

so,

$$\int_{\Omega} (\mathbf{N}^P)^T \mathbf{m}'\mathbf{B} d\Omega \cdot \dot{\bar{\mathbf{u}}} + \int_{\Omega} n(\mathbf{N}^P)^T \mathbf{m}\mathbf{B} d\Omega \dot{\bar{\mathbf{w}}} = 0 \tag{4.33}$$

where **m=** the vector form of Kronecker delta, {1 1 1 0 0 0}

m' =the modified vector form of Kronecker delta, {m_1 m_2 m_3 0 0 0}, which is determined by $\left(J\mathbf{F}^{-T}\mathbf{F}^{-1}\right)$

Equation (4.33) can be written as

$$\mathbf{M}_{up} \cdot \dot{\bar{\mathbf{u}}} + \mathbf{M}_{wp} \cdot \dot{\bar{\mathbf{w}}} = 0 \tag{4.34}$$

where

$$\mathbf{M}_{up} = \int_{\Omega} (\mathbf{N}^P)^T \mathbf{m}'\mathbf{B} d\Omega \tag{4.35}$$

$$\mathbf{M}_{wp} = \int_{\Omega} n(\mathbf{N}^P)^T \mathbf{m}\mathbf{B} d\Omega \tag{4.36}$$

Therefore, **C** and $\overline{\mathbf{F}}$ matrixes in equation (4.26) become

$$\mathbf{C} = \begin{bmatrix} 0 & 0 & 0 \\ 0 & \mathbf{M}_d & 0 \\ \mathbf{M}_{up} & \mathbf{M}_{wp} & 0 \end{bmatrix} \tag{4.37}$$

$$\overline{\mathbf{F}} = \begin{Bmatrix} \bar{\mathbf{f}}_u - \int_{\Omega} \mathbf{B}^T \mathbf{T} d\Omega \\ \bar{\mathbf{f}}_w \\ \mathbf{0} \end{Bmatrix} \tag{4.38}$$

4.2 FINITE ELEMENT FORM OF THE ELECTROCHEMICAL MODEL

The governing equation of the electrochemical model is given by equations (3.81) and (3.82)

$$\nabla \cdot \mathbf{J}^+ - \nabla \cdot \mathbf{J}^- = 0 \tag{4.39}$$

$$\frac{\partial c^k}{\partial t} + \nabla \cdot \mathbf{J}^+ + \nabla \cdot \mathbf{J}^- + \nabla \cdot (c^k \mathbf{v}^s) = 0 \tag{4.40}$$

Multiplying the above equation by the testing function ψ, gives

$$\int_\Omega (\nabla \cdot \mathbf{J}^+ - \nabla \cdot \mathbf{J}^-)\psi \; d\Omega = 0 \tag{4.41}$$

$$\int_\Omega (\nabla \cdot \mathbf{J}^+)\psi \; d\Omega - \int_\Omega (\nabla \cdot \mathbf{J}^-)\psi \; d\Omega = 0 \tag{4.42}$$

With equation (3.73), the first term of the above equation becomes

$$\begin{aligned} \int_\Omega (\nabla \cdot \mathbf{J}^+)\psi \; d\Omega &= \int_\Omega (\nabla \cdot (k_1^+ c^+ \nabla \hat{\mu}^+ + k_2^+ c^+ \nabla \hat{\mu}^-))\psi \; d\Omega \\ &= \int_\Omega (\nabla \cdot (k_1^+ c^+ \nabla \hat{\mu}^+))\psi \; d\Omega + \int_\Omega (\nabla \cdot (k_2^+ c^+ \nabla \hat{\mu}^-))\psi \; d\Omega \end{aligned} \tag{4.43}$$

Using integration by parts on the first term, yields

$$\int_\Omega (\nabla \cdot (k_1^+ c^+ \nabla \hat{\mu}^+))\psi \; d\Omega = \int_\Omega \nabla \cdot (k_1^+ c^+ \nabla \hat{\mu}^+ \psi) d\Omega - \int_\Omega (\nabla \psi) \cdot (k_1^+ c^+ \nabla \hat{\mu}^+) d\Omega \tag{4.44}$$

and applying Green's theorem, we have

$$\int_\Omega (\nabla \cdot (k_1^+ c^+ \nabla \hat{\mu}^+))\psi \; d\Omega = \int_s (k_1^+ c^+ \nabla \hat{\mu}^+ \psi) \cdot \mathbf{n} ds - \int_\Omega (\nabla \psi) \cdot (k_1^+ c^+ \nabla \hat{\mu}^+) d\Omega \tag{4.45}$$

Similarly,

$$\int_\Omega (\nabla \cdot (k_2^+ c^+ \nabla \hat{\mu}^-))\psi \; d\Omega = \int_s (k_2^+ c^+ \nabla \hat{\mu}^- \psi) \cdot \mathbf{n} ds - \int_\Omega (\nabla \psi) \cdot (k_2^+ c^+ \nabla \hat{\mu}^-) d\Omega \tag{4.46}$$

so that,

$$\int_{\Omega}(\nabla\cdot\mathbf{J}^{+})\psi\ d\Omega=\int_{\Omega}(k_1^{+}c^{+}\nabla\hat{\mu}^{+}\psi)\cdot\mathbf{n}ds-\int_{\Omega}(\nabla\psi)\cdot(k_1^{+}c^{+}\nabla\hat{\mu}^{+})d\Omega$$

$$+\int_{\Omega}(k_2^{+}c^{+}\nabla\hat{\mu}^{-}\psi)\cdot\mathbf{n}ds-\int_{\Omega}(\nabla\psi)\cdot(k_2^{+}c^{+}\nabla\hat{\mu}^{-})d\Omega \tag{4.47}$$

and also,

$$\int_{\Omega}(\nabla\cdot\mathbf{J}^{-})\psi\ d\Omega=\int_{\Omega}(k_1^{-}c^{-}\nabla\hat{\mu}^{-}\psi)\cdot\mathbf{n}ds-\int_{\Omega}(\nabla\psi)\cdot(k_1^{-}c^{-}\nabla\hat{\mu}^{-})d\Omega$$

$$+\int_{\Omega}(k_2^{-}c^{-}\nabla\hat{\mu}^{+}\psi)\cdot\mathbf{n}ds-\int_{\Omega}(\nabla\psi)\cdot(k_2^{-}c^{-}\nabla\hat{\mu}^{+})d\Omega \tag{4.48}$$

Thus, the electroneutrality condition becomes

$$\int_{\Omega}(k_1^{+}c^{+}\nabla\hat{\mu}^{+}\psi)\cdot\mathbf{n}ds-\int_{\Omega}(\nabla\psi)\cdot(k_1^{+}c^{+}\nabla\hat{\mu}^{+})d\Omega+\int_{\Omega}(k_2^{+}c^{+}\nabla\hat{\mu}^{-}\psi)\cdot\mathbf{n}ds-\int_{\Omega}(\nabla\psi)\cdot(k_2^{+}c^{+}\nabla\hat{\mu}^{-})d\Omega$$
$$-\int_{\Omega}(k_1^{-}c^{-}\nabla\hat{\mu}^{-}\psi)\cdot\mathbf{n}ds+\int_{\Omega}(\nabla\psi)\cdot(k_1^{-}c^{-}\nabla\hat{\mu}^{-})d\Omega-\int_{\Omega}(k_2^{-}c^{-}\nabla\hat{\mu}^{+}\psi)\cdot\mathbf{n}ds+\int_{\Omega}(\nabla\psi)\cdot(k_2^{-}c^{-}\nabla\hat{\mu}^{+})d\Omega=0 \tag{4.49}$$

Choosing weight function as $\psi=\mathbf{N}^{c}$

$$\int_{\Omega}(k_1^{+}c^{+}\nabla\hat{\mu}^{+}\mathbf{N}^{c})\cdot\mathbf{n}ds-\int_{\Omega}(\nabla\mathbf{N}^{c})\cdot(k_1^{+}c^{+}\nabla\hat{\mu}^{+})d\Omega+\int_{\Omega}(k_2^{+}c^{+}\nabla\hat{\mu}^{-}\mathbf{N}^{c})\cdot\mathbf{n}ds-\int_{\Omega}(\nabla\mathbf{N}^{c})\cdot(k_2^{+}c^{+}\nabla\hat{\mu}^{-})d\Omega$$
$$-\int_{\Omega}(k_1^{-}c^{-}\nabla\hat{\mu}^{-}\mathbf{N}^{c})\cdot\mathbf{n}ds+\int_{\Omega}(\nabla\mathbf{N}^{c})\cdot(k_1^{-}c^{-}\nabla\hat{\mu}^{-})d\Omega-\int_{\Omega}(k_2^{-}c^{-}\nabla\hat{\mu}^{+}\mathbf{N}^{c})\cdot\mathbf{n}ds+\int_{\Omega}(\nabla\mathbf{N}^{c})\cdot(k_2^{-}c^{-}\nabla\hat{\mu}^{+})d\Omega=0 \tag{4.50}$$

and collecting term, the above equation can be written as

$$\int_{\Omega}(k_1^{+}c^{+}\nabla\hat{\mu}^{+}\mathbf{N}^{c}+k_2^{+}c^{+}\nabla\hat{\mu}^{-}\mathbf{N}^{c}-k_1^{-}c^{-}\nabla\hat{\mu}^{-}\mathbf{N}^{c}-k_2^{-}c^{-}\nabla\hat{\mu}^{+}\mathbf{N}^{c})\cdot\mathbf{n}ds$$
$$+\int_{\Omega}(-k_1^{+}c^{+}+k_2^{-}c^{-})(\nabla\mathbf{N}^{c})\cdot(\nabla\mathbf{N}^{c})d\Omega\cdot\overline{\hat{\boldsymbol{\mu}}}^{+}+\int_{\Omega}(-k_2^{+}c^{+}+k_1^{-}c^{-})(\nabla\mathbf{N}^{c})\cdot(\nabla\mathbf{N}^{c})d\Omega\cdot\overline{\hat{\boldsymbol{\mu}}}^{-}=0 \tag{4.51}$$

or in matrix form

$$\mathbf{M}_1^{+}\overline{\hat{\boldsymbol{\mu}}}^{+}+\mathbf{M}_1^{-}\overline{\hat{\boldsymbol{\mu}}}^{-}=\mathbf{f}_1^{c} \tag{4.52}$$

Where

$$\mathbf{M}_1^+ = \int_\Omega (-k_1^+ c^+ + k_2^- c^-)(\nabla \mathbf{N}^c)\cdot(\nabla \mathbf{N}^c) d\Omega \tag{4.53}$$

$$\mathbf{M}_1^- = \int_\Omega (-k_2^+ c^+ + k_1^- c^-)(\nabla \mathbf{N}^c)\cdot(\nabla \mathbf{N}^c) d\Omega \tag{4.54}$$

$$\mathbf{f}_1^c = \int_\Omega (k_1^- c^- \nabla \hat{\mu}^- \mathbf{N}^c + k_2^- c^- \nabla \hat{\mu}^+ \mathbf{N}^c - k_1^+ c^+ \nabla \hat{\mu}^+ \mathbf{N}^c - k_2^+ c^+ \nabla \hat{\mu}^- \mathbf{N}^c)\cdot \mathbf{n} ds \tag{4.55}$$

Multiplying equation (4.40) by the testing function Ψ , gives

$$\int_\Omega (\frac{\partial c^k}{\partial t} + \nabla\cdot\mathbf{J}^+ + \nabla\cdot\mathbf{J}^- + \nabla\cdot(c^k \mathbf{v}^s))\Psi d\Omega = 0 \tag{4.56}$$

The third term of the above equation can be converted to:

$$\int_\Omega [\nabla\cdot c^k \mathbf{v}^s)]\Psi d\Omega = \int_\Omega \nabla\cdot(c^k \mathbf{v}^s \Psi) d\Omega - \int_\Omega (\nabla\Psi)\cdot(c^k \mathbf{v}^s) d\Omega \tag{4.57}$$

and using the divergence theorem, this term can be transformed as:

$$\int_\Omega [\nabla\cdot c^k \mathbf{v}^s)]\Psi d\Omega = \int_s (c^k \mathbf{v}^s \Psi)\cdot \mathbf{n} ds - \int_\Omega (\nabla\Psi)\cdot(c^k \mathbf{v}^s) d\Omega \tag{4.58}$$

Substituting equations (4.58), (4.48) into (4.56) , and choosing weight function $\Psi = \mathbf{N}^c$,

$$\begin{aligned}
&\int_\Omega \frac{\partial c^k}{\partial t}\mathbf{N}^c d\Omega + \int_s (c^k \mathbf{v}^s \mathbf{N}^c)\cdot \mathbf{n} ds - \int_\Omega (\nabla \mathbf{N}^c)\cdot(c^k \mathbf{v}^s) d\Omega \\
&+ \int_\Omega (k_1^+ c^+ \nabla \hat{\mu}^+ \mathbf{N}^c + k_2^+ c^+ \nabla \hat{\mu}^- \mathbf{N}^c + k_1^- c^- \nabla \hat{\mu}^- \mathbf{N}^c + k_2^- c^- \nabla \hat{\mu}^+ \mathbf{N}^c)\cdot \mathbf{n} ds \\
&- \int_\Omega (k_1^+ c^+ + k_2^- c^-)(\nabla \mathbf{N}^c)\cdot(\nabla \mathbf{N}^c) d\Omega \cdot \bar{\hat{\boldsymbol{\mu}}}^+ - \int_\Omega (k_2^+ c^+ + k_1^- c^-)(\nabla \mathbf{N}^c)\cdot(\nabla \mathbf{N}^c) d\Omega \cdot \bar{\hat{\boldsymbol{\mu}}}^- = 0
\end{aligned} \tag{4.59}$$

or

$$\mathbf{B}_c \dot{\bar{\mathbf{c}}}^k = \bar{\mathbf{f}}_2^c \tag{4.60}$$

where

$$\mathbf{B}_c = \int_{\Omega} [(\mathbf{N}^c)^T \mathbf{N}^c] d\Omega \tag{4.61}$$

$$\begin{aligned}
\bar{\mathbf{f}}_2^c &= -\int_s (c^k \mathbf{v}^s \mathbf{N}^c) \cdot \mathbf{n} ds + \int_{\Omega} (\nabla \mathbf{N}^c) \cdot (c^k \mathbf{v}^s) d\Omega \\
&- \int_{\Omega} (k_1^+ c^+ \nabla \hat{\mu}^+ \mathbf{N}^c + k_2^+ c^+ \nabla \hat{\mu}^- \mathbf{N}^c + k_1^- c^- \nabla \hat{\mu}^- \mathbf{N}^c + k_2^- c^- \nabla \hat{\mu}^+ \mathbf{N}^c) \cdot \mathbf{n} ds \\
&+ \int_{\Omega} (k_1^+ c^+ + k_2^- c^-)(\nabla \mathbf{N}^c) \cdot (\nabla \mathbf{N}^c) d\Omega \cdot \bar{\hat{\boldsymbol{\mu}}}^+ + \int_{\Omega} (k_2^+ c^+ + k_1^- c^-)(\nabla \mathbf{N}^c) \cdot (\nabla \mathbf{N}^c) d\Omega \cdot \bar{\hat{\boldsymbol{\mu}}}^-
\end{aligned} \tag{4.62}$$

4.3 TIME INTEGRATION

There are two kinds of time integration schemes utilized for the finite element method. One is explicit time integration such as the central difference method, and the other is an implicit time integration such as trapezoidal rule. For the explicit time, it has low computation cost because it dose not need to perform inversion, but it is conditionally stable, which requires a small time increment. On the other hand, the implicit time integration has opposite features.

In this study, the Newmark-β method is applied for equation (4.26) and the backward-Euler method for equations (4.52) and (4.60).

4.3.1 Newmark-β method

The discrete equation of motion is formulated by the following equation.

$$\mathbf{M}\ddot{\mathbf{X}}^n + \mathbf{C}\dot{\mathbf{X}}^n + \mathbf{K}\mathbf{X}^n = \bar{\mathbf{F}}^n \tag{4.63}$$

and in n+1 step,

$$\mathbf{M}\ddot{\mathbf{X}}^{n+1} + \mathbf{C}\dot{\mathbf{X}}^{n+1} + \mathbf{K}\mathbf{X}^{n+1} = \overline{\mathbf{F}}^{n+1} \tag{4.64}$$

When Newmark-β is used, $\dot{\mathbf{X}}^n$ and $\ddot{\mathbf{X}}^n$ are approximated as follows:

$$\dot{\mathbf{X}}^{n+1} = \dot{\mathbf{X}}^n + \frac{\Delta t}{2}(\ddot{\mathbf{X}}^n + \ddot{\mathbf{X}}^{n+1}) \tag{4.65}$$

$$\mathbf{X}^{n+1} = \mathbf{X}^n + \Delta t\dot{\mathbf{X}}^n + \frac{\Delta t^2}{2}\{(1-2\beta)\ddot{\mathbf{X}}^n + 2\beta\ddot{\mathbf{X}}^{n+1}\} \tag{4.66}$$

Equations (4.65) and (4.66) are finite difference formulas. The parameter β determines the characteristics of stability and accuracy of this algorithm.

The Newmark – β method has an advantage of unconditionally stability under the condition of $\beta \geq 1/4$.

4.3.2 Formulation

The Newmark – β method is applied to solve equation (4.26). In case of $\gamma = 1/2, \beta = 1/4$, it's unconditionally stable. With these paremeters, equations (4.64), (4.65) and (4.66) become

$$\mathbf{M}\ddot{\mathbf{X}}^{n+1} + \mathbf{C}\dot{\mathbf{X}}^{n+1} = \overline{\mathbf{F}}^{n+1} \tag{4.67}$$

$$\dot{\mathbf{X}}^{n+1} = \dot{\mathbf{X}}^n + \frac{\ddot{\mathbf{X}}^n + \ddot{\mathbf{X}}^{n+1}}{2}\Delta t \tag{4.68}$$

$$\mathbf{X}^{n+1} = \mathbf{X}^n + \dot{\mathbf{X}}^n\Delta t + \left[\frac{\ddot{\mathbf{X}}^n + \ddot{\mathbf{X}}^{n+1}}{4}\right]\Delta t^2 \tag{4.69}$$

Using the above equations to eliminate $\dot{\mathbf{X}}^{n+1}$ and $\ddot{\mathbf{X}}^{n+1}$ gives

$$\left[\frac{4}{\Delta t^2}\mathbf{M} + \frac{2}{\Delta t}\mathbf{C}\right]\mathbf{X}^{n+1} = \overline{\mathbf{F}}^{n+1} + \hat{\mathbf{M}}\left[\frac{4}{\Delta t^2}\mathbf{X}^n + \frac{4}{\Delta t}\dot{\mathbf{X}}^n + \ddot{\mathbf{X}}^n\right] + \mathbf{C}\left[\frac{2}{\Delta t}\mathbf{X}^n + \dot{\mathbf{X}}^n\right] \tag{4.70}$$

Then, the terms $\dot{\mathbf{X}}^{n+1}$ and $\ddot{\mathbf{X}}^{n+1}$ are updated using the formulas,

$$\ddot{\mathbf{X}}^{n+1} = \frac{4}{\Delta t^2}(\mathbf{X}^{n+1} - \mathbf{X}^n - \Delta t\dot{\mathbf{X}}^n) - \ddot{\mathbf{X}}^n \tag{4.71}$$

$$\dot{\mathbf{X}}^{n+1} = \frac{2}{\Delta t}(\mathbf{X}^{n+1} - \mathbf{X}^n) - \dot{\mathbf{X}}^n \tag{4.72}$$

where $\mathbf{X}^n$, $\dot{\mathbf{X}}^n$ and $\ddot{\mathbf{X}}^n$ are known from the previous step of the calculations. Thus, if $\mathbf{X}^{n+1}$ is determined from equation (4.70), $\dot{\mathbf{X}}^{n+1}$ and $\ddot{\mathbf{X}}^{n+1}$ can be obtained from equations (4.71) and (4.72). So, the key point of this problem is to solve the nonlinear equation (4.70).

Equation (4.70) can be written as

$$\mathbf{G}(\mathbf{X}) = RHS - LHS = 0 \tag{4.73}$$

In order to solve the above nonlinear equation, Newton's method [74] is applied to make the residual, $\mathbf{G}(\mathbf{X})$ very small (Fig.4.1) with successive corrections until it is less than some tolerance. Thus, it is necessary to linearize equation (4.73) for matrix K [54].

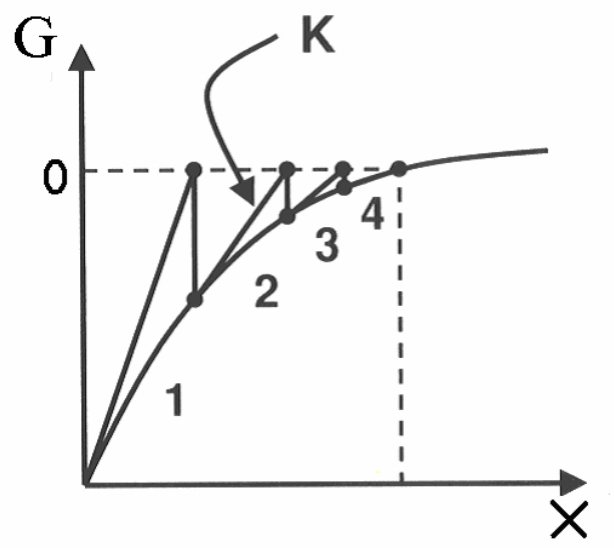

Fig.4.1 Schematic of Newton's method

This is done by writing equation (4.73) as

$$\mathbf{G}_{n+1}(\mathbf{X}^n + \Delta\mathbf{X}) = \mathbf{G}_n + \Delta\mathbf{G} = \mathbf{G}_n + \frac{\partial \mathbf{G}}{\partial \mathbf{X}}\Delta\mathbf{X} = \mathbf{G}_n + \mathbf{K}(\Delta\mathbf{X}) = 0 \tag{4.74}$$

The above equation indicates how **K** matrix to be constructed. It can be expressed as a collection of columns in the form.

$$\left[\frac{\partial \mathbf{G}}{\partial \mathbf{X}}\right] = \left[\left\{\frac{\partial \mathbf{G}}{\partial X_1}\right\}\left\{\frac{\partial \mathbf{G}}{\partial X_2}\right\}\cdots\left\{\frac{\partial \mathbf{G}}{\partial X_j}\right\}\cdots\left\{\frac{\partial \mathbf{G}}{\partial X_N}\right\}\right] \tag{4.75}$$

Each column can be determined as follows:

$$\left\{\frac{\partial \mathbf{G}}{\partial X_j}\right\} = \frac{\mathbf{G}(X_1, X_2 \cdots X_j + \delta X_j, \cdots, X_N) - \mathbf{G}(X_1, X_2 \cdots X_j, \cdots, X_N)}{\delta X_j} \tag{4.76}$$

where δX_j dependents on the specific problem. In this work, a good value for δX_j was found to be $X_j / 10000$. Every degree of the freedom has its corresponding column obtained by equation (4.76).

Once the global stiffness matrix is determined, the increments $\Delta\mathbf{X}$ can be obtained by equation (4.75), and then the vector $\mathbf{X}$ is updated by $\mathbf{X}^{n+1} = \mathbf{X}^n + \Delta\mathbf{X}$. Thus equation (4.75) is updated and the process is repeated until $\|\mathbf{G}\|$ is less than tolerance. Now the current step quantities $\mathbf{X}$ at every node are known and satisfy the governing equations. Subsequent time steps can be done until the final time is reached.

A simplified flow chart of X and G iterative process and time integration can be seen in Fig. 4.2.

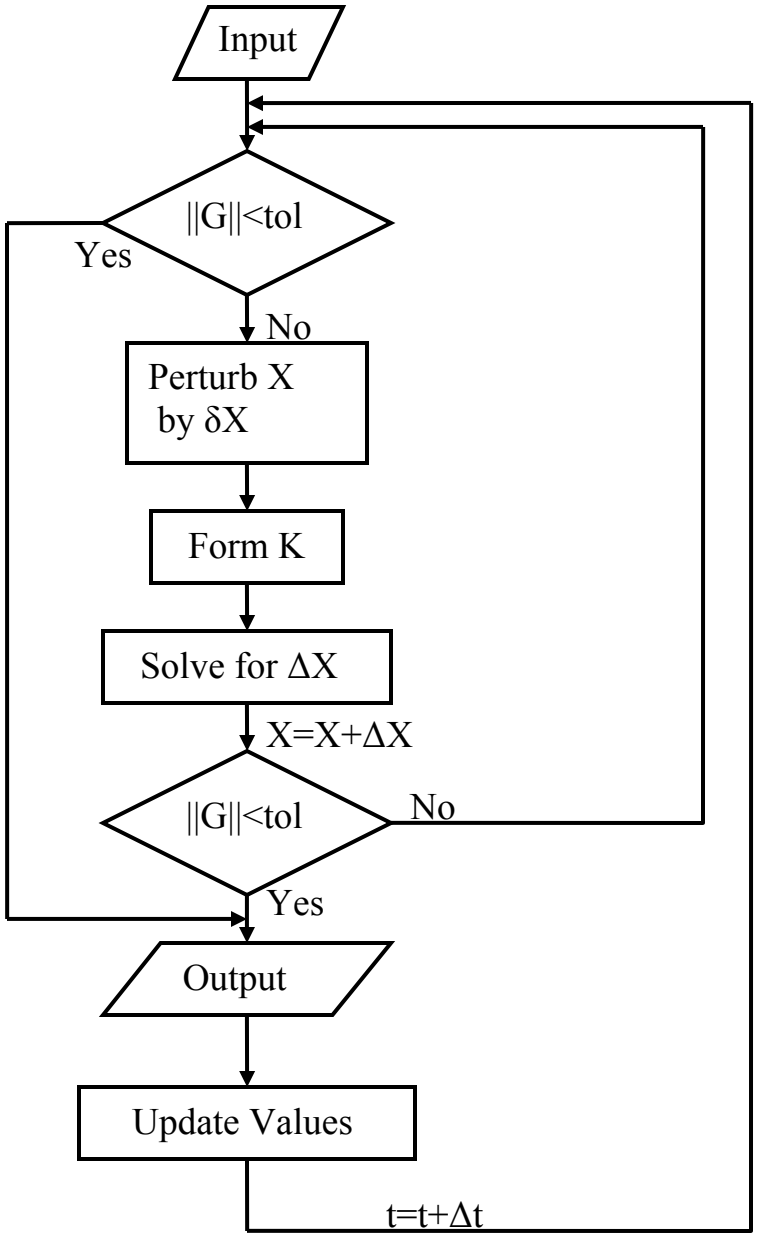

Fig.4.2 Flow chart of solution of the system of equations

4.3.3. The backward - Euler method for the electrochemical model

The backward-Euler method as an implicit method utilized to solve equation (4.60) [74]. This method approximates the derivative as follows:

$$\dot{x}(t_{n+1}) = \frac{1}{\Delta t}(x(t_{n+1} - t_n)) \tag{4.77}$$

The backward-Euler method offers a better numerical stability than the explicit Euler method, which means that generally the time step size Δt can be chosen larger with the explicit method and still yield results of the same accuracy as the explicit method.

So equations (4.52) and (4.60) become

$$(\mathbf{M}_1^+)^{n+1}(\bar{\hat{\boldsymbol{\mu}}}^+)^{n+1} + (\mathbf{M}_1^-)^{n+1}(\bar{\hat{\boldsymbol{\mu}}}^-)^{n+1} = (\mathbf{f}_1^c)^{n+1} \tag{4.78a}$$

$$\frac{\mathbf{B}_c}{\Delta t}((\bar{\mathbf{c}}^k)^{n+1} - (\bar{\mathbf{c}}^k)^n) = (\bar{\mathbf{f}}_2^c)^{n+1} \tag{4.78b}$$

In the above equations, $\bar{\mathbf{c}}^+$ and $\bar{\mathbf{c}}^-$ are the unknowns. And $\bar{\mathbf{c}}^k$, $\bar{\hat{\boldsymbol{\mu}}}^+$, $\bar{\hat{\boldsymbol{\mu}}}^-$, $\mathbf{M}_1^+$ and $\mathbf{M}_1^-$ are the functions of $\bar{\mathbf{c}}^+$ and $\bar{\mathbf{c}}^-$, so these equations are nonlinear, and can be solved by Newton's method described in the section 4.3.2.

4.4 SELECTION OF THE ELEMENT

In order to solve equations (4.70) and (4.78), the Galerkin finite element method is employed. With this approach the domain is discretized into elements and the unknown variable is

approximated in each element. In this approach, the unknowns, for example, the unknown field of displacement, u, should be represented in the following way:

$$u = \sum_{i=1}^{N} u_i N_i \tag{4.79}$$

where N_i, known as shape or basis functions. u_i is the nodal value of the unknown function to be determined and N is the number of nodes each element contains.

The discrete surface of the current configuration can be mapped into discrete elements in order to determine the unknown coefficients, and the key point is how to select suitable N_i for our problem.

This mathematical porous model involves the solid, the fluid and pressure, which means it's a mixed problem. For this kind of problem, the selection of the interpolations for displacement and pressure is very important [64], and it is frequently noted that inappropriate interpolations yield very poor approximations.

For the soft tissue, the solid and fluid phases are always considered as nearly incompressible, which may cause mesh locking. In mathematics, the discrete Babuska-Brezzi (BBL) condition was proved to be a critical requirement for the mixed finite element method to be stable and convergent. This theory was given in detail in Oden and Carey [63].

However, in practice, a quick and simple tool is given to describe the discrete system behaviors in the different interpolations. The constraint ratio, r, is defined by

$$r = \frac{n_{eq}}{n_c} \tag{4-80}$$

Where for two dimensional problems,

r>2 too few incompressibility constraints

r=2 optimal

r<2 too many incompressibility constraints

r≤1 locking

Some typical elements are listed as follows.

(1) The biquadratic displacement – biquadratic pressure quadrilateral (Ub2/Pb2)(Fig.4.3)

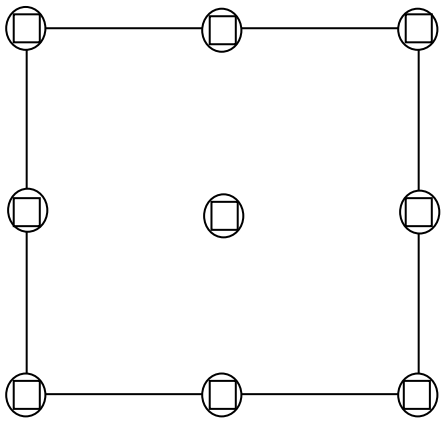

Fig.4.3 Ub2/Pb2 element (□ - Pressure, ◯ - Displacement)

r=2, which is optimal, but this element violates the BBL condition, which means it may exhibit spurious pressure modes.

(2) The biquadratic displacement – bilinear pressure quadrilateral (Ub2/Pb1) (Fig.4.4)

r=8, which is very high (i.e., there are too few incompressibility constraints). Although it satisfies the BBL condition, sometimes, it yields very poor approximations. However, it is widely used.

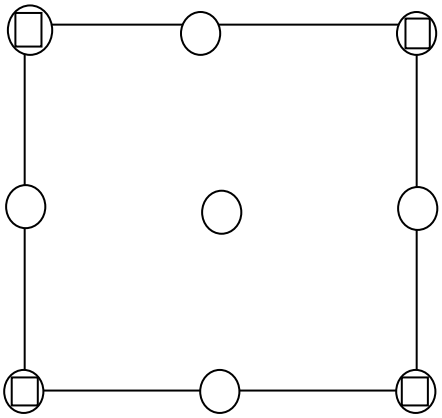

Fig.4.4 Ub2/Pb1 element (□ - Pressure, ◯ - Displacement)

(3) The biquadratic displacement – linear pressure quadrilateral (Ub2/P1) (Fig. 4.5)

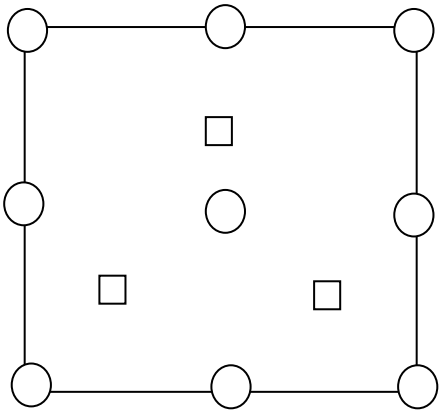

Fig.4.5 Ub2/P1 element (□ - Pressure, ◯ - Displacement)

R=2.67, which is relatively optimal. This element satisfies the BBL conditions. But pressure in the element is discontinuous, which has inconvenience in defining boundary conditions of pressure.

In our study, we employ mainly Ub2/Pb2 elements in 2-D and 3- D problems, although they don't satisfy the BBL conditions, they usually display good converge and yield satisfactory results. More important, no stability difficulties have been encountered in our problems. In addition, we also developed the Ub2/Pb1 and Ub2/P1 elements (referred to Appendix A), which can substitute for Ub2/Pb2 element if stability difficulties occur with the Ub2/Pb2 element.

4.5 Ub2/Pb2 FINITE ELEMENT DESCRIPTION

4.5.1 Element for Ub2/Pb2

In this section, the 3-dimensional (3-D) Ub2/Pb2 finite element will be described because the 2-dimensional (2-D) finite element is similar to the 3-D finite element, and the 3-D finite element can be reduced to be 2-D finite element.

The 3-D element is a 27 node isoparametric element with local coordinates ξ, η, and ζ ranging from –1 to 1 (Figure 4.6). The corresponding shape functions are listed in Table 4.1. The five unknowns u, w, p, c^+, c^-, are discretized as follows:

$$\begin{aligned} u_j &= N_{Kj}^{u}\overline{u}_{Kj} \\ w_j &= N_{Kj}^{w}\overline{w}_{Kj} \\ p &= N_K^{p}\overline{p}_K \\ c^+ &= N_K^{c}\overline{c}_K^{+} \\ c^- &= N_K^{c}\overline{c}_K^{-} \end{aligned} \tag{4.81}$$

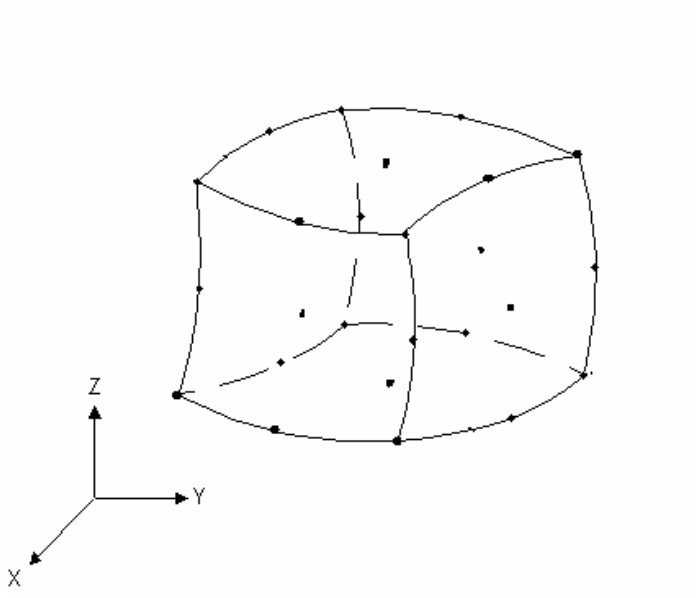

(a) The global element

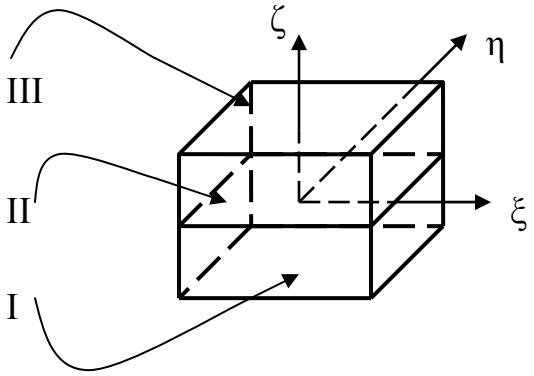

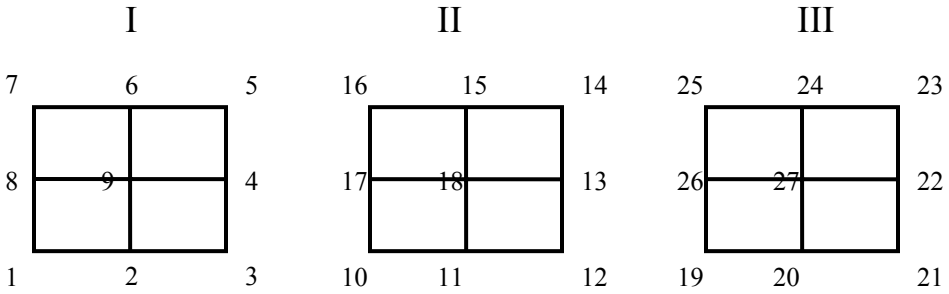

(b) The local element

Fig. 4.6 Mapping of the global element into the local element

Table 4.1 Shape functions of 27-node isoparametric element

Node	Shape function	Node	Shape function	Node	Shape function
1	$\frac{1}{8}\xi(\xi-1)\eta(\eta-1)\zeta(\zeta-1)$	10	$\frac{1}{4}\xi(\xi-1)\eta(\eta-1)(1-\zeta^2)$	19	$\frac{1}{8}\xi(\xi-1)\eta(\eta-1)\zeta(\zeta+1)$
2	$\frac{1}{4}(1-\xi^2)\eta(\eta-1)\zeta(\zeta-1)$	11	$\frac{1}{2}(1-\xi^2)\eta(\eta-1)(1-\zeta^2)$	20	$\frac{1}{4}(1-\xi^2)\eta(\eta-1)\zeta(\zeta+1)$
3	$\frac{1}{8}\xi(\xi+1)\eta(\eta-1)\zeta(\zeta-1)$	12	$\frac{1}{4}\xi(\xi+1)\eta(\eta-1)(1-\zeta^2)$	21	$\frac{1}{8}\xi(\xi+1)\eta(\eta-1)\zeta(\zeta+1)$
4	$\frac{1}{4}\xi(\xi+1)(1-\eta^2)\zeta(\zeta-1)$	13	$\frac{1}{2}\xi(\xi+1)(1-\eta^2)(1-\zeta^2)$	22	$\frac{1}{4}\xi(\xi+1)(1-\eta^2)\zeta(\zeta+1)$
5	$\frac{1}{8}\xi(\xi+1)\eta(\eta+1)\zeta(\zeta-1)$	14	$\frac{1}{4}\xi(\xi+1)\eta(\eta+1)(1-\zeta^2)$	23	$\frac{1}{8}\xi(\xi+1)\eta(\eta+1)\zeta(\zeta+1)$
6	$\frac{1}{4}(1-\xi^2)\eta(\eta+1)\zeta(\zeta-1)$	15	$\frac{1}{2}(1-\xi^2)\eta(\eta+1)(1-\zeta^2)$	24	$\frac{1}{4}(1-\xi^2)\eta(\eta+1)\zeta(\zeta+1)$
7	$\frac{1}{8}\xi(\xi-1)\eta(\eta+1)\zeta(\zeta-1)$	16	$\frac{1}{4}\xi(\xi-1)\eta(\eta+1)(1-\zeta^2)$	25	$\frac{1}{8}\xi(\xi-1)\eta(\eta+1)\zeta(\zeta+1)$
8	$\frac{1}{4}\xi(\xi-1)(1-\eta^2)\zeta(\zeta-1)$	17	$\frac{1}{2}\xi(\xi-1)(1-\eta^2)(1-\zeta^2)$	26	$\frac{1}{4}\xi(\xi-1)(1-\eta^2)\zeta(\zeta+1)$
9	$\frac{1}{2}(1-\xi^2)(1-\eta^2)\zeta(\zeta-1)$	18	$(1-\xi^2)(1-\eta^2)(1-\zeta^2)$	27	$\frac{1}{2}(1-\xi^2)(1-\eta^2)\zeta(\zeta+1)$

4.5.2 The gradient of the displacement

In equations (4.70) and (4.78), the gradients of **u**, **w**, p, $\mathbf{c}^+$ and $\mathbf{c}^-$ have to be calculated. As an example, the gradient of the displacement field **u** is evaluated as follows:

$$\nabla \mathbf{u} = \begin{Bmatrix} \sum_i^N u_{xi} \frac{\partial N_i}{\partial x} & \sum_i^N u_{xi} \frac{\partial N_i}{\partial y} & \sum_i^N u_{xi} \frac{\partial N_i}{\partial z} \\ \sum_i^N u_{yi} \frac{\partial N_i}{\partial x} & \sum_i^N u_{yi} \frac{\partial N_i}{\partial y} & \sum_i^N u_{yi} \frac{\partial N_i}{\partial z} \\ \sum_i^N u_{zi} \frac{\partial N_i}{\partial x} & \sum_i^N u_{zi} \frac{\partial N_i}{\partial y} & \sum_i^N u_{zi} \frac{\partial N_i}{\partial z} \end{Bmatrix} \tag{4.82}$$

In the above equation, the partial derivatives with respect to the current coordinates, x, y and z, of the shape functions are needed and defined by

$$\begin{aligned} \frac{\partial N_i}{\partial x} &= \frac{\partial N_i}{\partial \xi}\frac{\partial \xi}{\partial x} + \frac{\partial N_i}{\partial \eta}\frac{\partial \eta}{\partial x} + \frac{\partial N_i}{\partial \zeta}\frac{\partial \zeta}{\partial x} \\ \frac{\partial N_i}{\partial y} &= \frac{\partial N_i}{\partial \xi}\frac{\partial \xi}{\partial y} + \frac{\partial N_i}{\partial \eta}\frac{\partial \eta}{\partial y} + \frac{\partial N_i}{\partial \zeta}\frac{\partial \zeta}{\partial y} \\ \frac{\partial N_i}{\partial z} &= \frac{\partial N_i}{\partial \xi}\frac{\partial \xi}{\partial z} + \frac{\partial N_i}{\partial \eta}\frac{\partial \eta}{\partial z} + \frac{\partial N_i}{\partial \zeta}\frac{\partial \zeta}{\partial z} \end{aligned} \tag{4.83}$$

The derivative of the shape functions with respect to ξ, η and ζ can be easily evaluated because the shape functions are explicit functions of the coordinates ξ, η and ζ. The approach to calculate the partial derivatives of ξ, η and ζ with respect to the current coordinates x, y and z is done using the identity:

$$\begin{bmatrix} \frac{\partial x}{\partial x} & \frac{\partial x}{\partial y} & \frac{\partial x}{\partial z} \\ \frac{\partial y}{\partial x} & \frac{\partial y}{\partial y} & \frac{\partial y}{\partial z} \\ \frac{\partial z}{\partial x} & \frac{\partial z}{\partial y} & \frac{\partial z}{\partial z} \end{bmatrix} = \begin{bmatrix} \frac{\partial x}{\partial \xi} & \frac{\partial x}{\partial \eta} & \frac{\partial x}{\partial \zeta} \\ \frac{\partial y}{\partial \xi} & \frac{\partial y}{\partial \eta} & \frac{\partial y}{\partial \zeta} \\ \frac{\partial z}{\partial \xi} & \frac{\partial z}{\partial \eta} & \frac{\partial z}{\partial \zeta} \end{bmatrix} \begin{bmatrix} \frac{\partial \xi}{\partial x} & \frac{\partial \xi}{\partial y} & \frac{\partial \xi}{\partial z} \\ \frac{\partial \eta}{\partial x} & \frac{\partial \eta}{\partial y} & \frac{\partial \eta}{\partial z} \\ \frac{\partial \zeta}{\partial x} & \frac{\partial \zeta}{\partial y} & \frac{\partial \zeta}{\partial z} \end{bmatrix} = \begin{bmatrix} 1 & 0 & 0 \\ 0 & 1 & 0 \\ 0 & 0 & 1 \end{bmatrix} \tag{4.84}$$

which gives

$$\begin{bmatrix} \frac{\partial \xi}{\partial x} & \frac{\partial \xi}{\partial y} & \frac{\partial \xi}{\partial z} \\ \frac{\partial \eta}{\partial x} & \frac{\partial \eta}{\partial y} & \frac{\partial \eta}{\partial z} \\ \frac{\partial \zeta}{\partial x} & \frac{\partial \zeta}{\partial y} & \frac{\partial \zeta}{\partial z} \end{bmatrix} = \begin{bmatrix} \frac{\partial x}{\partial \xi} & \frac{\partial x}{\partial \eta} & \frac{\partial x}{\partial \zeta} \\ \frac{\partial y}{\partial \xi} & \frac{\partial y}{\partial \eta} & \frac{\partial y}{\partial \zeta} \\ \frac{\partial z}{\partial \xi} & \frac{\partial z}{\partial \eta} & \frac{\partial z}{\partial \zeta} \end{bmatrix}^{-1} \tag{4.85}$$

Specifically the terms on the right hand side of equation (4.85) can be evaluated as follows

$$\begin{aligned} &\frac{\partial x}{\partial \xi} = \sum_{i=1}^{N} x_i \frac{\partial N_i}{\partial \xi} \qquad \frac{\partial x}{\partial \eta} = \sum_{i=1}^{N} x_i \frac{\partial N_i}{\partial \eta} \qquad \frac{\partial x}{\partial \zeta} = \sum_{i=1}^{N} x_i \frac{\partial N_i}{\partial \zeta} \\ &\frac{\partial y}{\partial \xi} = \sum_{i=1}^{N} y_i \frac{\partial N_i}{\partial \xi} \qquad \frac{\partial y}{\partial \eta} = \sum_{i=1}^{N} y_i \frac{\partial N_i}{\partial \eta} \qquad \frac{\partial y}{\partial \zeta} = \sum_{i=1}^{N} y_i \frac{\partial N_i}{\partial \zeta} \\ &\frac{\partial z}{\partial \xi} = \sum_{i=1}^{N} z_i \frac{\partial N_i}{\partial \xi} \qquad \frac{\partial z}{\partial \eta} = \sum_{i=1}^{N} z_i \frac{\partial N_i}{\partial \eta} \qquad \frac{\partial z}{\partial \zeta} = \sum_{i=1}^{N} z_i \frac{\partial N_i}{\partial \zeta} \end{aligned} \tag{4.86}$$

The following well known formula [54] is also needed,

$$dxdydz = J_e d\xi d\eta d\zeta \tag{4.87}$$

In the finite element calculations, each of the elements is mapped onto the same base element of Fig.4.6. Because of the complexity of the calculations, numerical integration is needed and the formula for Gauss integration is given by,

$$\int_{-1}^{1}\int_{-1}^{1}\int_{-1}^{1} \Phi(\xi,\eta,\zeta) d\xi d\eta d\zeta \cong \sum_{j}^{n_j}\sum_{i}^{n_i}\sum_{k}^{n_k} \Phi(\xi_i,\eta_{j,}\zeta_k) w_i w_j w_k \tag{4.88}$$

where $\Phi(\xi,\eta,\zeta)$ is arbitrary function evaluated at the Gauss point (ξ_i,η_j,ζ_k) with the associated weighting values of w_i, w_j and w_k. In this study, 3 gauss points were used in each direction of integration, so $n_i = n_j = n_k = 3$.

4.6 COMPUTATION OF THE INTERNAL FORCE

In case of the large deformation and viscoelasticity, the computation of the internal force is complicated. In order to solve it numerically, the kinematical equations and viscoelastic constitutive equations should be linearized. Here we adopt the method of Jason Aaron given in [54].

4.6.1 Linearization of kinematical equations

With an increment in time, all the gradients have an increment. In the following equations, a superposed hat is used to signify the incremented or current value. Thus,

$$\hat{\mathbf{F}} = \mathbf{F} + \Delta\mathbf{F} = (\mathbf{F}^e + \Delta\mathbf{F}^e)(\mathbf{F}^v + \Delta\mathbf{F}^v) = \widehat{\mathbf{F}}^e\widehat{\mathbf{F}}^v \tag{4.89}$$

where

$$\mathbf{F} + \Delta\mathbf{F} = \mathbf{F} + \nabla(\Delta\mathbf{u}) = \mathbf{I} + \nabla(\mathbf{u} + \Delta\mathbf{u}) \tag{4.90}$$

With the Cauchy-Green strain tensor formulation, the current strain associated with $\widehat{\mathbf{F}}$ can then be obtained by

$$\hat{\mathbf{E}} = \frac{1}{2}(\hat{\mathbf{F}}^T\hat{\mathbf{F}} - \mathbf{I}) = \frac{1}{2}\widehat{\mathbf{F}}^{v^T}(\widehat{\mathbf{F}}^{e^T}\widehat{\mathbf{F}}^e - \mathbf{I})\widehat{\mathbf{F}}^v + \frac{1}{2}(\widehat{\mathbf{F}}^{v^T}\widehat{\mathbf{F}}^v - \mathbf{I}) \tag{4.91}$$

This can be rewritten as:

$$\hat{\mathbf{E}} = \widehat{\mathbf{F}}^{v^T}\widehat{\mathbf{E}}^e\widehat{\mathbf{F}}^v + \widehat{\mathbf{E}}^v \tag{4.92}$$

where

$$\widehat{\mathbf{E}}^e = \frac{1}{2}(\widehat{\mathbf{F}}^{e^T}\widehat{\mathbf{F}}^e - \mathbf{I}) \tag{4.93}$$

$$\widehat{\mathbf{E}}^{v} = \frac{1}{2}(\widehat{\mathbf{F}}^{v^T}\widehat{\mathbf{F}}^{v} - \mathbf{I}) \tag{4.94}$$

In order to simplify the solution process, $\Delta\mathbf{L}^{v}$, the viscoelastic increment, is introduced here as,

$$\Delta\mathbf{L}^{v} = \Delta\mathbf{F}^{v}\mathbf{F}^{v^{-1}} \tag{4.95}$$

It was mentioned in chapter 3 that rotation is assumed absent in the permanent parts of the deformation gradient $\mathbf{F}^{v}$, so the viscoelastic increment has no component of rotation. As a result, $\Delta\mathbf{L}^{v}$ becomes a symmetric tensor:

$$\Delta\mathbf{L}^{v} = \Delta\mathbf{L}^{v^T} \tag{4.96}$$

The current viscoelastic deformation gradient can be expressed as:

$$\widehat{\mathbf{F}}^{v} = \mathbf{F}^{v} + \Delta\mathbf{F}^{v} = (\mathbf{I} + \Delta\mathbf{L}^{v})\mathbf{F}^{v} \tag{4.97}$$

Thus, the current viscoelastic strain is:

$$\widehat{\mathbf{E}}^{v} = \frac{1}{2}(\mathbf{F}^{v^T}\mathbf{F}^{v} - \mathbf{I}) + \frac{1}{2}\mathbf{F}^{v^T}(\Delta\mathbf{L}^{v^T} + \Delta\mathbf{L}^{v} + \Delta\mathbf{L}^{v^T}\Delta\mathbf{L}^{v})F^{v} = \mathbf{E}^{v} + \Delta\mathbf{E}^{v} \tag{4.98}$$

Therefore, the increment of the viscoelastic strain is given by

$$\Delta\mathbf{E}^{v} = \frac{1}{2}\mathbf{F}^{v^T}(\Delta\mathbf{L}^{v^T} + \Delta\mathbf{L}^{v} + \Delta\mathbf{L}^{v^T}\Delta\mathbf{L}^{v})\mathbf{F}^{v} \tag{4.99}$$

Finally, substituting equation (4.99) into equation (4.92), the current elastic strain can be given by

$$\widehat{\mathbf{E}}^{e} = [(\mathbf{I} + \Delta\mathbf{L}^{v})\mathbf{F}^{v}]^{-T}(\hat{\mathbf{E}} - \mathbf{E}^{v} - \frac{1}{2}\mathbf{F}^{v^T}(\Delta\mathbf{L}^{v^T} + \Delta\mathbf{L}^{v} + \Delta\mathbf{L}^{v^T}\Delta\mathbf{L}^{v})\mathbf{F}^{v})[(\mathbf{I} + \Delta\mathbf{L}^{v})\mathbf{F}^{v}]^{-1} \tag{4.100}$$

Because the displacement of solid remains unchanged over the increment, $\hat{\mathbf{E}}$ in the above equation is known. And $\mathbf{F}^{v}$ and $\mathbf{E}^{v}$ are the values of the previous time step. Therefore the above

equation is a nonlinear function of the viscoelastic increment, $\Delta\mathbf{L}^v$ to express the current value of the elastic strain.

With the expression of the current value of the elastic strain, the current elastic stress can be expressed as:

$$\widehat{\mathbf{S}}^e = \mathbf{D} : \widehat{\mathbf{E}}^e = \mathbf{D} : [\widehat{\mathbf{F}}^{v^{-T}} (\hat{\mathbf{E}} - \mathbf{E}^v - \Delta\mathbf{E}^v)\widehat{\mathbf{F}}^{v^{-1}}] \tag{4.101}$$

The elastic stress measure, $\mathbf{S}^e$ can be converted to the viscoelastic stress measure, $\mathbf{S}^v$, by

$$\widehat{\mathbf{S}}^v = \widehat{\mathbf{F}}^{v^{-1}} \widehat{\mathbf{S}}^e \widehat{\mathbf{F}}^{v^{-T}} = \widehat{\mathbf{F}}^{v^{-1}} \{\mathbf{D} : [\widehat{\mathbf{F}}^{v^{-T}} (\hat{\mathbf{E}} - \mathbf{E}^v - \Delta\mathbf{E}^v)\widehat{\mathbf{F}}^{v^{-1}}]\}\widehat{\mathbf{F}}^{v^{-T}} \tag{4.102}$$

Subtracting the stress of the previous time step from the stress at the current time, yields the increment of the viscoelastic stress,

$$\Delta\mathbf{S}^v = \widehat{\mathbf{S}}^v - \mathbf{S}^v = \widehat{\mathbf{F}}^{v^{-1}} \{\mathbf{D} : [\widehat{\mathbf{F}}^{v^{-T}} (\hat{\mathbf{E}} - \mathbf{E}^v - \Delta\mathbf{E}^v)\widehat{\mathbf{F}}^{v^{-1}}]\}\widehat{\mathbf{F}}^{v^{-T}} - \mathbf{S}^v \tag{4.103}$$

4.6.2. Linearization of viscoelastic constitutive equations [54]

As mentioned in Chapter 3, the integral form of the viscoelastic constitutive relation is used in this work as:

$$\mathbf{E}^v(t) = \int_0^t \frac{\partial \mathbf{J}_v(t-\tau)}{\partial(t-\tau)} \mathbf{S}^v(\tau) d\tau \tag{4.104}$$

A widely used form of the creep compliance $\mathbf{J}^v$ is chosen here,

$$\mathbf{J}_v(t-\tau) = \mathbf{D}_v^{-1} \sum_{i=1}^{m} A_i [1 - e^{-\frac{t-\tau}{\tau_i}}] \tag{4.105}$$

The viscoelastic matrix $\mathbf{D}_v$ is material property, which is determined by the experimental study. With the differentiation of the above equation, yields

$$\frac{\partial \mathbf{J}_v(t-\tau)}{\partial(t-\tau)} = \mathbf{D}_v^{-1}\sum_{i=1}^{m}\frac{A_i}{\tau_i}[e^{-\frac{t-\tau}{\tau_i}}] \tag{4.106}$$

so, equation (4.104) becomes

$$\mathbf{E}^v(t) = \mathbf{D}_v^{-1}\sum_{i=1}^{m}\frac{A_i}{\tau_i}\int_0^t[e^{-\frac{(t-\tau)}{\tau_i}}] : \mathbf{S}^v(\tau)d\tau \tag{4.107}$$

The increment of the viscoelastic strain in an increment of time can be expressed by

$$\Delta\mathbf{E}^v = \mathbf{E}^v(t+\Delta t) - \mathbf{E}^v(t) \tag{4.108}$$

Substituting equation (4.104) into the above equation yields,

$$\Delta\mathbf{E}^v(t) = \mathbf{D}_v^{-1}\sum_{i=1}^{m}\frac{A_i}{\tau_i}\int_0^{t+\Delta t}[e^{-\frac{(t+\Delta t-\tau)}{\tau_i}}] : \mathbf{S}^v(\tau)d\tau - \mathbf{D}_v^{-1}\sum_{i=1}^{m}\frac{A_i}{\tau_i}\int_0^t[e^{-\frac{(t-\tau)}{\tau_i}}] : \mathbf{S}^v(\tau)d\tau \tag{4.109}$$

Using a linear approximation of $\mathbf{S}^v$ and $\mathbf{E}^v$ from the interval t to $t+\Delta t$, and taking the integration intervals from $\int_0^t$ and $\int_t^{t+\Delta t}$, we have

$$\mathbf{D}_v : \Delta\mathbf{E}^v = \sum_{i=1}^{m}\{\frac{A_i}{\tau_i}[e^{-\frac{\Delta t}{\tau_i}} - 1]\mathbf{I}_i + A_i\,\mathbf{S}^v(t)[1-e^{-\frac{\Delta t}{\tau_i}}] + A_i\Delta\mathbf{S}^v(t)[1-\frac{\tau_i}{\Delta t}(1-e^{-\frac{\Delta t}{\tau_i}})]\} \tag{4.110}$$

where

$$\mathbf{I}_i(t) = \int_0^t e^{-\frac{t-\tau}{\tau_i}}\mathbf{S}^v(\tau)d\tau \tag{4.111}$$

For simplification, equation (4.110) can be rearranged in terms of p_v, w_v, and $\mathbf{h}_v$.

$$\mathbf{D}_v : \Delta\mathbf{E}^v = \mathbf{h}_v + p_v\mathbf{S}^v(t) + w_v\Delta\mathbf{S}^v(t) \tag{4.112}$$

where

$$\mathbf{h}_v = \sum_{i=1}^{m} \frac{A_i}{\tau_i}[e^{-\frac{\Delta t}{\tau_i}} - 1]\mathbf{I}_i \tag{4.113}$$

$$p_v = \sum_{i=1}^{m} A_i\,[1 - e^{-\frac{\Delta t}{\tau_i}}] \tag{4.114}$$

$$w_v = \sum_{i=1}^{m} A_i[1 - \frac{\tau_i}{\Delta t}(1 - e^{-\frac{\Delta t}{\tau_i}})] \tag{4.115}$$

Therefore, the increment of the viscoelastic stress, $\Delta\mathbf{S}^v$, can be obtained from equation (4.112) by

$$\Delta\mathbf{S}^v = \frac{1}{w_v}(\mathbf{D}_v : \Delta\mathbf{E}^v - \mathbf{h}_v - p_v\mathbf{S}^v) \tag{4.116}$$

4.6.3. Nonlinear local incremental solution

From equation (4.103) and equation (4.116), we can see that the increment of the viscoelastic stress is given in two different ways, one is from the kinematical equations, and another is based on the constitutive equation. Combining equation (4.103) and (4.116), yields,

$$\frac{1}{w_v}(\mathbf{D}_v : \Delta\mathbf{E}^v - \mathbf{h}_v - p_v\mathbf{S}^v) = \widehat{\mathbf{F}}^{v^{-1}}\{\mathbf{D} : [\widehat{\mathbf{F}}^{v^{-T}}(\hat{\mathbf{E}} - \mathbf{E}^v - \Delta\mathbf{E}^v)\widehat{\mathbf{F}}^{v^{-1}}]\}\widehat{\mathbf{F}}^{v^{-T}} - \mathbf{S}^v \tag{4.117}$$

In the above equation, there is only one unknown, the viscoelastic increment $\Delta\mathbf{L}^v$. Other terms are either known from the previous time step or expressed as a function of $\Delta\mathbf{L}^v$, therefore, using Newton's method (referred to 4.3.2), $\Delta\mathbf{L}^v$ can be calculated numerically.

Once $\Delta\mathbf{L}^v$ is obtained, a schematic of the solution process is: $\Delta\mathbf{L}^v \xrightarrow{Eqn(4.98)} \hat{\mathbf{E}}^v \xrightarrow{Eqn(4.100)} \hat{\mathbf{E}}^e \xrightarrow{Eqn(4.101)} \widehat{\mathbf{S}}^e$, thus the second Piola-Kirchhoff stress can be calculated and used to formulate the internal force.

5.0 VERIFICATION OF MODEL

Verification of the computer model is hard to accomplish because of the complication of the problem. Here, we study the problems which have the analytical solutions. The verification can be done by comparing numerical results to analytical solutions for well established problems. These problems we select are: (1) solid phase (only); (2) fluid phase (only); (3) verification of the electroneutrality condition; (4) verification of the diffusive equation (one dimension); (5) solid-fluid phase (coupled, one dimension).

5.1 SOLID PHASE

Since in the small strain problems, the higher order terms of large strain theory can be considered negligible, the numerical results obtained by the proposed model should be almost the same as the result of small strain elastic theory. This provides a possibility to verify our program. Here the small uniaxial tension model is chosen (shown in Fig.5.1). The upper edge is loaded with pressure 90 Pa, and the corresponding loading history is shown in Fig.5.2. The bottom edge is constrained. The material properties are selected (referred to Table 5.1). Because the velocity and acceleration are relatively small, the static solution is considered as our analytical solution.

Table 5.1 Material properties of the element (Solid)

E(Pa)	ν	$\rho_{s(kg/m^3)}$	$\rho_{f(kg/m^3)}$	n	$k(\ m^4/N-s\ )$
45500	0.0	1016	1000	0.0001	1E-16

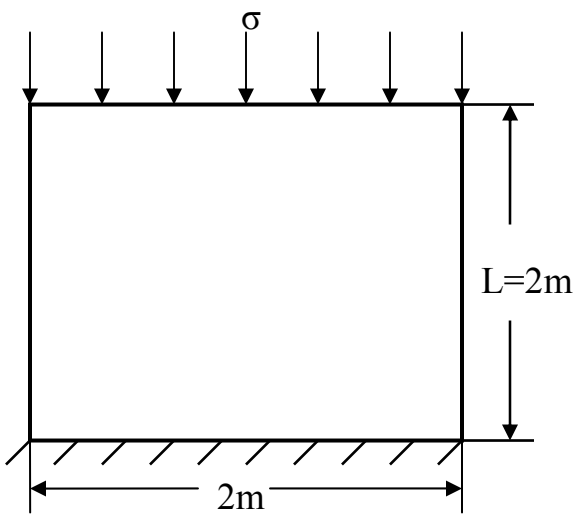

(a) Physical model

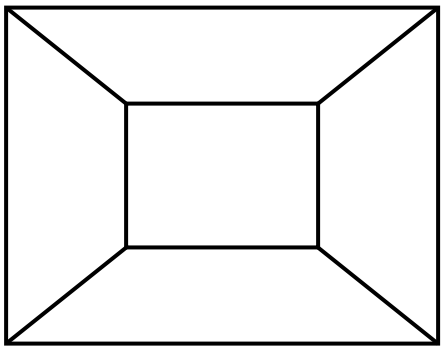

(b) Finite element model

Fig.5.1 The uniaxial tension model

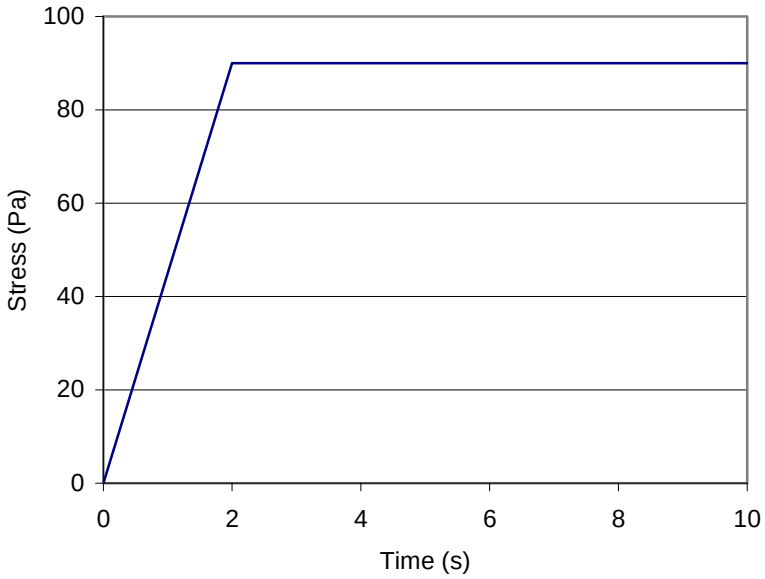

Fig.5.2.The loading history

For viscoelastic properties in equation (4.105), the amplitude A is selected as 0.00014 and the relaxation time τ as 20.

5.1.1 Elastic response

In the small strain uniaxial tension, the analytical static results is

$$u(t) = L\frac{\sigma}{E} \tag{5.1}$$

Figure 5.3 shows the result given by the proposed model is nearly the exact same result as the analytical solution.

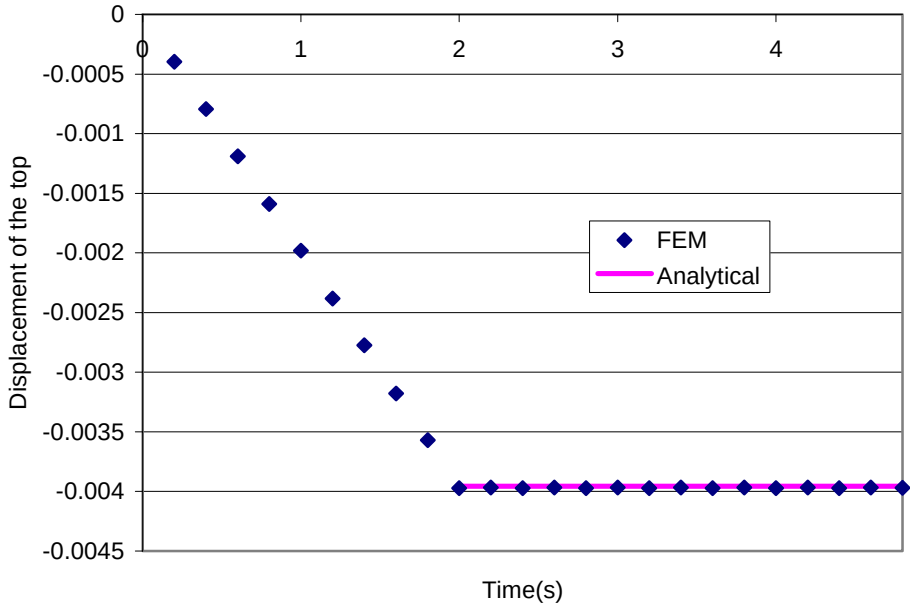

Fig.5.3 Variation of Uy at top with time (elasticity)

5.1.2 Viscoelastic response

The small strain constitutive relation for the small strain viscoelastic theory is

$$\varepsilon(t) = \frac{\sigma}{E} - \int_0^t \frac{\partial J_v}{\partial \tau}\sigma(\tau)d\tau \tag{5.2}$$

Here, the relaxation function is given by:

$$J_v = A_i\left(1 - e^{-\frac{t-\tau}{\tau_i}}\right) \tag{5.3}$$

Substituting equation (5.3) into equation (5.2), we get

$$\varepsilon(t) = \frac{\sigma}{E} + A_i\sigma\left[1 - e^{-\frac{t}{\tau_i}}\right] \tag{5.4}$$

In case of small loads, the strain kinematical relation can be well obtained by

$$\varepsilon = \Delta L / L \tag{5.5}$$

Therefore, the final expression of displacement can be written as

$$u(t) = L\frac{\sigma}{E} + LA_i\sigma\left[1 - e^{-\frac{t}{\tau_i}}\right] \tag{5.6}$$

Figure 5.4 indicates that the result of the proposed nonlinear model is in accordance with the linear small stain analytical solution.

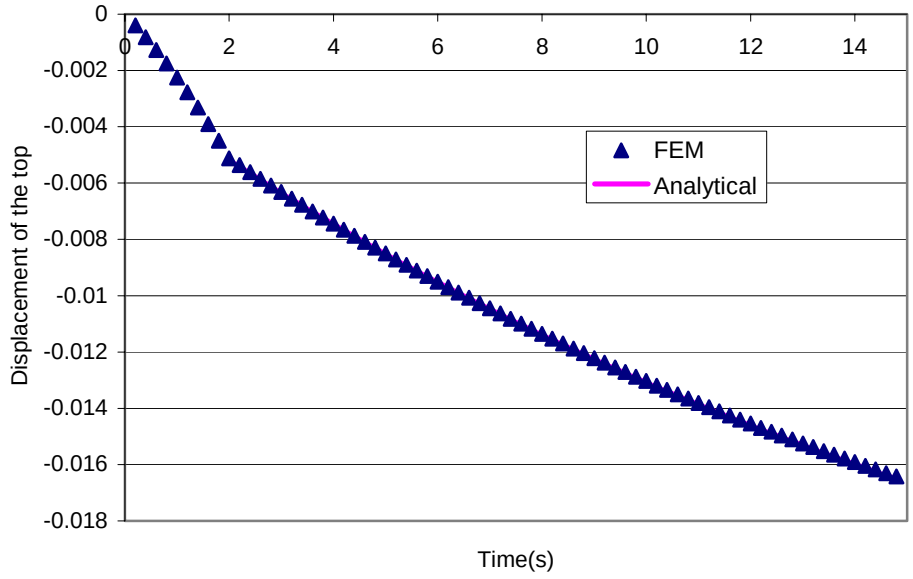

Fig.5.4 Variation of Uy at top with time (viscoelasticity)

Thus, the results of the computation model correspond well to analytical solutions for elastic and viscoelastic solid problems.

5.2 FLUID PHASE

A one dimensional fluid problem is examined to verify the porous computations of the program. The problem is show in Fig.5.5, and the displacement of solid is fixed, and a pressure is applied on the fluid. The fluid properties are given in Table 5.2. 12 2-D elements are arranged in a line, but only the motion in X direction is allowed.

Table5.2 Material properties of the element

$\rho_{f(kg/m^3)}$	n	$k(\ m^4/N-s\ )$
1000	0.1	0.3

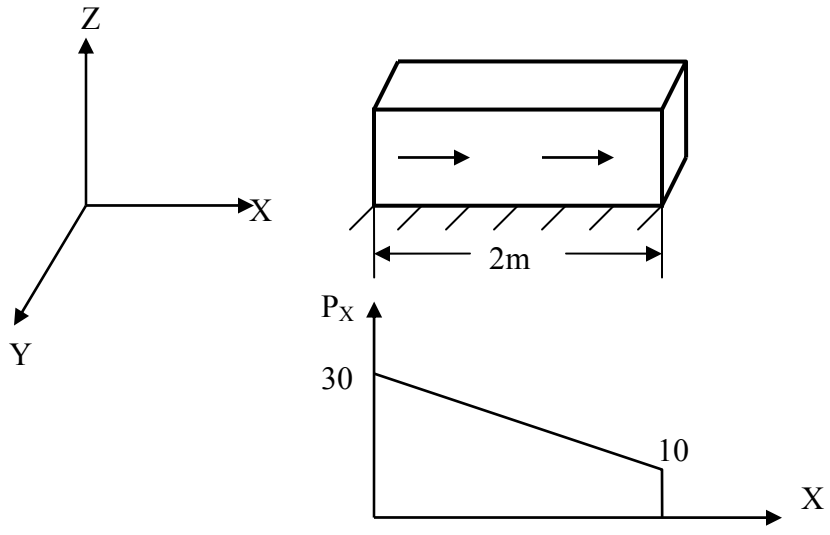

Fig.5.5 The fluid model and the distribution of pressure along X axis

In the case of an uncoupled fluid phase and the absent of a body force, equation (3.51) can be simplified as

$$\nabla p - \frac{n}{k}\dot{\mathbf{w}} - \rho_f \ddot{\mathbf{w}} = 0 \tag{5.7}$$

Assuming ∇p is a constant in the total field, and only one dimension (x) is considered, the fluid velocity V_x is given by

$$V_x = A_f e^{-\frac{k\rho_f}{n}} + (dp/dx)\cdot(k/n) \tag{5.8}$$

The initial condition gives the value of A. When $V_x = 0$ at t=0,

$$A_f = -\frac{dp}{dx}\frac{k}{n} \tag{5.9}$$

Thus,

$$V_x = \frac{dp}{dx}\frac{k}{n}(1 - e^{-\frac{k\rho_f}{n}t}) \tag{5.10}$$

From Fig.5.6, we can see that the overall results from the proposed model fit the fluid analytical solutions very well. The small difference may be done due to neglecting $\ddot{\mathbf{X}}^0$. In our computation, it is assumed to 0 for convenience.

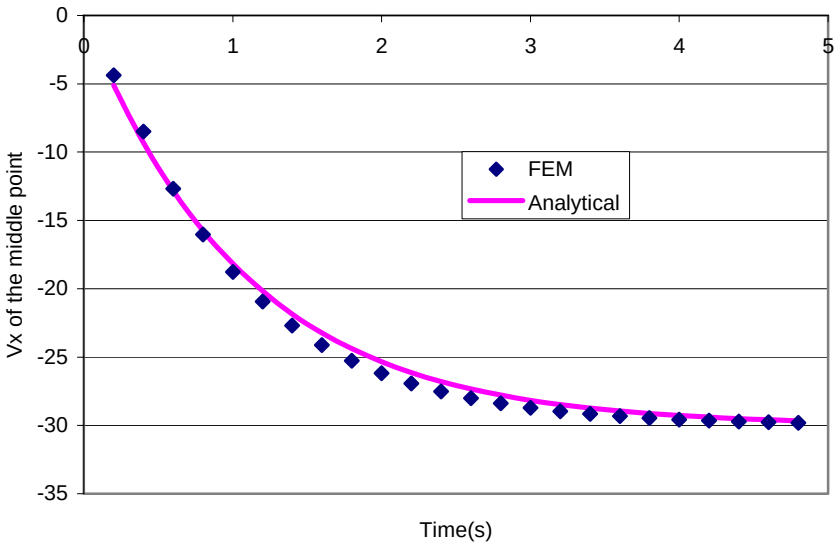

Fig.5.6 Variation of fluid velocity at the center with time

5.3 VERIFICATION OF ELECTRONEUTRALITY CONDITIONS

A simple 2-D model (referred to Fig.5.7a) is used to study the electroneutrality conditions. A 1×1 square is filled with two monovalent ion species, i.e., anion (-) and cation (+). The cation and anion concentrations at point A are 3. For other points in the field, the concentrations are selected as 2 (referred to Fig.5.7b).

The results about point A and point B (close to A) are shown in Fig. (5.8). For A and B, the concentration of anions is the same as that of cations during the whole time, which indicates the electroneuality condition is satisfied. In addition, the concentration at A decreases with time, and approaches to the same value of B, which is in accordance with the diffusive equation.

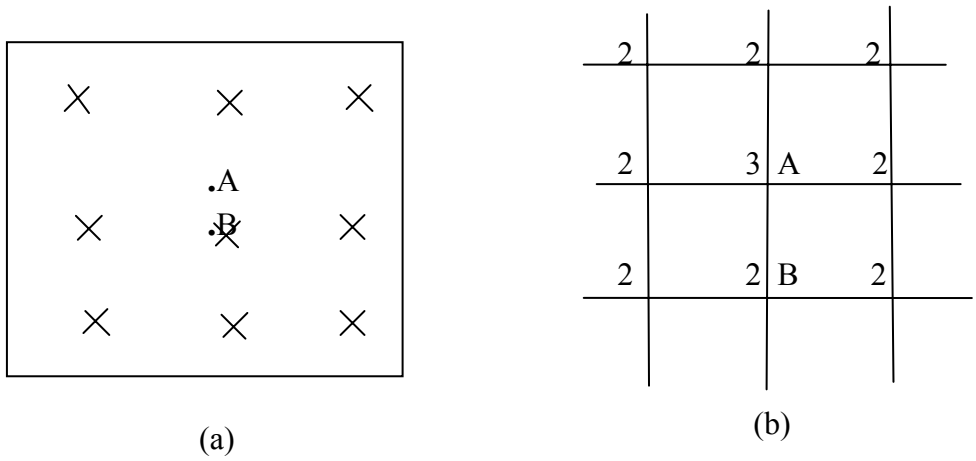

Fig.5.7 Electric-chemical model

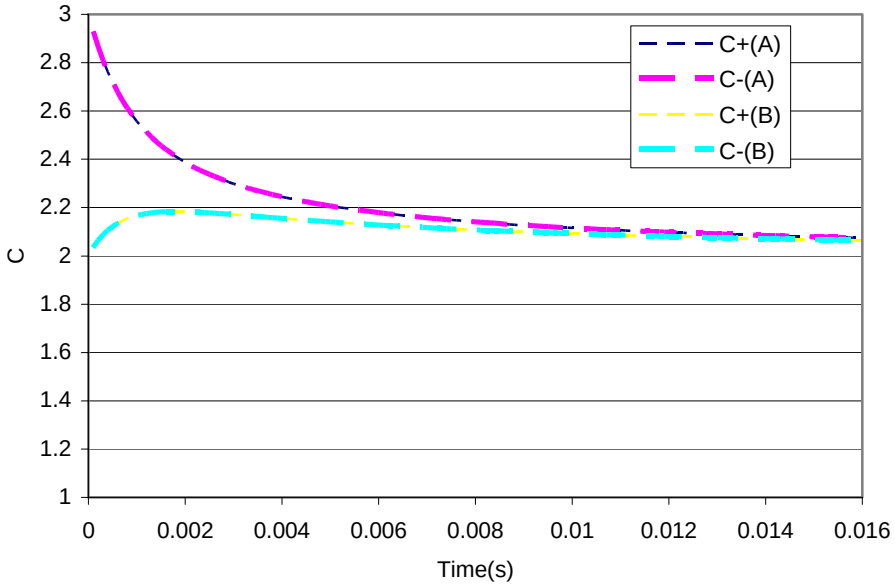

Fig.5.8 Concentration of A and B with time

5.4 STUDY OF DIFFUSIVE EQUATION

The program is used to analyze the diffusion in a one-dimensional rod of length l_0. Equation (4.60) is transformed to the typical diffusive equation (5.11) to obtain an analytical result. The governing equation describing the problem is

$$\frac{dc}{dt} = D_{cc} \frac{d^2 c}{dx^2} \tag{5.11}$$

where Dcc is the diffusive coefficient.

The boundary conditions for the problem are

$$\frac{dc}{dt} = 0 \qquad \text{at } x = 0, x = l_0 \quad t > 0 \tag{5.12a}$$

and the initial condition is

$$c(x,t) = 10x \quad \text{for } t = 0, \ 0 \le x \le l_0 \tag{5.12b}$$

The analytical solution to this problem is given by

$$c(x,t) = 10l_0 - \sum_{n=1}^{\infty} \frac{20l_0}{(n\pi)^2} [1-(-1)^n] \cos\frac{n\pi x}{l_0} e^{-n^2\pi^2 / l_0^2 * D_{cc} t} \tag{5.13}$$

where the diffusion coefficient D_{cc} is selected as 2, and $l_0 = 6$.

12 2-D elements are arranged in a line, but only the motion in X direction is allowed. It can be seen that in Fig.5.9, the analytical solution and the numerical solution correlate well, which demonstrates the performance of the computation program in modeling diffusion.

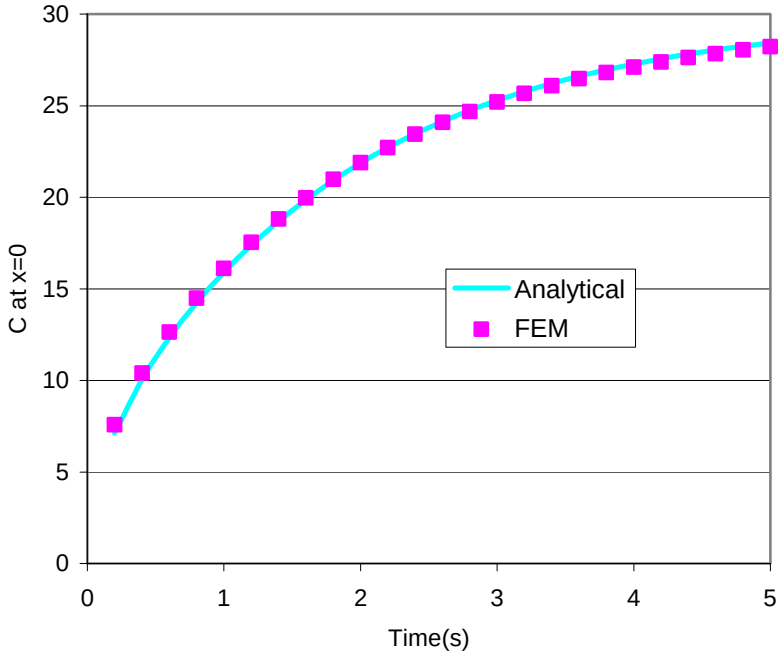

Fig. 5.9 Variation of c at x=0 with time

5.5 PORO-ELASTIC PROBLEM (NEARLY INCOMPRESSIBLE) [57, 69]

A one-dimensional poroelastic problem is shown in Fig.5.10, which describes the motion of porous elastic material along the x-axis. The material properties are given to Table 5.3.

Table 5.3 Material properties of the element

E(Pa)	ν	$\rho_{s(kg/m^3)}$	$\rho_{f(kg/m^3)}$	n	k($m^4/N-s$)	Ks(Pa)	K_f(Pa)
3000	0.2	0.306	0.2977	0.333	0.004883	5005	61060

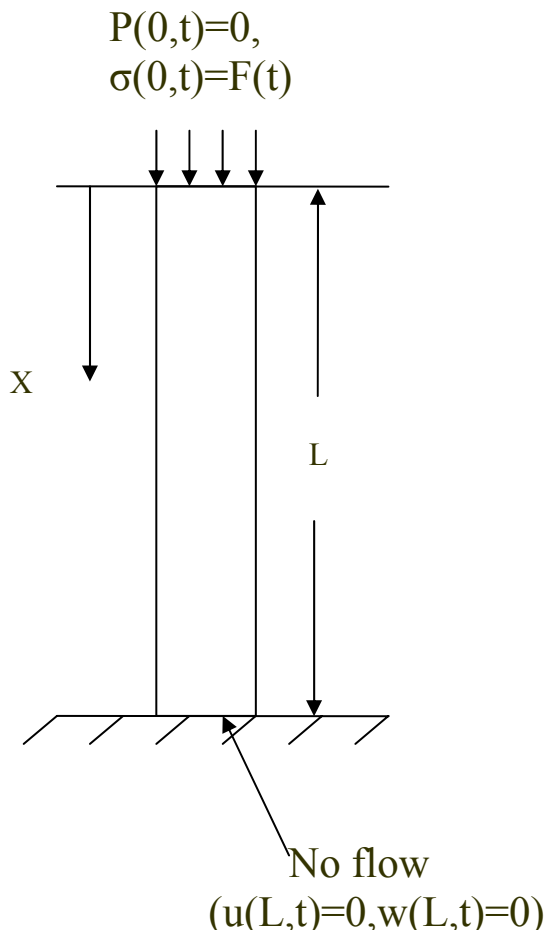

Fig.5.10 A one-dimensional boundary value problem

(No flow or displacement on lateral boundaries)

The boundary conditions are

$$\sigma(0,t) = F(t) \tag{5.14a}$$

and

$$p(0,t) = 0 \tag{5.14b}$$

and the initial conditions are

$$u(x,0) = \dot{u}(x,0) = w(x,0) = \dot{w}(x,0) = 0 \tag{5.14c}$$

In order to assess the accuracy of our proposed model, the analytical solution obtained by Simon et al. [57, 69] for this problem is given as follows.

A non-dimensional u-w form of the field equation is [57, 69]

$$u_{,\xi\xi} + \alpha k w_{,\xi\xi} = u_{,\tau\tau} + \beta w_{,\tau\tau} \tag{5.15a}$$

$$\alpha k u_{,\xi\xi} + k w_{,\xi\xi} = \beta u_{,\tau\tau} + \gamma w_{,\tau\tau} + w_{,\tau} \tag{5.15b}$$

where

$$\xi = x_1 / (\rho k V_c) \tag{5.16}$$

$$\tau = t / (\rho k) \tag{5.17}$$

$$u_{,\xi\xi} = \partial^2 u / \partial \xi^2 \tag{5.18}$$

$$\beta = \rho_f / \rho \tag{5.19}$$

$$\gamma = \beta / n \tag{5.20}$$

$$k = Q / (\lambda + 2\mu + \alpha^2 Q) \tag{5.21}$$

And where V_c is the speed of propagation for waves that move through the porous medium with w=0, defined as

$$V_c = \sqrt{(\lambda + 2\mu + \alpha^2 Q) / \rho} \tag{5.22}$$

The boundary conditions are

$$f(\tau) = k / V_c \sigma(0,\tau) = k / V_c F(t) \qquad \text{at } \xi = 0 \tag{5.23}$$

$$p(0,\tau) = 0 \tag{5.24}$$

and the initial conditions are given by

$$u = u_{,\tau} = w = w_{,\tau} = 0 \text{ for } \tau = 0 \tag{5.25}$$

An analytical solution of equation (5.15) could not be obtained for arbitrary materials. However, under the condition of arbitrary f(t), and an infinite domain (no reflections) composed of solid and fluid materials that are dynamically compatible ($\alpha k = \beta$), an analytical solution was given in [57,69] as

$$w = w(\xi,\tau) = c_a \int_0^{\tau} f(\tau-\bar{\tau}) e^{-\frac{b\bar{\tau}}{2a}} I_0\left(\frac{b\sqrt{\bar{\tau}^2 - a\xi^2}}{2a}\right) 1(\bar{\tau} - \sqrt{a\xi})\, d\bar{\tau} \tag{5.26a}$$

$$u = u(\xi,\tau) = -\int_0^{\tau} f(\tau-\bar{\tau}) 1(\bar{\tau}-\xi)\, d\bar{\tau} - \beta w(\xi,\tau) \tag{5.26b}$$

where

$$a = (\gamma - \beta^2) b \tag{5.27}$$

$$b = 1/(k - \beta^2) \tag{5.28}$$

$$c_a = \alpha\sqrt{a(1-\alpha\beta)} \tag{5.29}$$

In this solution, there are two dilatational waves: a Biot's wave with a non-dimensional speed, $v_1 = 1$, and a slower Biot's wave with a non-dimensional speed, $v_2 = \frac{1}{\sqrt{a}}$. Therefore, the testing time is selected as 0.2 second so that no reflected waves were present in the region of interest in the finite element model (which has a finite length).

In this problem, a step load, $\sigma = \sigma_0 1(t)$, and free flow, $p = 0$, were prescribed at the free top surface of a one-dimensional porous medium (see Figure 5.10). 12 2-D elements are arranged in a line (X direction). Three element formulations, Ub2/Pb2, Ub2/Pb1, and Ub2/P1 are considered here. Fig.5.11 and Fig.5.12 indicate how the solid and fluid displacements at the top vary with time. Fig.5.13 and Fig.5.14 gives the displacements of the solid and fluid phases along the X axis at time t=0.05 s. Fig.5.15 shows the distribution of pressure at time t=0.05s.

Comparing the finite element results with the analytical solutions, we can see that with these elements, the results for Ub2/Pb2 in both phases are in accordance with the analytical result with high accuracy. The Ub2/Pb1 and Ub2/P1 elements have good agreement for the solid behavior, but have large difference in the field of the fluid phase. This example demonstrates the performance of the Ub2/Pb2 element in a solid-fluid coupled problem.

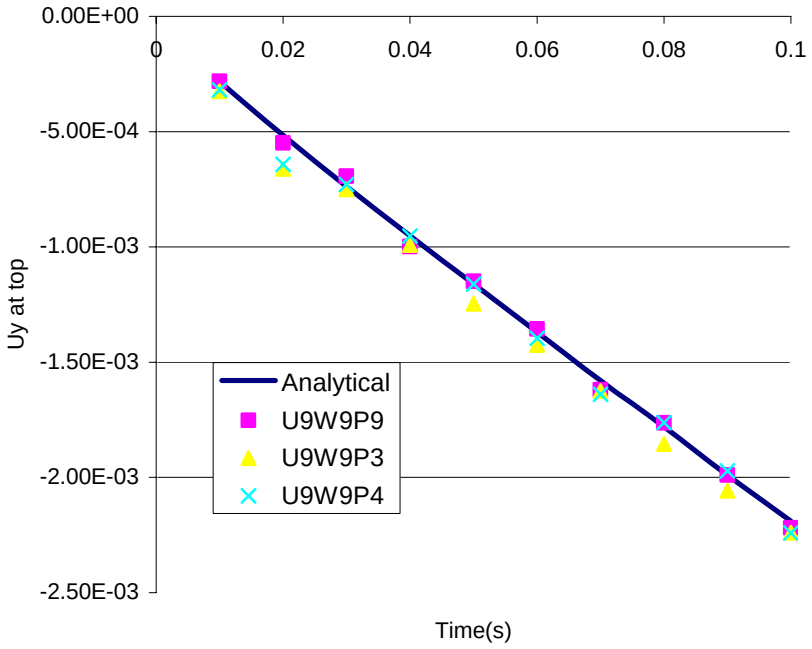

Fig.5.11 Variation of u_y at top with time (near compressibility)

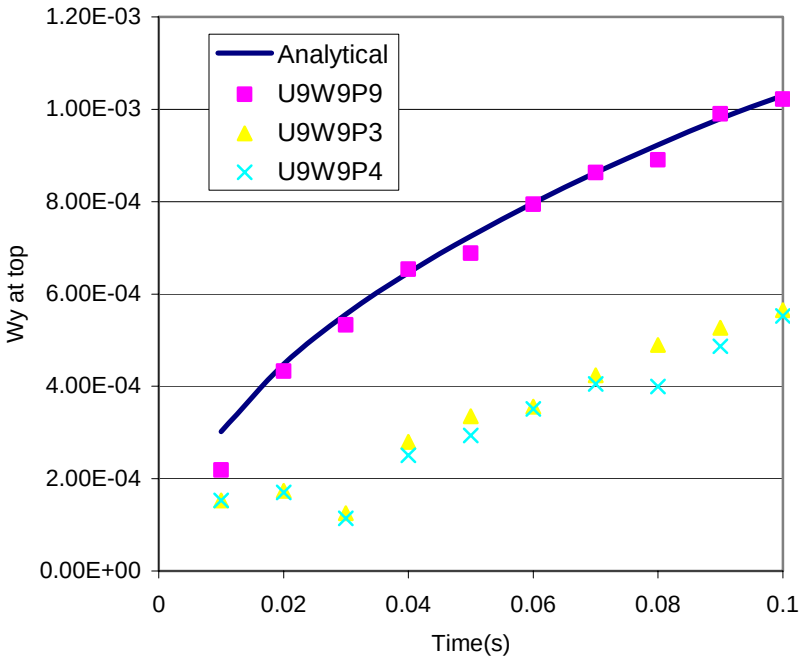

Fig. 5.12 Variation of Wy at top with time(near compressibility)

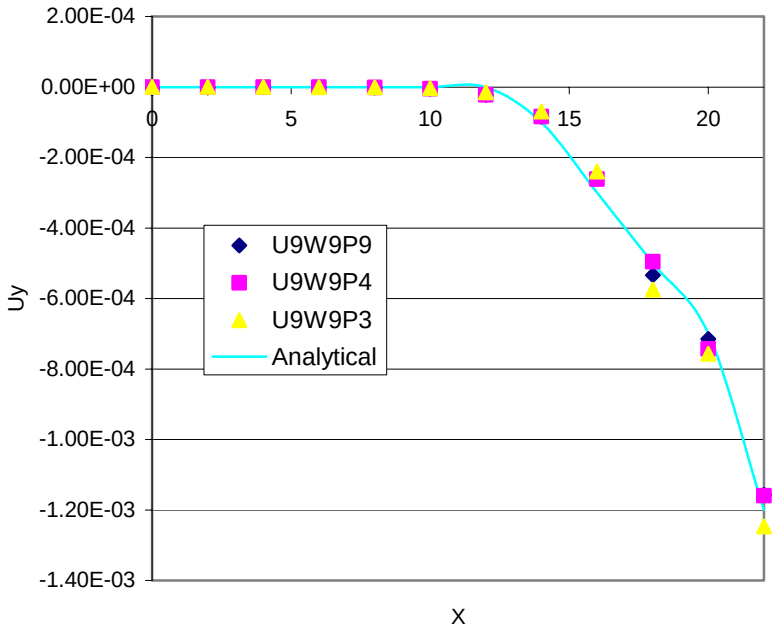

Fig.5.13 Distribution of Uy along X axis (t=0.05s)

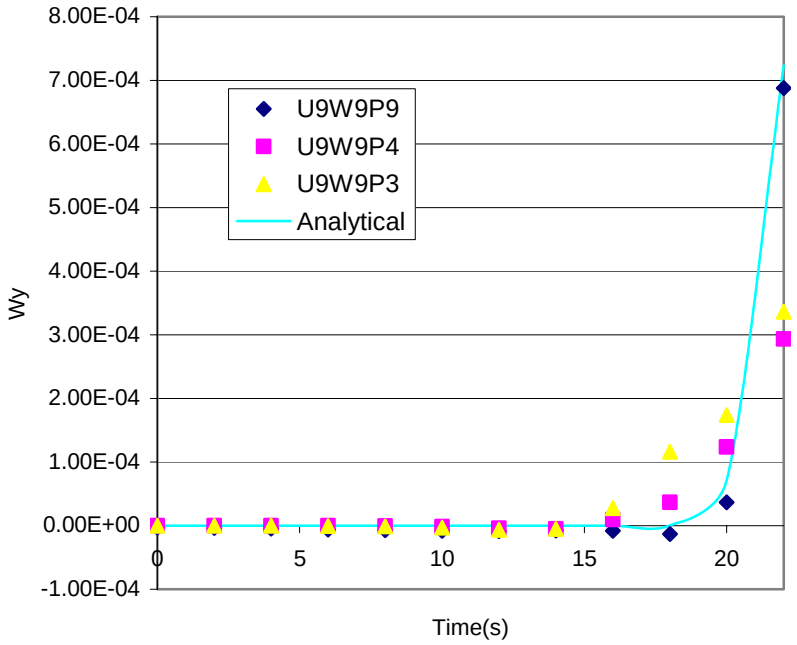

Fig.5.14 Distribution of Wy along X axis (t=0.05s)

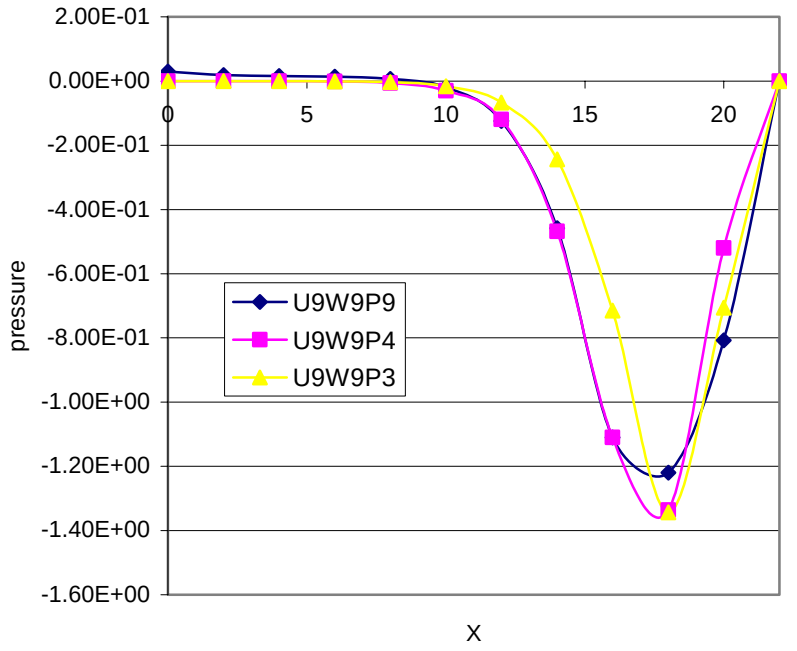

Fig.5.15 Distribution of pressure along X axis (t=0.05s)

5.6 SOLID-FLUID COUPLED PROBLEM (FULLY INCOMPRESSIBLE)

The previous example is also used to study the performance of the program for fully incompressible problems. Because of the mathematical difficulty, the analytical solution can not be obtained directly; however, there is a simple way to testify our program. For the continuity condition, in one dimensional problems with small strains, becomes,

$$\frac{d\dot{u}(x,t)}{dx} + n\frac{d\dot{w}(x,t)}{dx} = 0 \tag{5.30}$$

The integral of the above equation becomes

$$\dot{u}(x,t) + n\dot{w}(x,t) = \phi'(t) \tag{5.31}$$

Then integrating with respect to time, yields

$$u(x,t) + nw(x,t) = \int \phi'(t)dt = \phi(t) \tag{5.32}$$

with the boundary condition $u(0,t) = w(0,t) = 0$, we have

$$\phi(t) = 0 \tag{5.33}$$

Thus,

$$u(x,t) + nw(x,t) = 0 \tag{5.34}$$

Equation (5.34) reveals the relations between the displacement of fluid and solid in this one-dimensional problem. 12 2-D elements are arranged in a line (X direction). Ub2/Pb2 element formulation is considered here. Figure 5.16 gives the displacement of fluid and solid of top point with time, which agrees with equation (5.34) with high accuracy.

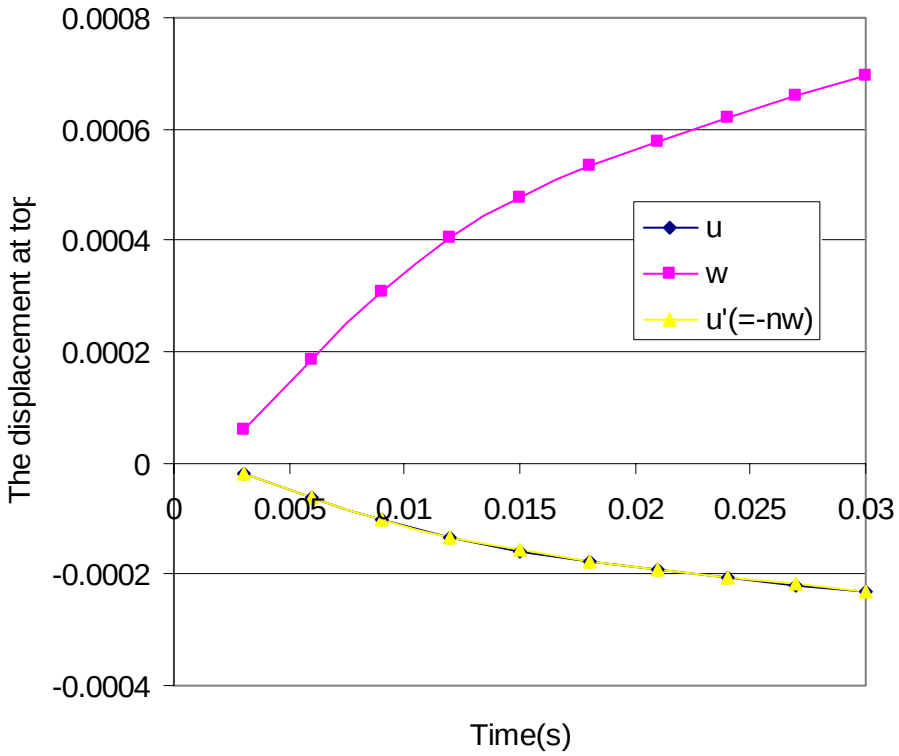

Fig. 5.16 The displacement of solid and fluid at top with time

In order to compare the difference between fully incompressible and nearly incompressible behavior, the "true "Possion's ratio is selected as 0.49 for the solid phase in the nearly incompressible case, and the corresponding results are given in Fig. 5.17-5.21.

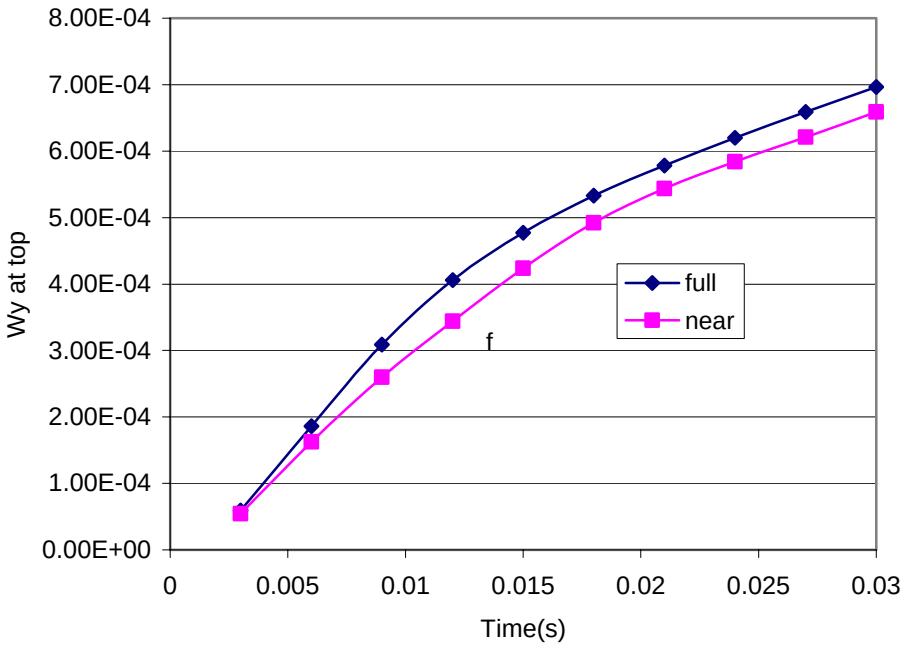

Fig.5.17 Wy at top in the full and near incompressibility

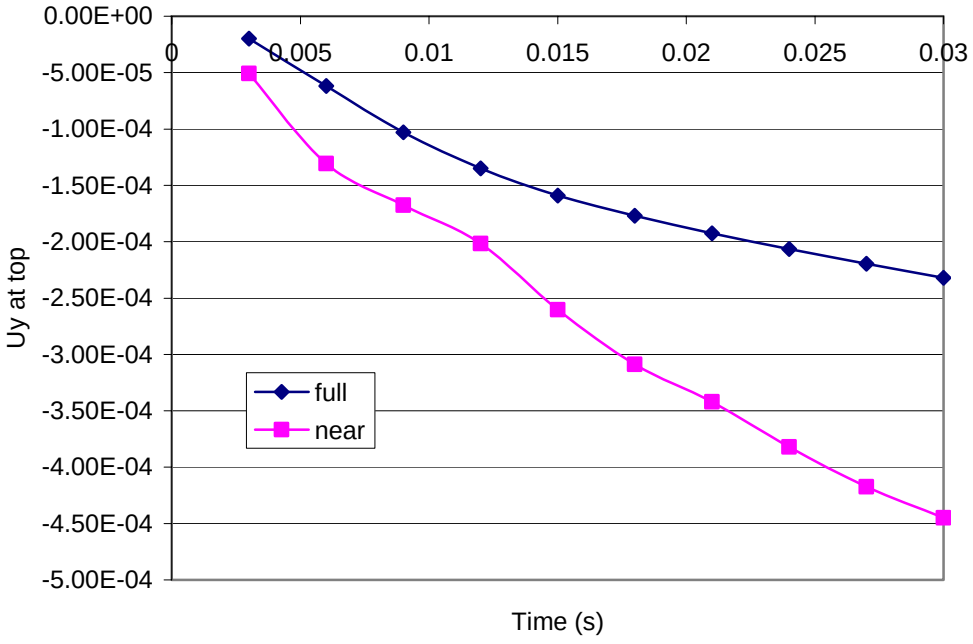

Fig.5.18 Uy at top in the full and near incompressibility

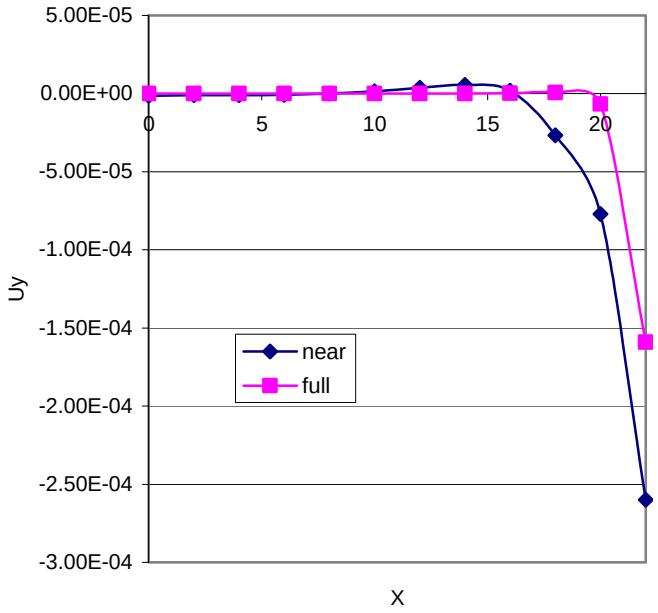

Fig.5.19 Uy distribution along X axis (t=0.015s)

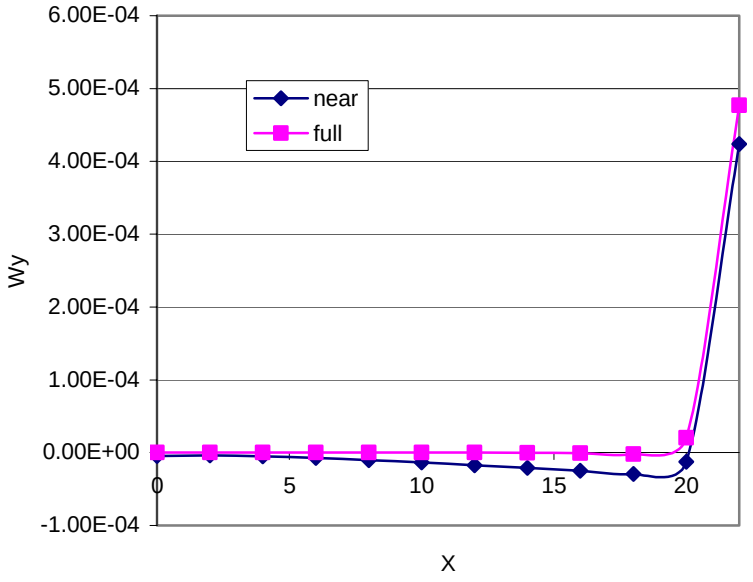

Fig.5.20 Wy distribution along X axis (t=0.015s)

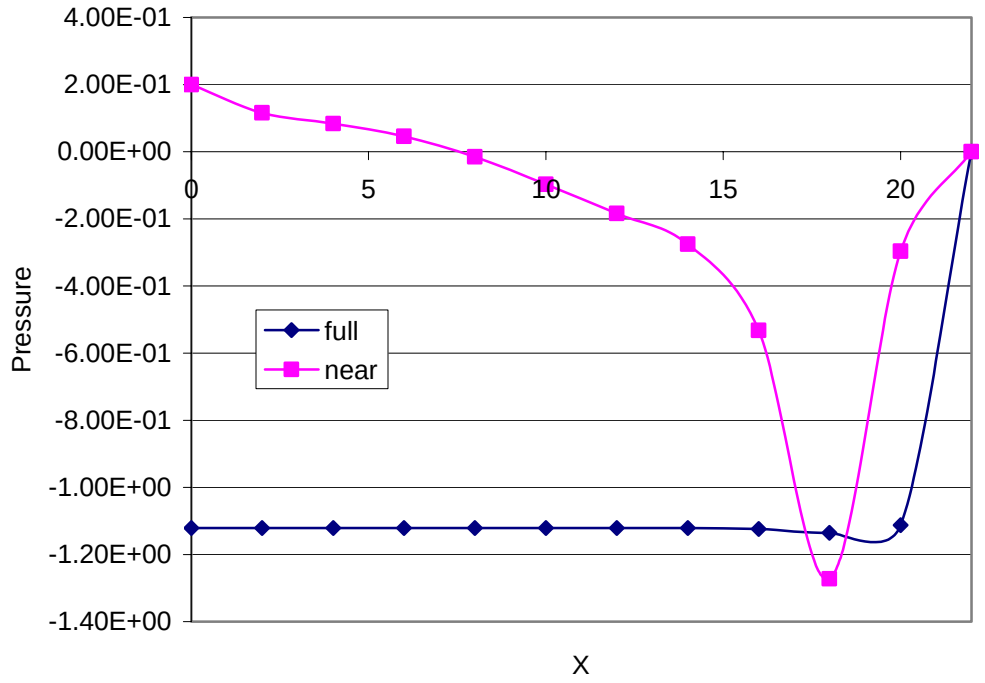

Fig.5.21 Pressure distribution along X axis (t=0.015s)

Figures 5.17 and 5.18 show that there is little difference between the near and full incompressibility in the response of fluid, but in the response of solid, the difference becomes more pronounced. Figures 5.19 and 5.20 reveal that with the wave transportation at time 0.015second, the points close to the force point are stimulated; others far from the force point have no response. Figure 5.21 indicates that in case of the full incompressibility, the pressure wave goes through the whole domain, on the contrary, for the near incompressibility, the pressure varies gradually along X axis.

For the full incompressibility, since the pressure wave goes through the whole domain, the initial conditions of pressure become significant. However, the initial pressure conditions in some problems are difficult to define. This is the disadvantage of the full incompressibility. So in the quasi-static problem, the penalty method is applied to make the pressure implicit. However,

in the dynamical problem, it's hard to find a right penalty number for the computation because of the various scales of the solutions with time. Consequently, the penalty method is not suitable in the dynamical problem. For the near incompressibility, although it has no such difficulty because the pressure varies gradually, this method needs to have the "true "poisson's ratio of the solid phase, which is hard to define it sometimes. Therefore, it is always chosen a value close to 0.5 [39-40]. In principle, the penalty method is close to the near incompressibility because the gigantic penalty number is used in the penalty method.

6.0 PARAMETRIC STUDY OF A 2-D MODEL

In this chapter, some numerical examples are considered show the importance of the finite deformations, the viscoelasticity, and the electric-chemical effect on the mechanical response of porous solids.

6.1 COMPARISON OF SMALL STRAN AND LARGE STRAIN

The geometry chosen for study is a square domain (Fig.6.1). For the solid phase, the bottom edge is fixed, others are free. For the fluid phase, all edges are free. The top edge is loaded with pressure P. In order to compare the difference between the large strain and small strain without the effect of the inertial terms, a long duration (200s) is applied (shown in Fig. 6.2), and the value of P is chosen as 100% of E. The material properties of the human disc are selected [44]: E=$2.25\times10^{5}\,Pa$, $\upsilon=0.45$, $k=1\times10^{-14}\,m^{4}/N-s$, $\rho_s=1026kg/m^{3}$, $\rho_f=1000kg/m^{3}$. Two different porosities 0.5 and 0.7 are considered.

Figure 6.3 shows that with increasing time, the difference in the displacement of point A between the large strain case and the small strain case increases. At the time of 200s, the difference is almost 100%. Figure 6.3 also indicates that the displacement of point A with n=0.5

is larger than that with n=0.7. Figures 6.5-6.8 present the deformation of the total model at time 200s with the different porosities.

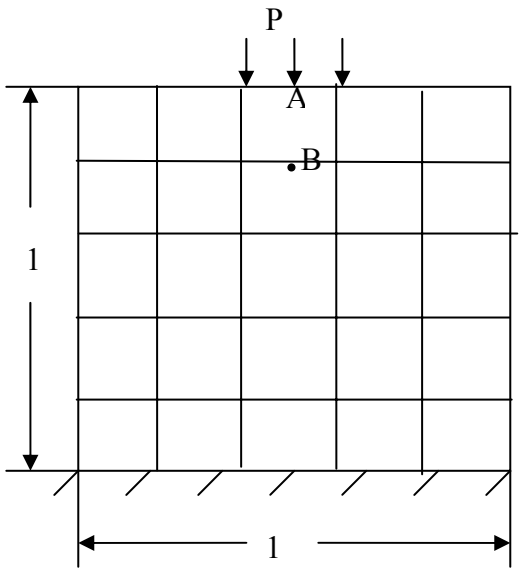

Fig.6.1 The testing model

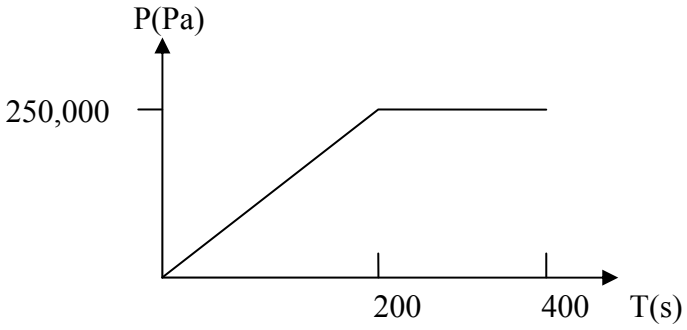

Fig.6.2 The loading process

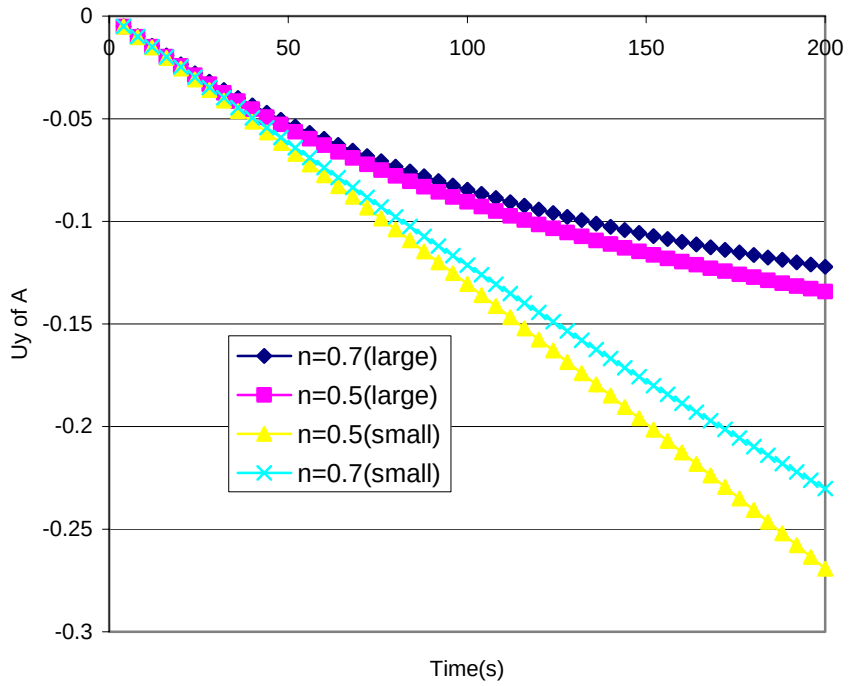

Fig. 6.3 Comparison of Uy of A in case of the large strain and small strain

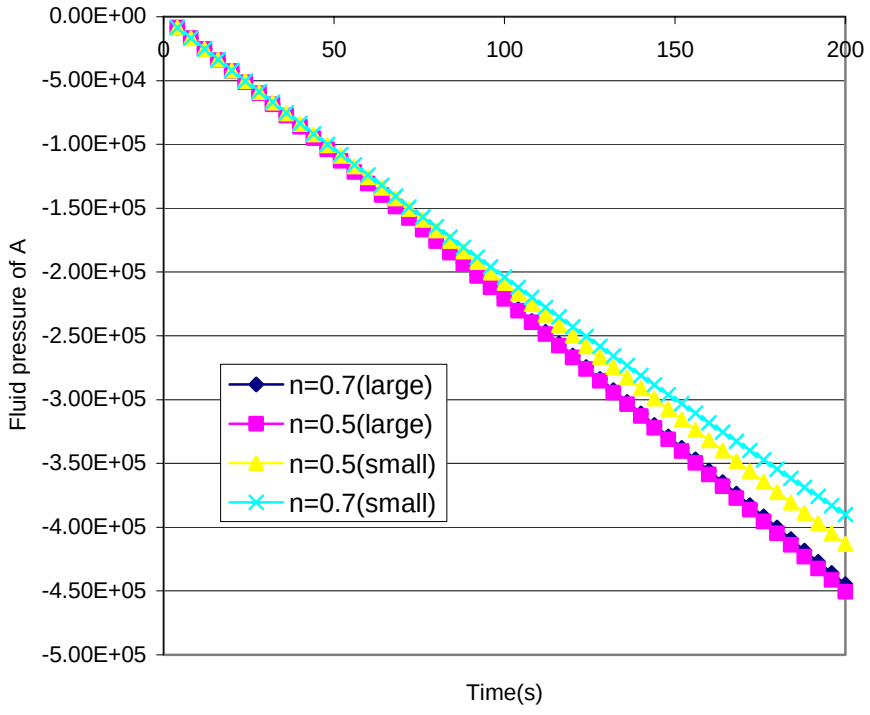

Fig. 6.4 Comparison of Pressure of A in case of the large strain and small strain

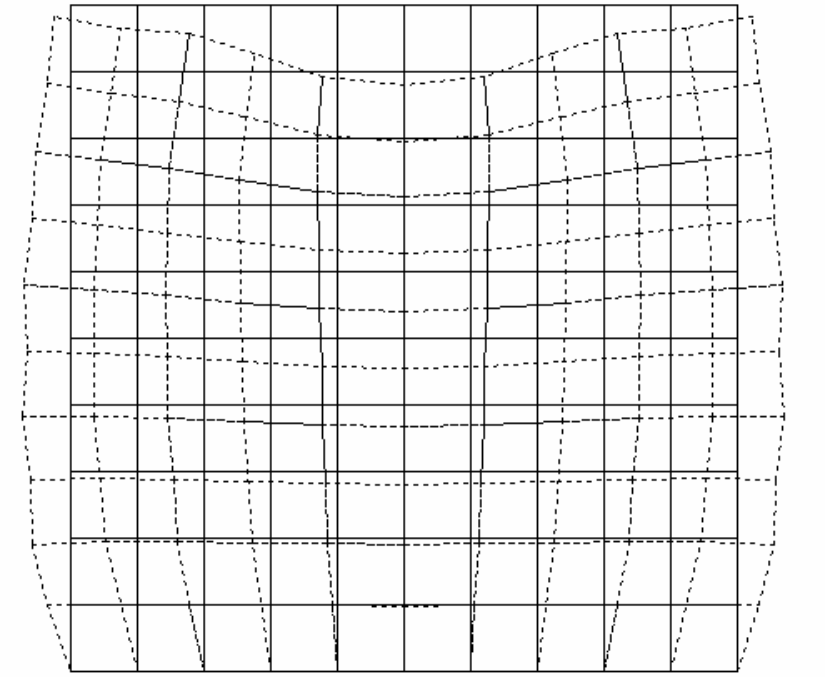

Fig.6.5 Deformation in case of the large strain (T=200s, n=0.7)

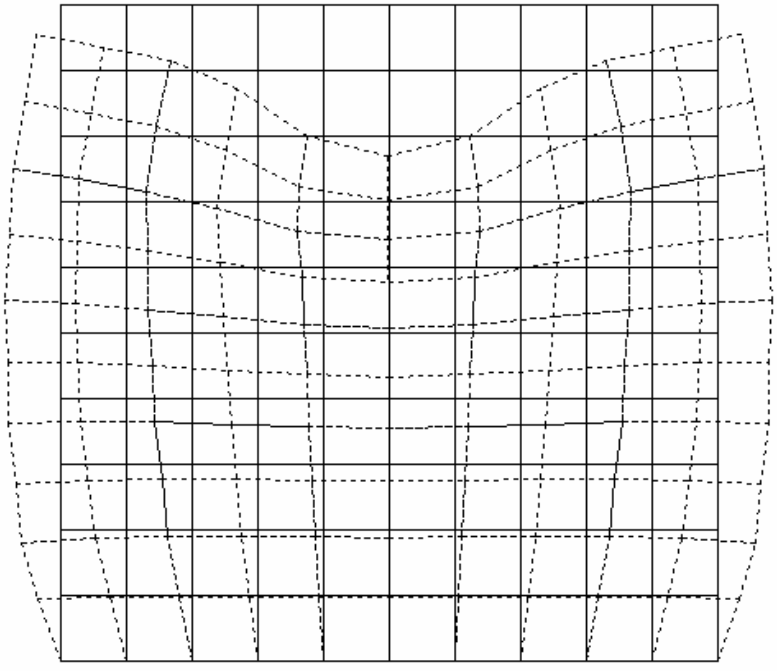

Fig.6.6 Deformation in case of the small strain (T=200s, n=0.7)

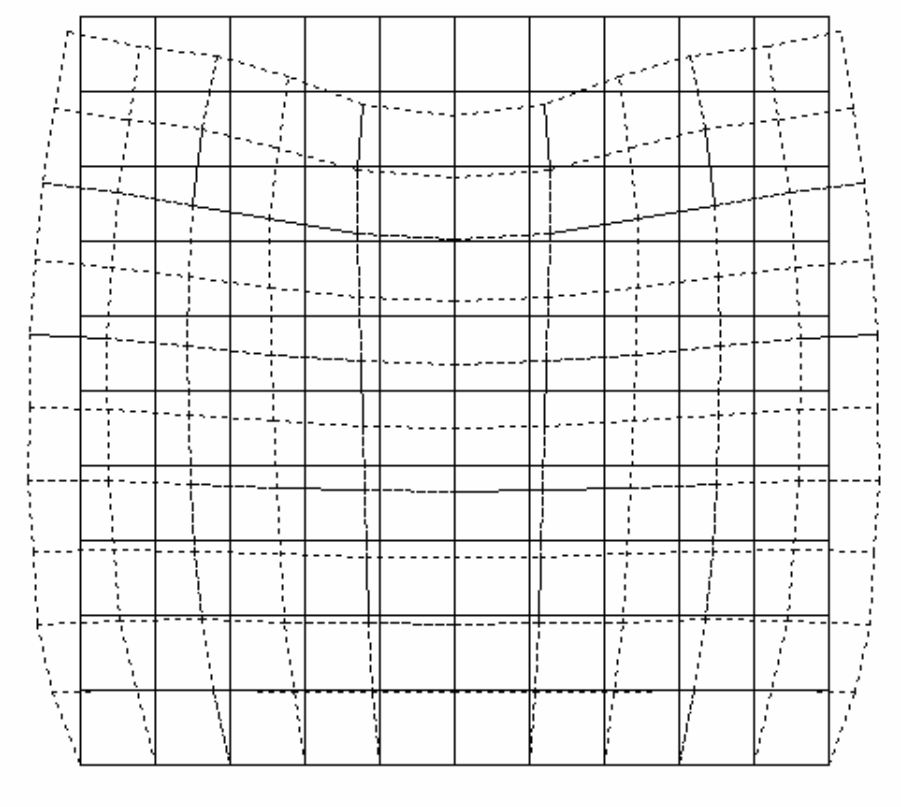

Fig.6.7. Deformation in case of the large strain (T=200s, n=0.5)

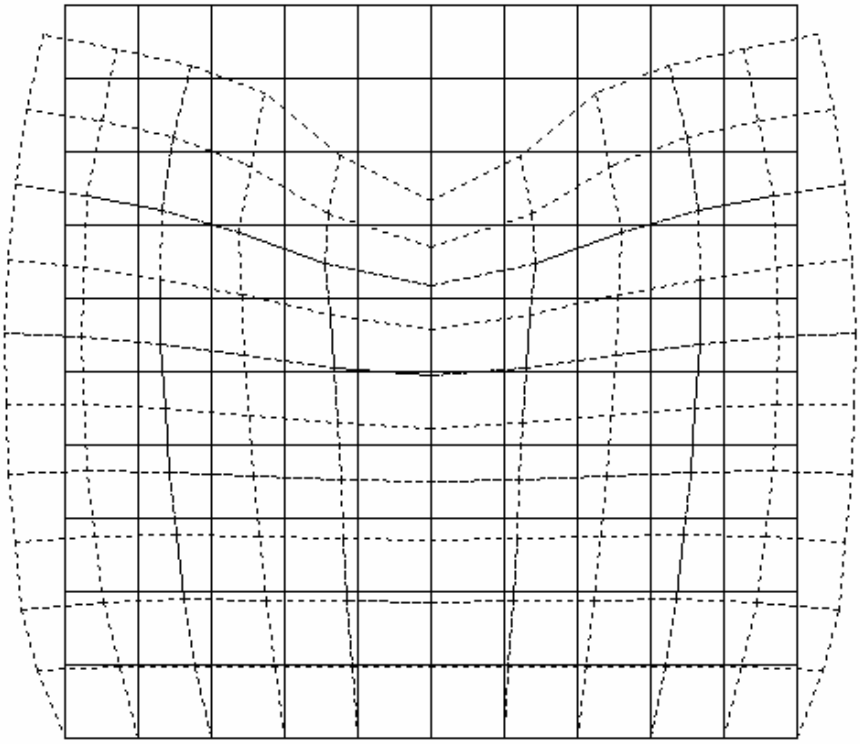

Fig.6.8 Deformation in case of the small strain (T=200s, n=0.5)

For the comparison of the small strain and large strain, when a poroelastic material is in compression, the component in compression direction of the gradient of the deformation **F** is less than 1 because from equation 3.84 because of the compression deformation in this direction,

$$\mathbf{F} \equiv \nabla \mathbf{r} = \mathbf{I} + \nabla \mathbf{u} \tag{6.1}$$

As a result, since

$$p = nQ\hat{w}_{i,i} + J\alpha Q\left[\frac{\partial X_r}{\partial x_k} E_{rs} \frac{\partial X_s}{\partial x_k}\right] \tag{6.2}$$

Equation (6.2) involves the inversion of **F**, pressure increases (shown in Fig.6.4).

The stress of the solid phase is composed of the effective stress and the fluid pressure *p* [39],

$$\boldsymbol{\sigma} = \boldsymbol{\sigma}' + \alpha \mathbf{m} p \tag{6.3}$$

Thus, when the pressure in the large strain case is greater than that of the small strain case, the effective stress of the small strain should be larger than that of the large strain case for the same pressure loaded. Therefore, the deformation in the small strain problem should be greater than that of the large strain problem.

With the decrease of the porosity, the quantity α defined in equation (3.55) decreases also [57]. Therefore, this causes the effective stress in the low porosity case to be larger than that of the large porosity case with the same pressure loaded.

6.2 COMPARISON OF THE ELASTICITY AND VISCOELASTICITY

As we mentioned in chapter three, the material of the biological tissue is viscoelastic, therefore, the comparison of the elasticity and viscoelasticity is done in this section to show the effect of the viscoelasticity.

The model and the loading are the same as the previous section, except including the viscoelastic material properties, which are selected in the range of [73]: A=1e-5, τ=100

Figure 6.9 shows the significant difference between the viscoelasticity and the elasticity, which states the effect of the viscoelasticity is not negligible. Figure 6.10 indicates the displacement of A at n=0.5 is larger than that at n=0.7. Figures 6.11, 12, and 13 present the deformation of the solid phase at time 200 s.

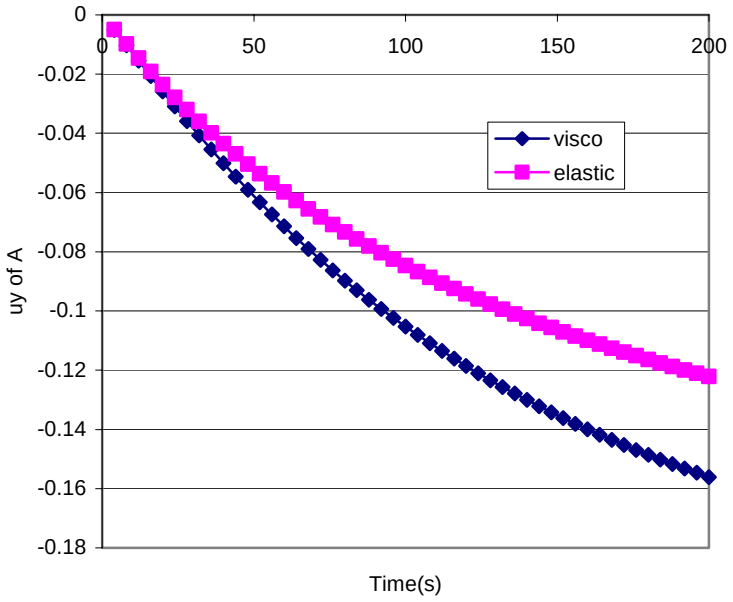

Fig.6.9 Uy of A with time in case of the elasticity and viscoelasticity (n=0.7)

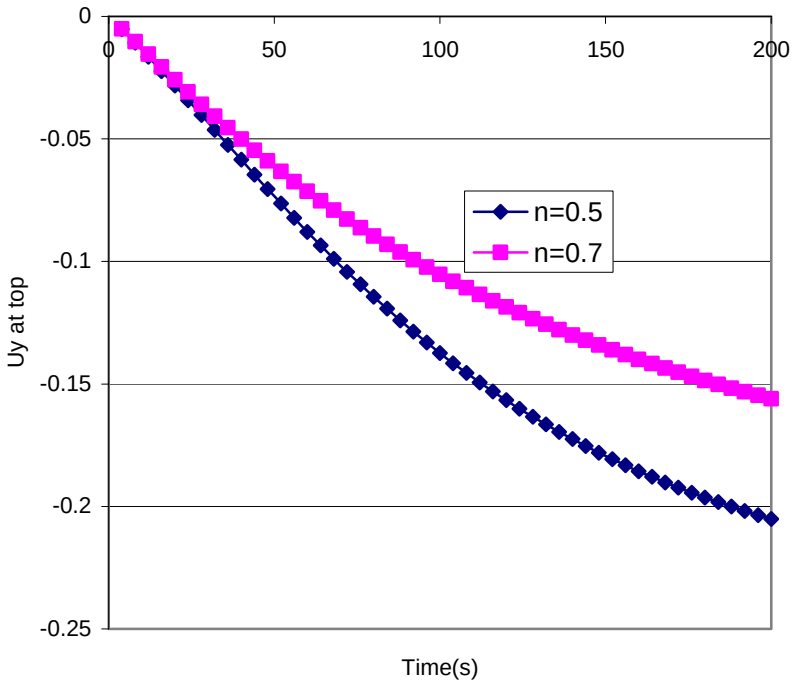

Fig.6.10 Uy of A with time at different porosities

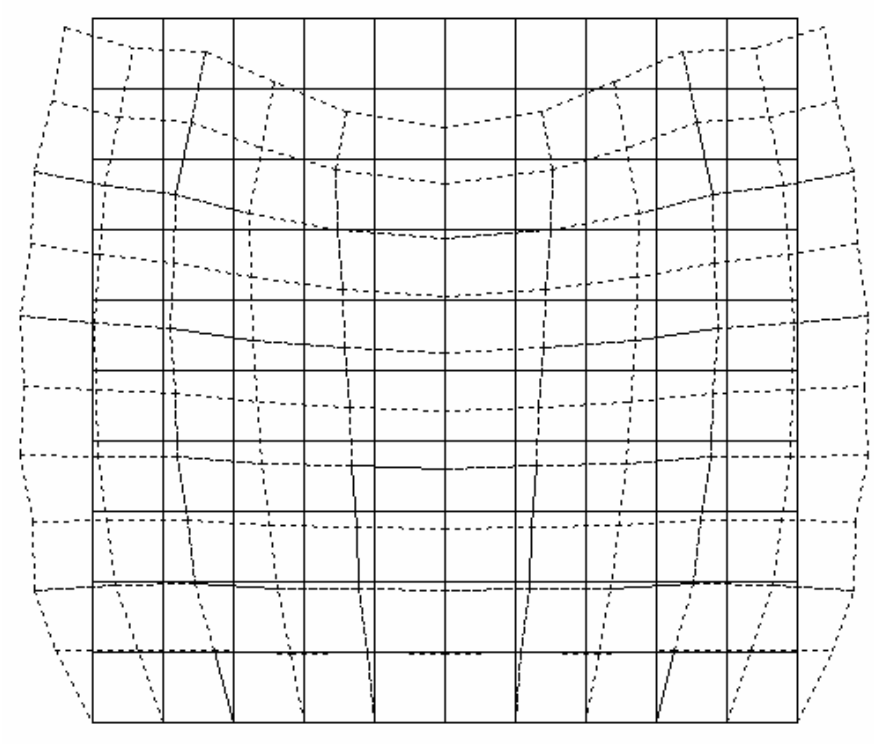

Fig.6.11 Deformation with the viscoelasticity (T=200s, n=0.7)

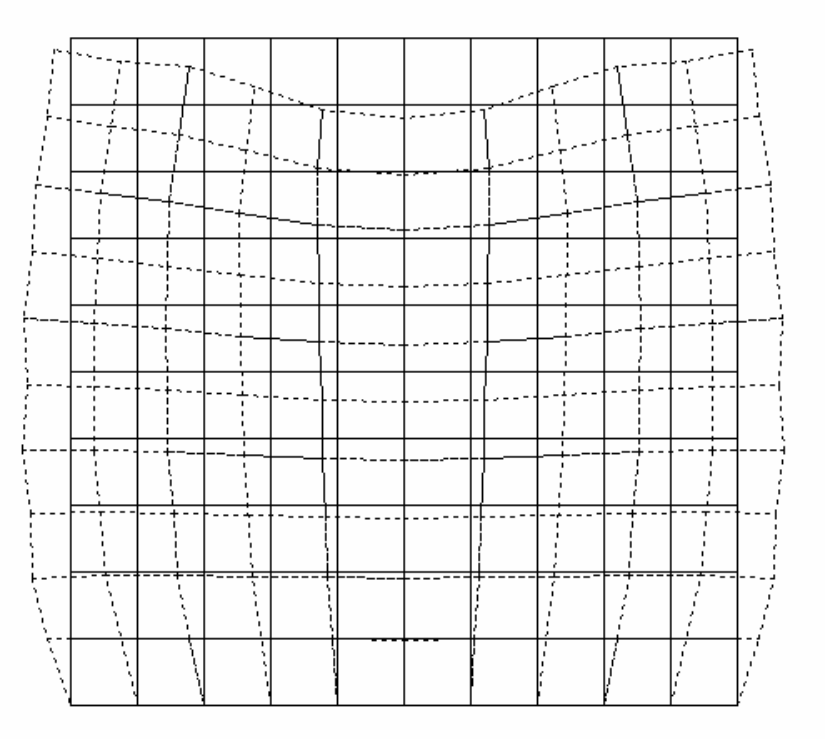

Fig.6.12 Deformation with the elasticity (T=200s, n=0.7)

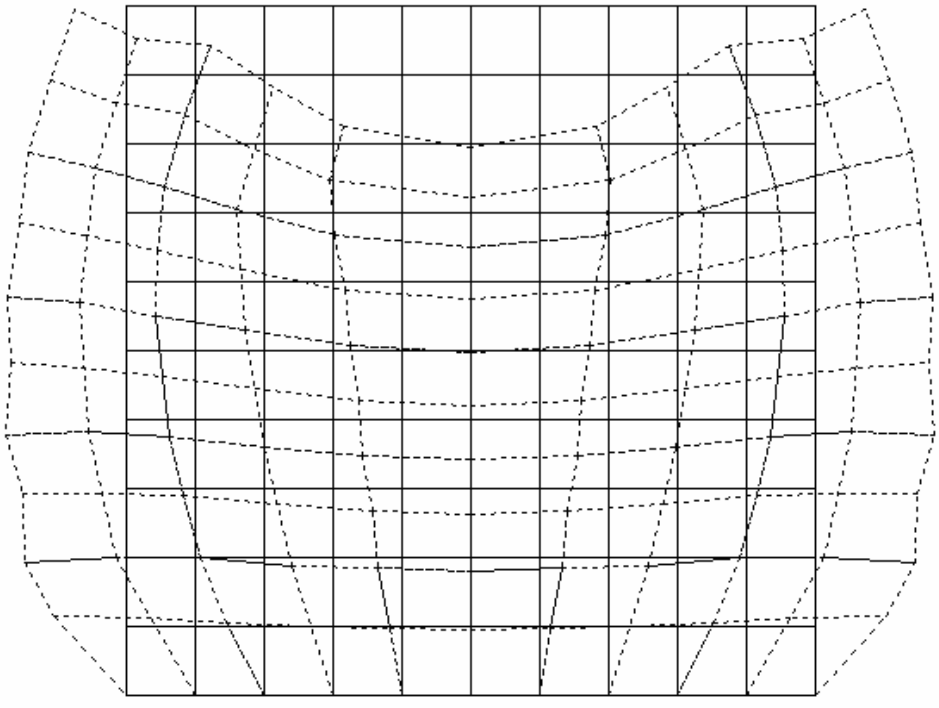

Fig.6.13 Deformation with the viscoelasticity (T= 200s, n=0.5)

6.3 BEHAVIOR UNDER RAPID LOADING

The model and the material properties are the same as the previous section, except the loading history, which is selected as 0.1 second (Fig. 6.14)

Figures 6.15-6.17 show that under rapid loading, the displacement and fluid pressure at top have a little bit of vibration after the loading time 0.1second.

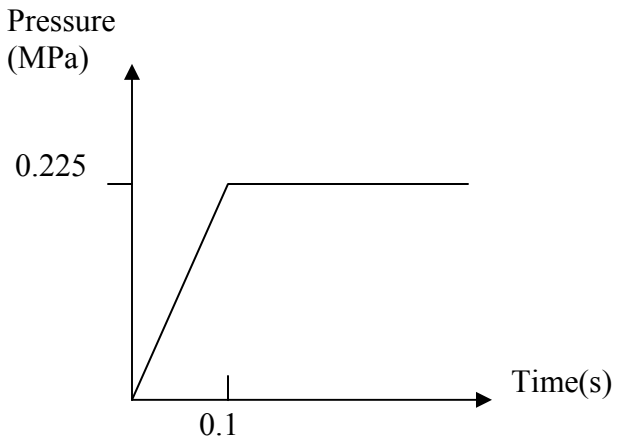

Fig.6.14 The loading history

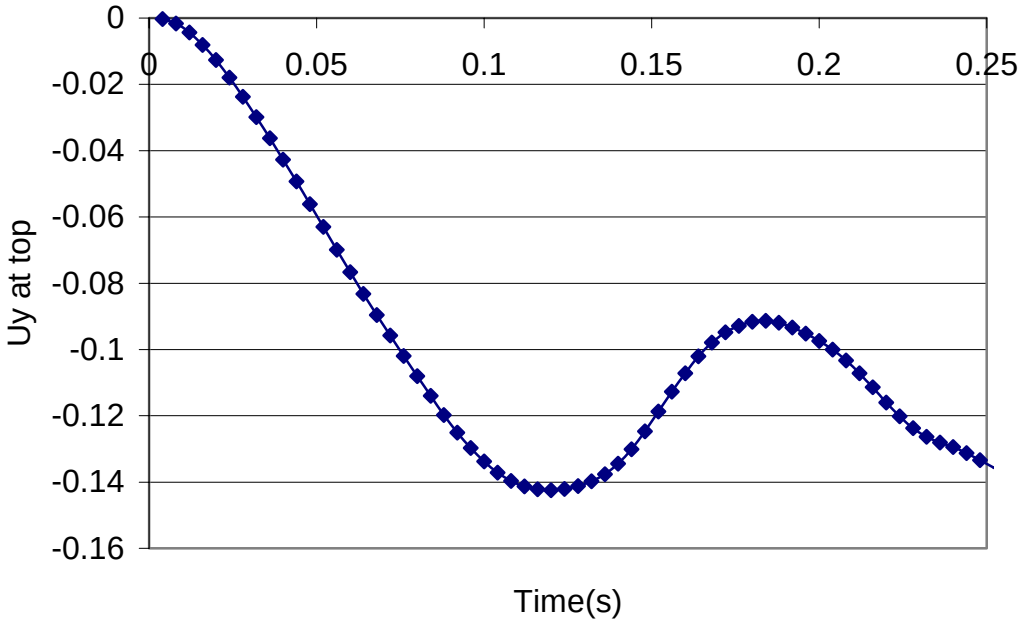

Fig.6.15 Uy at top with time

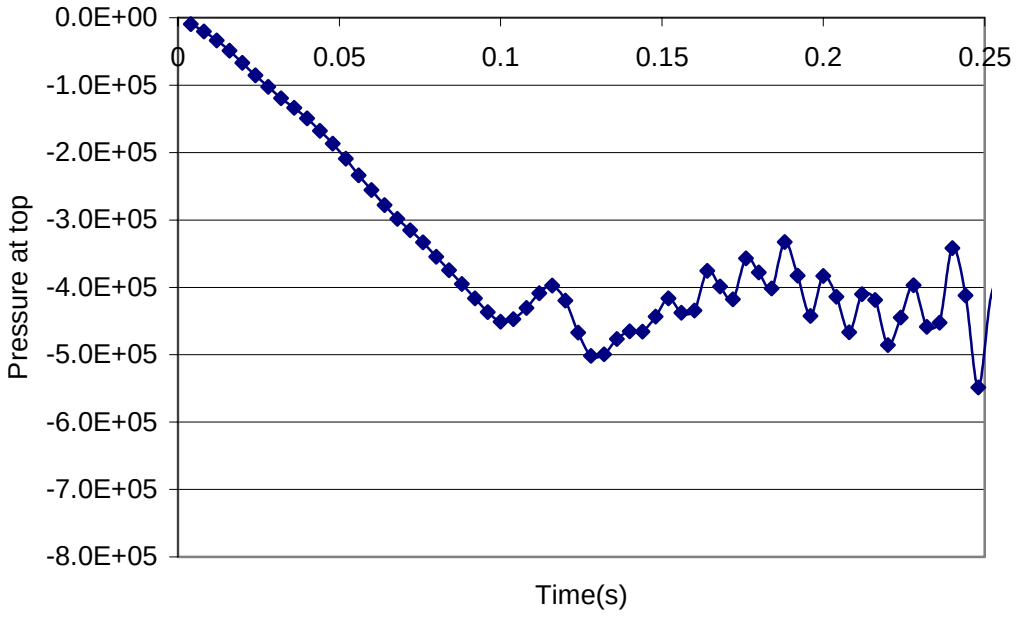

Fig.6.16 Fluid pressure at top with time

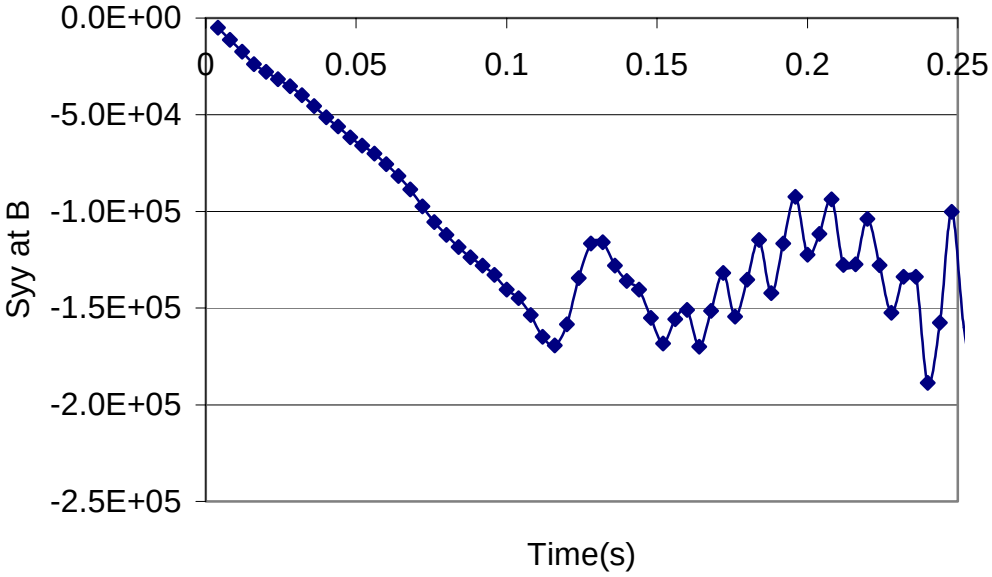

Fig.6.17 Syy at B with time

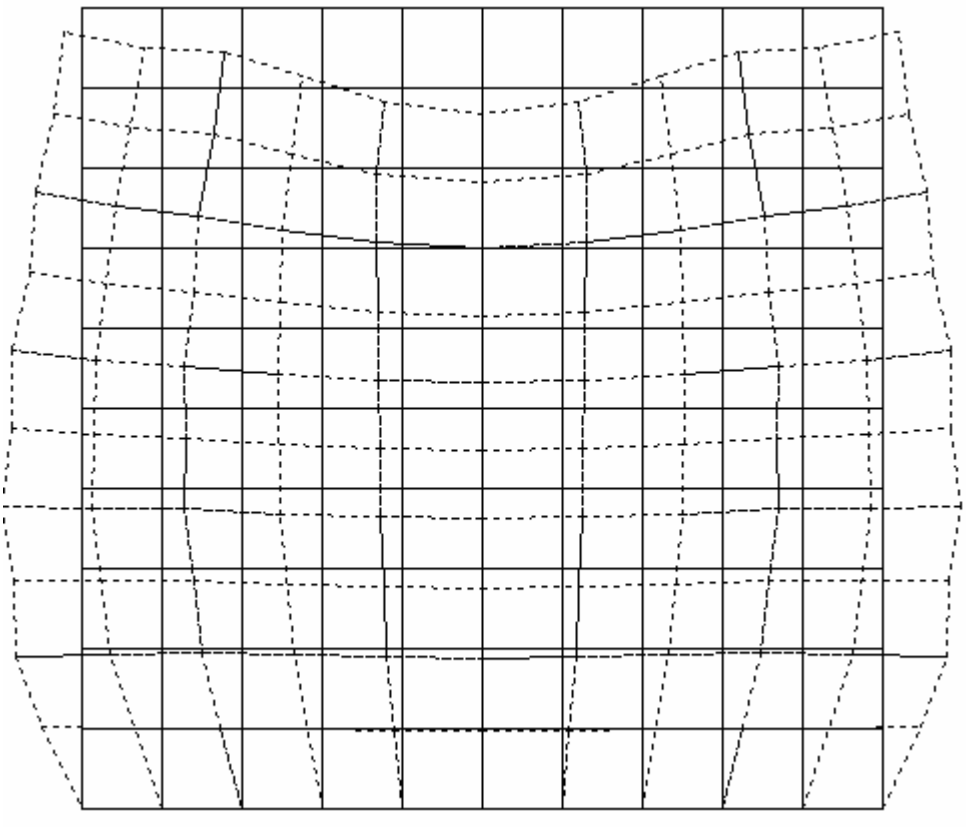

Fig.6.18 Deformation of solid phase at t=0.1s

6.4 THE CHEMICAL ELECTRIC SWELLING MODEL

The electro-chemical model is given in Figure 6.19. A soft tissue is putted in a 1cm×1cm square cup ABCD in which 0.1M NaCl is filled with. ABCD is connected with a NaCl bath which concentration is 0.3M. DC edge is fixed for the solid phase of the soft tissue, but is permeable to allow NaCl to go through. AD and BC are constrained, and only one dimensional movement is allowed. At the beginning, the soft tissue is in equilibrium that means the pressure outside is equal to the swelling pressure caused by 0.1M NaCl. The porous material properties are the same as those in the previous section, and the material properties in the electro-chemical model are selected in the range of literature [44]:

$$\text{T=310K, R=8318}\frac{liter-Pa}{mole-K},\ f_{+sw}=f_{-sw}=f_{+-}=f_{-+}=1.0\times10^{8}\frac{N-s}{m^{4}}$$

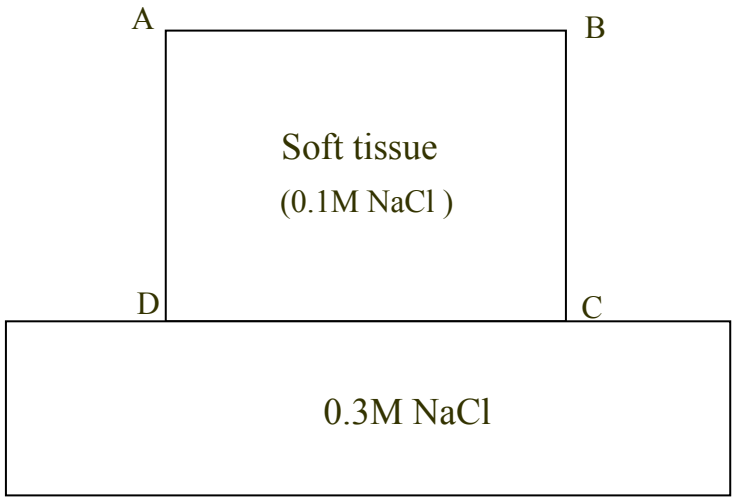

Fig.6.19 The electro-chemical model

Since the concentration at DC is constant as 0.3M, and the initial concentration for ABCD is 0.1M, NaCl ions diffuse from DC to the total square. Thus, the concentration in ABCD becomes larger with time, and eventually approaches to 0.3M, which is in accordance with the computational results (Fig. 6.20). As a result, with the increase of the ion concentrations, the swelling pressure at AB becomes larger than the outside pressure, which makes the soft tissue swell (Fig. 6.21 and 22).

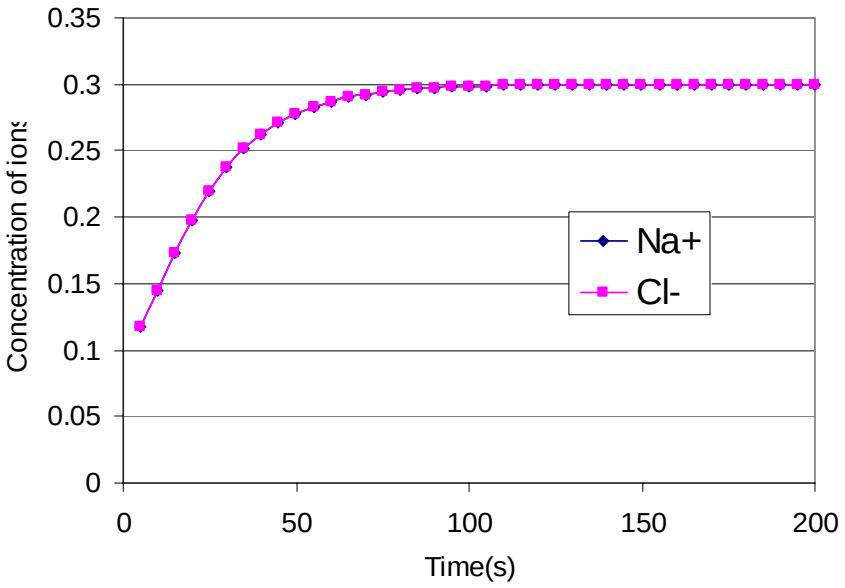

Fig.6.20 Ion concentrations of AB edge with time

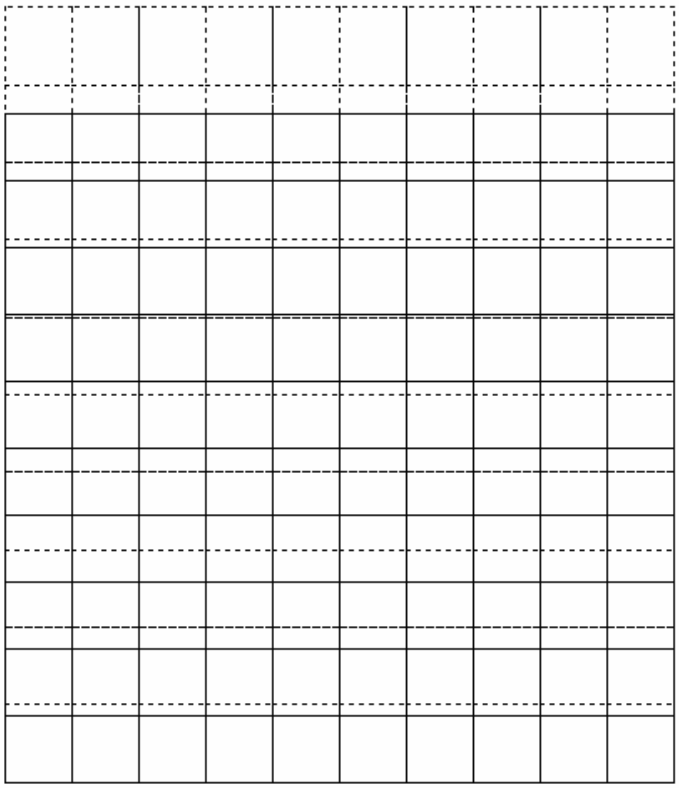

Fig. 6.21 Deformation of the solid phase at 200s

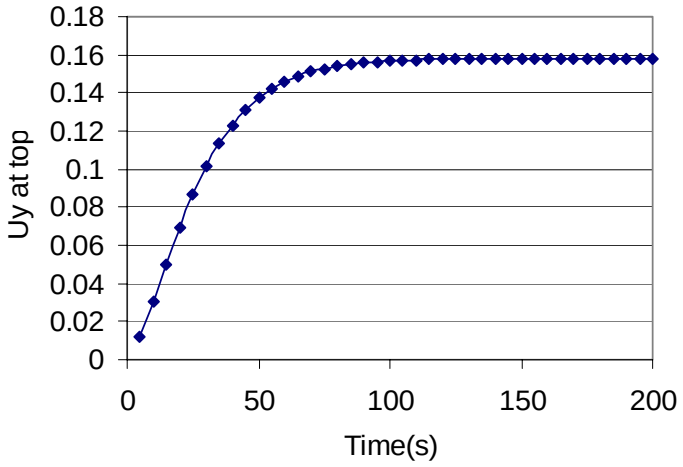

Fig.6.22 Displacement of edge AB with time

6.5 STUDY OF BRAIN TISSUE (APPLICATION)

Traumatic brain injury (TBI) frequently occurs due to the blunt impact to the head. Many studies [75] have been done to understand the mechanical behavior and the injury mechanisms of brain. The brain is a hydrated soft tissue, which consists of about 78% water, 10-12% phospholipids, 8% protein, and small amounts of carbohydrates, inorganic salts, and soluble organic substances, our poroelastic program is applied to study the impact of the brain tissue.

A two-dimensional circular geometry is used to model the brain shown in Fig.6.23. The boundary is constrained (both solid and fluid phases) except a small loading window (between point E and F). A sinusoidal point force (Fig.6.24) is applied to simulate an impact load. The response up to 10 ms will be investigated. The material properties are chosen from the literature as: n=0.8, $k=10^{-8}m^4/N\text{-}s$. E=31300Pa, the solid density $\rho_s=1016kg/m^3$, the fluid density $\rho_f=1000kg/m^3$, the apparent Poisson ratio $\upsilon=0.36$, the true Poisson ration $\upsilon=0.49$ [62]. The viscoelastic properties are given as: A=1e-5, $\tau=100$[75]. The aim of this study is to find an appropriate scaling of P based on size. For the small model, the radius is selected as 0.5”(1.27cm), and for the larger model, it is 2.5” (6.35cm).

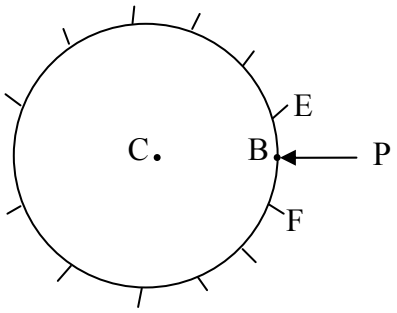

Fig. 6.23 The model of the brain impact

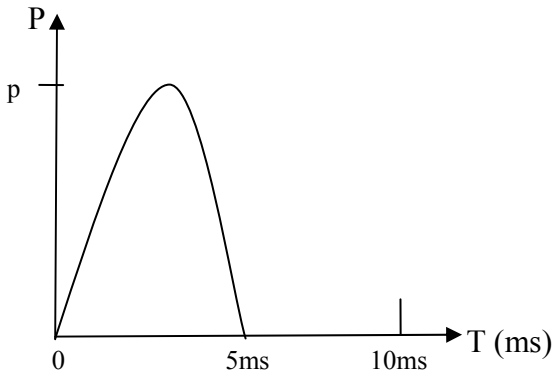

Fig.6.24 The loading history

(for the small model brain, p=1; for the large model, p=5)

Because the electrochemical effects in the brain tissue are unknown, only the poroelastic behavior is used to study the impact. Using a plane of symmetry, the finite element model is shown in Figure 6.25.

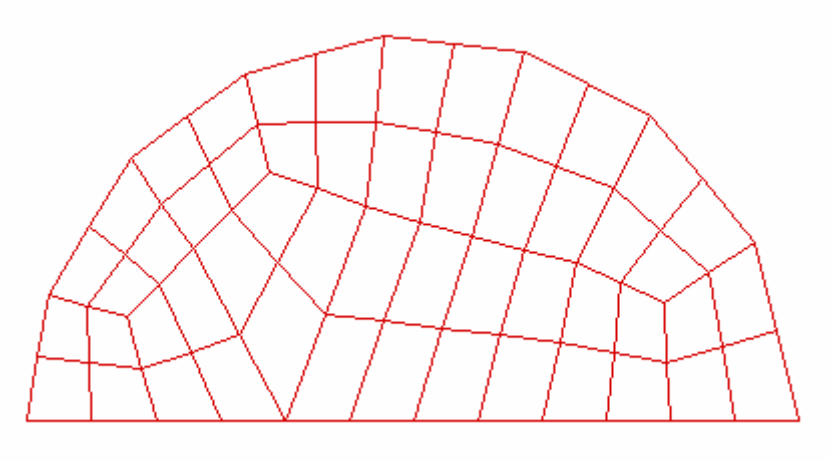

Fig.6.25 The finite element model

Figures 6.26 and 6.27 indicate the pressures and displacements of points B and C vary with time respectively. Figures 6.29 - 6.32 give the fluid pressure and solid deformation at time 2.5ms respectively. Figure 6.27 and 6.28 illustrate the fluid pressure and maximum of τ_{max} of points B and C are much close in case of radius 0.5” and 2.5”. Thus, scaling 5 is a proper choice for radius 0.5” and 2.5”.

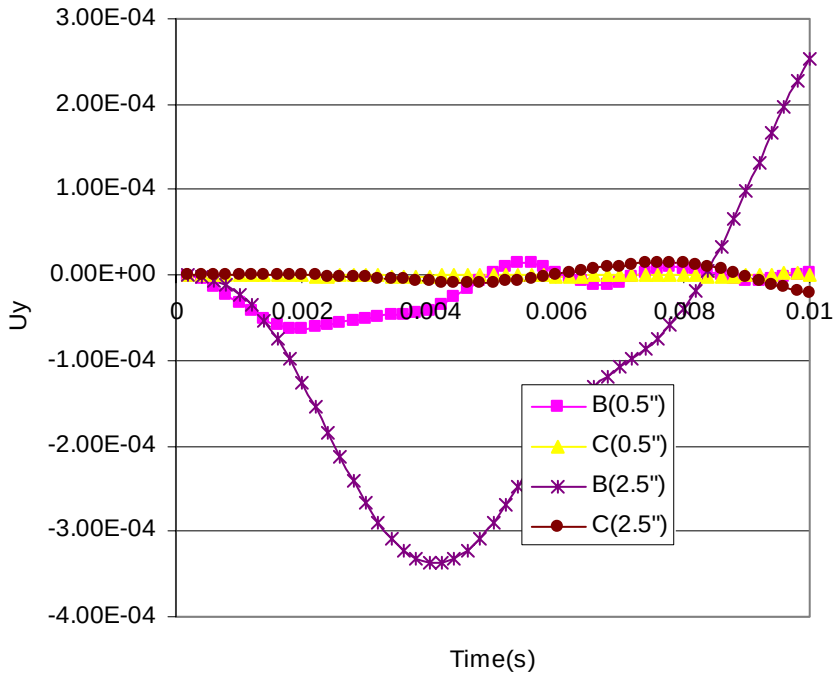

Fig.6.26 Displacement with time

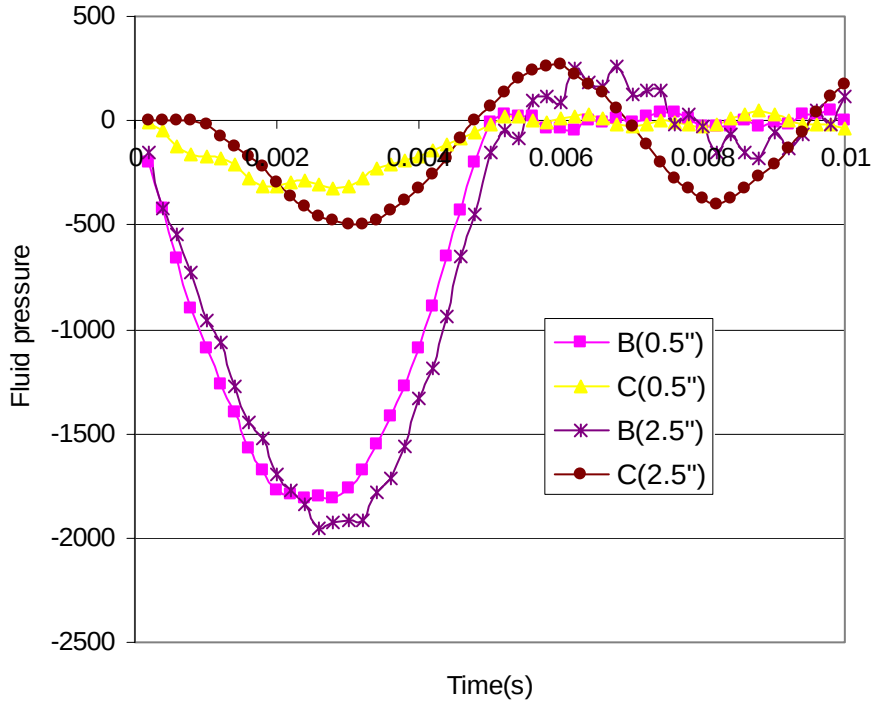

Fig.6.27 Fluid pressure with time

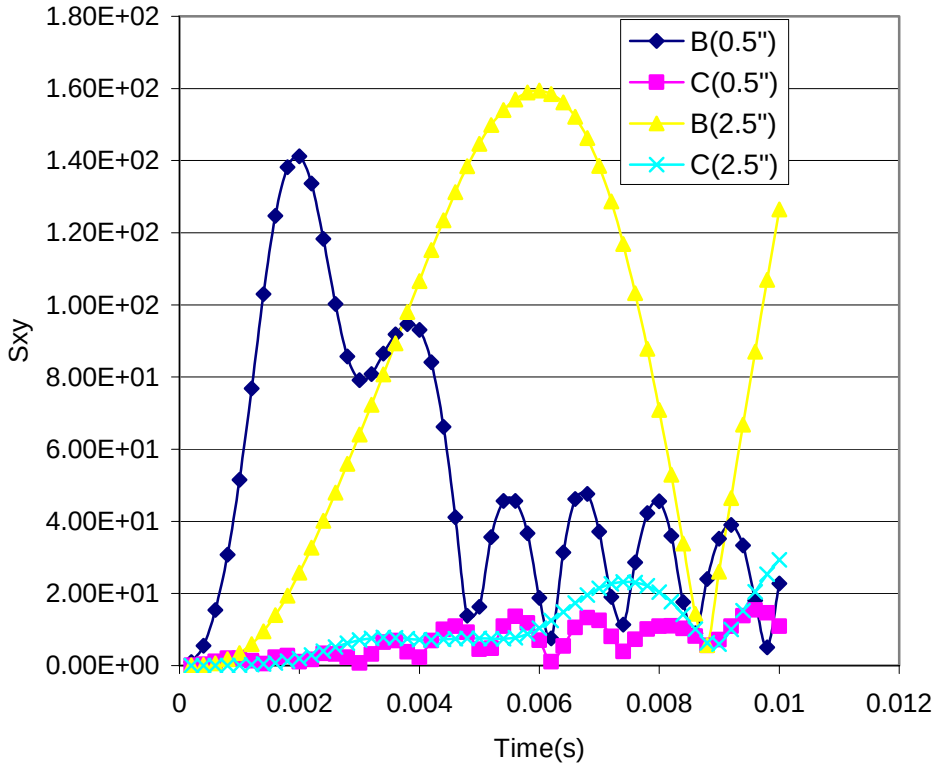

Fig.6.28 τ_{max} with time

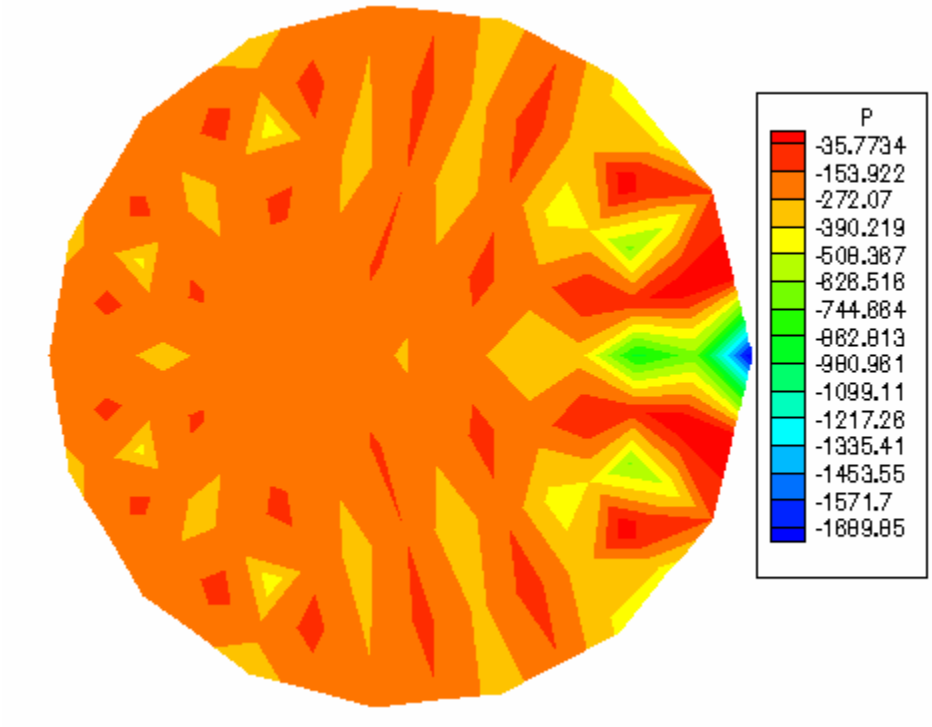

Fig.6.29 Fluid pressure (0.5", T=2.5ms)

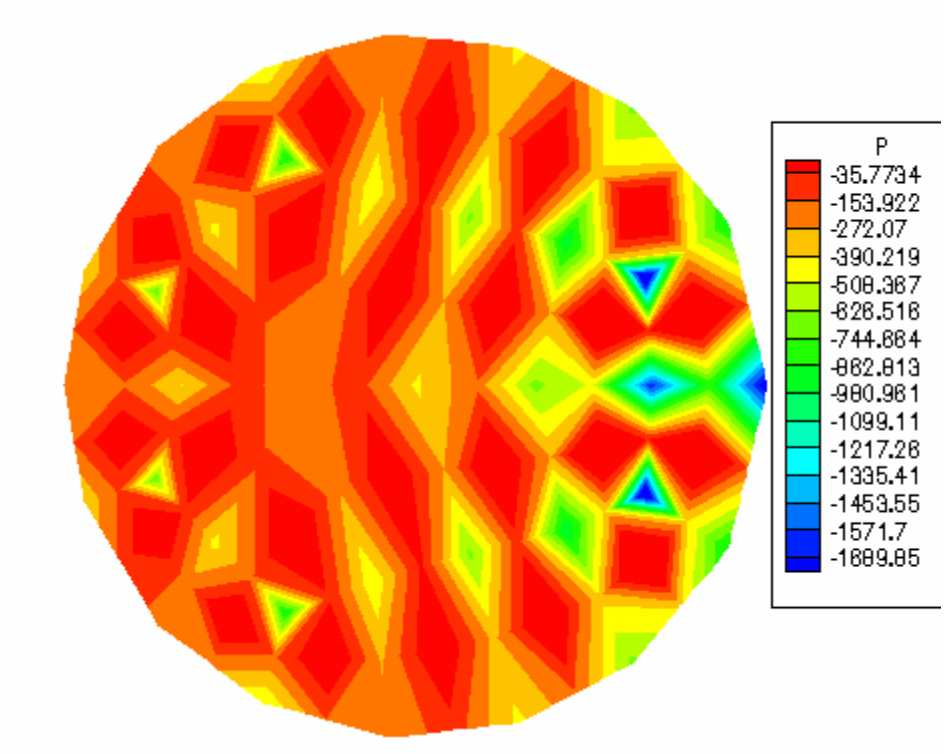

Fig.6.30 Fluid pressure (2.5”,T=2.5ms)

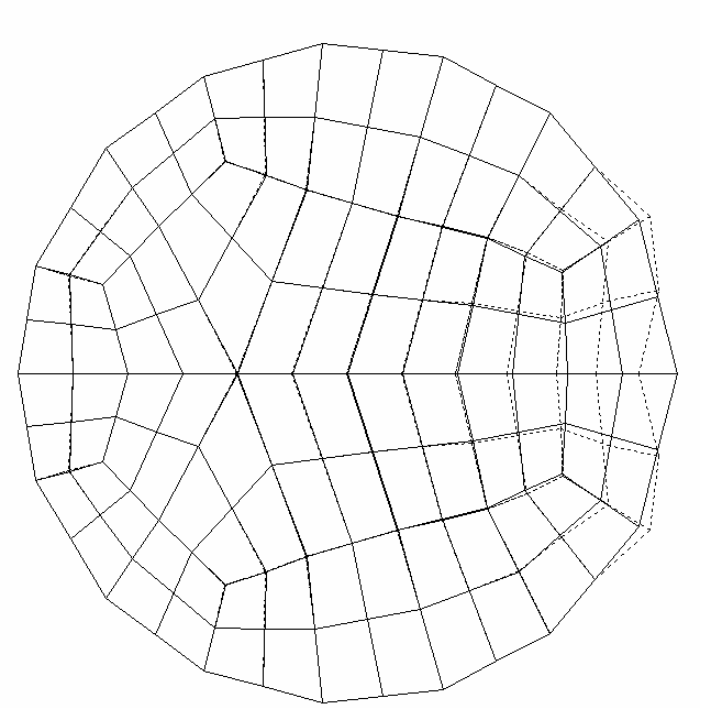

Fig.6.31 Deformation of the solid (0.5”, T=2.5ms)

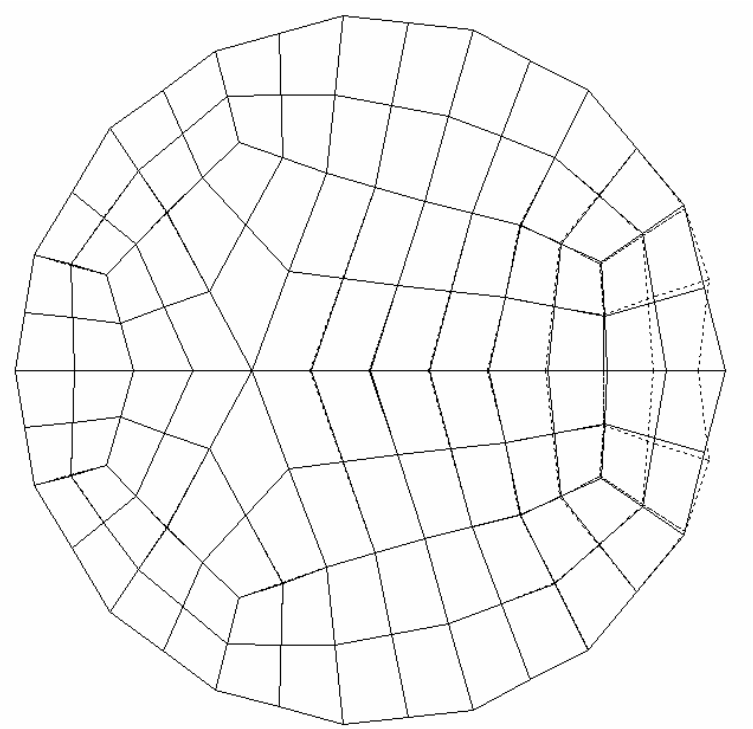

Fig.6.32 Deformation of the solid (2.5”, T=2.5ms)

7.0 CONCLUDING REMARKS

The work carried out for the present study was aimed mainly at building an infrastructure within the framework of finite elements for a better understanding of the mechanical behavior of biological tissue. The model developed for the study includes most important features of biological tissue, although it is no way complete.

Among the pertinent accomplishments of this work are:

- Introduce finite strains and inertial effects into the poroelastic model of biological tissues
- Develop the weak forms for the porous - electric-chemical model by treating cation and anion as variables
- Incorporate Newmark-β method, the backward method, and Newton's method into the implicit nonlinear solutions with the nearly incompressible and fully incompressible cases considered

This methodology and codes developed for the study have been verified with one –dimensional analytical solutions. Moreover, this study, using two dimensional examples, clearly demonstrates the importance of the finite deformation, the viscoelasticity of the material, and the electric-chemic effect. Finally, a preliminary work on the effect of impact loads on brain has show the capability of the present work in capturing sophisticated response behavior of the brain.

One of the potentially important features of biological tissue not included in the present study is the effects of nonlinear material properties. Neither does this study address the computational efficiency of the finite element implementation. The logical next step for a follow up research is to address these issues. Also an extension that can be readily achieved is to expand the implementation to three-dimensional based upon the formulation presented.

There are also research issues that are important from modeling perspectives: the needs to have a better material characterization and good scale test results database for model verification. Without complementary research in these areas, the analytical and numerical modeling alone can not be expected to provide a comprehensive and precise picture of the biological tissue behavior.

APPENDIX A

ELEMENT FORMULATION OF THE Ub2/P1 AND THE Ub2/Pb1 ELEMENTS

The two-dimensional element is considered here. As the displacement in these elements has the same approximation as in Ub2/Pb2, therefore, only the pressure approximation is given.

(1) Ub2/P1 element [62]

In this element, pressure is represented as a linear function:

$$p = a + bx + cy \tag{A1}$$

For the sake of convenience in the implementation of the algorithm, the pressure can be expressed in terms of the pressure and pressure gradient evaluated at the center node, node 9, of the element. Therefore,

$$p = p_9 + \left.\frac{\partial p}{\partial x}\right|_9 (x - x_9) + \left.\frac{\partial p}{\partial y}\right|_9 (y - y_9)$$

$$= \{1, (x - x_9), (y - y_9)\} \begin{Bmatrix} p_9 \\ \left.\frac{\partial p}{\partial x}\right|_9 \\ \left.\frac{\partial p}{\partial y}\right|_9 \end{Bmatrix} = \mathbf{N} \cdot \mathbf{P}_h^e \tag{A2}$$

where $\boldsymbol{N}$ is the pressure interpolation function and $\mathbf{P}_h^e$ is the element pressure vector calculated at the center node of the element.

(2)Ub2P/b1 element

In this element the local coordinates ξ, η range from –1 to 1(Fig.A1), and the pressure is described as

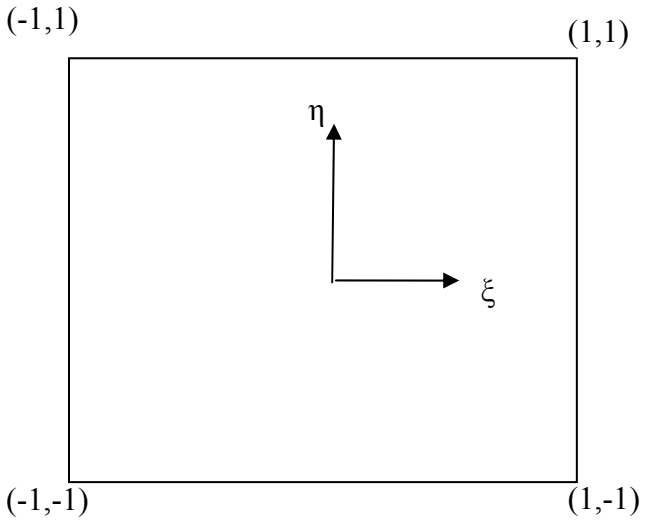

Fig. A1 P element in Ub2/Pb1 element

$$p = \sum_{i}^{4} N_i p_i \tag{A3}$$

where

$$\begin{aligned} N_1 &= \frac{1}{4}(1+\xi)(1+\eta) \\ N_2 &= \frac{1}{4}(1-\xi)(1+\eta) \\ N_3 &= \frac{1}{4}(1-\xi)(1-\eta) \\ N_4 &= \frac{1}{4}(1+\xi)(1-\eta) \end{aligned} \tag{A4}$$

APPENDIX B

THE RELATIONSHIP BETWEEN THE LAGRANGIAN FORM AND THE EULERIAN FORM

In the initial configuration (Fig.B1.a), the fluid moves through the face of dS_R, and **N** is unit normal to S_R. In the current configuration (Fig.B1.b), the fluid flows through the face of dS, and **n** is unit normal to dS.

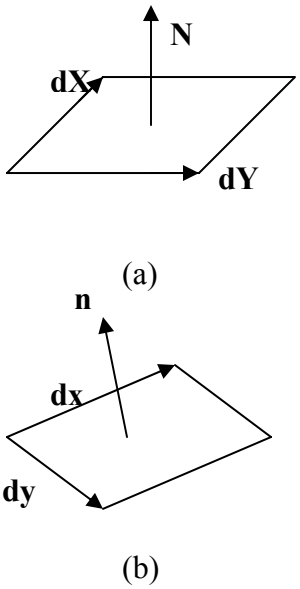

Fig.B1 The surface deformations of

(a) the initial configuration; (b) the current configuration

$$\hat{\mathbf{N}} dS_R = \mathbf{dX} \times \mathbf{dY} \tag{B.1}$$

and

$$\hat{\mathbf{n}} dS = \mathbf{dx} \times \mathbf{dy} \tag{B.2}$$

Or in rectangular Cartesian components

$$\hat{N}_I dS_R = e_{IJK} dX_J dY_K \tag{B.3}$$

$$\hat{n}_r dS = e_{rst} dx_s dy_t \tag{B.4}$$

Since

$$dX_J = \frac{\partial X_J}{\partial x_s} dx_s \tag{B.5}$$

and

$$dY_K = \frac{\partial Y_K}{\partial y_t} dy_t \tag{B.6}$$

Making use of equations (B.5) and (B.6), equation (B.3) becomes

$$\hat{N}_I dS_R = e_{IJK} \frac{\partial X_J}{\partial x_s} \frac{\partial X_K}{\partial x_t} dx_s dy_t \tag{B.7}$$

Multiplying both sides of this equation by $\frac{\partial X_I}{\partial x_r}$, we have

$$\frac{\partial X_I}{\partial x_r} \hat{N}_I dS_R = e_{IJK} \frac{\partial X_I}{\partial x_r} \frac{\partial X_J}{\partial x_s} \frac{\partial X_K}{\partial x_t} dx_s dy_t \tag{B.8}$$

From the definition of the determination of matrix, we know

$$e_{rst} J^{-1} = e_{IJK} \frac{\partial X_I}{\partial x_r} \frac{\partial X_J}{\partial x_s} \frac{\partial X_K}{\partial x_t} \tag{B.9}$$

where

$$J = \det\left|\frac{\partial \mathbf{x}}{\partial \mathbf{X}}\right| \tag{B.10}$$

Thus,

$$\frac{\partial X_I}{\partial x_r}\hat{N}_I dS_R = J^{-1} e_{rst} dx_s dy_t \tag{B.11}$$

Substituting equation (B.4) into the above equation, yields [71],

$$\hat{n}_r dS = J\frac{\partial X_I}{\partial x_r}\hat{N}_I dS_R \tag{B.12}$$

Since mass conservation of fluid should be satisfied, an equal relative fluid mass flow rate occurs, thus, the relative fluid velocity, $\dot{\hat{w}}_i$ is defined by [61],

$$\dot{m}_f = \int_S \rho^f \dot{w}_r \hat{n}_r dS = \int_{S_R} \rho_R^f \dot{\hat{w}}_I \hat{N}_I dS_R \tag{B.13}$$

For incompressible fluid,

$$\rho^f = \rho_R^f \tag{B.14}$$

Using equation (B.12), we have finally,

$$\dot{\hat{w}}_I = J\frac{\partial X_I}{\partial x_r}\dot{w}_r \tag{B.15}$$

or,

$$\dot{\hat{\mathbf{w}}} = J\frac{\partial \mathbf{X}}{\partial \mathbf{x}}\dot{\mathbf{w}} \tag{B.16}$$

BIBLIOGRAPHY

1. Encyclopedia Wikipedia, http://en.wikipedia.org/wiki/Biological_tissue

2. Paremer, A., S.Fumer, and D.P.Rice, 1992, Musculoskeletal Conditions in the United States. First ed., Park Ridge, Illinois: American Academy of Orthopaedic Surgeons

3. Rutlow I.M., 1986, "Orthopaedic Operation in the United States 1979-83" , Journal of Bone and Joint Surgery, Vol.68-A, pp. 716-719

4. Gower, W.E. and V.Pedrini, 1969, "Age-related variations in protein-polysaccharide from human nucleus pulposus, annulus fibrosus and costal cartilage", Journal of Bone and Joint Surgery, Vol. 51-A, p.1154

5. Adams, M.A., Hutton, W.C., 1982, "Prolapsed intervertebral disc: A hyperflexion injury", Spine, Vol. 7, pp. 184-191

6. Adams, M.A., Hutton, W.C., 1985, "Gradual disc prolapse", Spine, Vol.10. pp. 524-531

7. Adams, M.A., Dolan, P., Hutton, W.C., 1987, "Diurnal variations in the stresses on the lumbar spine", Spine, Vol. 12, pp. 130-137

8. Brinckmann, P., 1986, "Injury of the annulus fibrosus and disc protrusions: An in vitro investigation on human lumbar disc", Spine, Vol.11, No.2, pp. 149-153

9. Lars G.Gilbertson, Vijay K. Goel, Wayne Z. Kong and John D. Clausen, 1995, "Finite element methods in spine biomechanics research", Critical Reviews in Biomedical Engineering, Vol.23, No.5&6, pp. 411-473

10. Belytschko, T., Kulak, R.F., and Schultz, A., 1972, "Finite element stress analysis of an intervertebral disc", Journal of Biomechanics, Vol. 7, pp. 277-285

11. Kulak, R.F., Belytschko, T.B.,Schultz, A.B., and Galante, J.O., 1976, "Nonlinear behavior of the human intervertebral disc under axial load", Journal of Biomechanics, Vol. 9, pp.377-386

12. Spilker, R.L., 1980, "Mechanical behavior of a simple model of an intervertebral disc under compressive loading", Journal of Biomechanics, Vol.13, pp. 895-901

13. Spilker, R.L., Daugirda, D.M., and Schultz, A.B., 1984, "Mechanical response of a simple finite element model of the intervertebral disc under complex loading", Journal of Biomechanics, Vol. 17, pp. 103-112

14. Spilker, R.L., Jakobs, D.M., and Schultz, A.B., 1986, "Material constants for a finite element model of the intervertebral disc with a fiber composite annulus", Journal of Biomechanical Engineering, Vol.108, pp. 1-11

15. Shriazi-Adl, A., Shrivastava, S.C., and Ahmed, A.M.,1984, "Stress analysis of the lumbar disc body unit in compression", Spine, Vol. 9, pp.120-134

16. Shirazi-Adl, A., 1989, "On fiber composite material models of disc annulus-comparison of predicted stresses", Journal of Biomechanics, Vol. 22, pp. 337-365

17. Charnley, J., 1952, Imbibation of fluid as a cause of herniation of the nucleus pulposus, Lancet,

18. Hendry, N.G.C., 1958, "The hydration of the nucleus pulposus and its relation to intervertebral disc derangement", Journal of Bone and Joint Surgery, Vol. 40B,pp.132-144

19. Urban, J.P.G., Maroudas, A., Bayliss, M.T., Dillon, J., 1979, "Swelling pressures of proteoglycans at the concentrations found in cartilaginous tissues", Biorheology, Vol. 16, pp. 447-464

20. Maroudas, A., Bannon, C., 1981, "Measurement of swelling pressure in cartilage and comparison with the osmotic pressure of constituent proteoglycans", Biorheology, Vol. 18, pp. 619-632

21. Urban, J.P.G., McMullin, J.F., 1985, "Swelling pressure on the intervertebral disc: Influence of proteoglycan and collagen contents", Biorheology, Vol.22, pp.145-157

22. Urban, J.P.G., Maroudas, A., 1981, "Swelling of the intervertebral disc in-vitro", Connective Tissue Research, Vol. 8, pp.1-10

23. Maroudas, A., Grushko, G., 1990, Measurement of swelling pressure of cartilage, Methods in Cartilage Research. Edited by A. Maroudas, and K. Kuettner. London, Academic Press, Harcourt Brace Jovanovich

24. Mow, V.C., Holmes, M.H., Lai, W.M.,1984, "Fluid transport and mechanical properties of articular cartilage: A review", Journal of Biomechanics, Vol.17, pp. 377-394

25. Mow, V.C., Kuei, S.C., Lai, W.M., 1980, "Armstrong C.G., Biphasic creep and stress relaxation of articular cartilage: Theory and experiments", Journal of Biomechanical Engineering, Vol.102, pp. 73-84

26. Spilker, R.L. and Suh, J.-K.,1990, "Formulation and evaluation of a finite element model for the biphasic model of hydrated soft tissue", Computers & Structures, Vol.35, No. 4, pp. 425-439

27. Hayer, W.C., Bodine, A.J., 1978, "Flow-independent viscoelastic properties of articular cartilage matrix", Journal of Biomechanics, Vol. 11, pp. 407-419

28. Mak, A.F., 1986, "The apparent viscoelastic behavior of articular cartilage – The contributions from the intrinsic matrix viscoelasticity and interstitial fluid flows", ASME Journal of Biomechanical Engineering, Vol. 108, pp. 123-130

29. Fung, Y.C., 1972, "Stress-strain-history relations of soft tissues in simple elongation", in: Biomechanics: Its Foundations and Objectives, Fung, Y.C., Perrone, N., and Anliker, m., eds., Prentice-Hall, Englewood Cliffs, NJ.

30. Suh, J.K., and Bai, S., 1998, "Finite element formulation of biphasic poroviscoelastic model for articular cartilage", Journal of Biomechanical Engineering, Vol.120, pp.195-201

31. Suh, J.K., and DiSilvestro, M.R., 1999, "Biphasic poroviscoelastic behavior of hydrated biological soft tissue", Journal of Applied Mechanics, Vol. 66, pp. 528-535

32. Levenston, M.E., Frank, E.H., and Grodzinsky, A.J., 1998, "Variationally derived 3-field finite element formulations for quasi-static poroelastic analysis of hydrated biological tissues", Computer Methods in Applied Mechanics and Engineering, Vol.156, pp.231-246

33. Grodzinsky, A.J., Roth, V., Myers, E., Grossman, W.D., and Mow, V.C.,1981, "The significance of electromechanical and osmotic forces in the non-equilibrium swelling behavior of articular cartilage in tension", ASME Journal of Biomechanical Engineering, Vol. 103, pp. 221-231

34. Grodzinsky, A.J., 1990, "Mechanical and electrical properties and their relevance to physiological processes", Methods in Cartilage Research, Chapter 11, Sec. 65, Academic Press, New York, pp. 275-287

35. Lanir, Y.,1987, "Biorheology and fluid flux in swelling tissues I: Bicompartment theory for small deformations including ionic effects", Biorheology, Vol. 24, pp. 173-187

36. Lai, W.M., Hou, J.S., and Mow, V.C.,1991, "A triphasic theory for the swelling and deformation behavior of articular cartilage", ASME Journal of Biomechanical Engineering, Vol. 113, pp. 245-258

37. Huyghe, J.M., and Janssen, J.D.,1997, " Quadriphasic mechanics of swelling incompressible porous media", International Journal of Engineering Science, Vol.35, pp. 793-802

38. Frijns.A.J.H., Huyghe, J.M., Janssen, J.D.,1997, " A validation of the quadriphasic mixture theory for intervertebral disc tissue", International Journal of Engineering Science, Vol. 35, pp. 1419-1429

39. Simon, B.R., Wu, J.S.S., Carlton, M.W., Evans, J.H., Kazarian, L.E.,1985, " Structural models for human spinal motion segments based on a poroelastic view of the intervertebral disc", Journal of Biomechanical Engineering, Vol.107, pp. 327-335

40. Simon, B.R., Wu, J.S.S., Carlton, M.W., et al.,1985, "Poroelastic dynamic structural models of Rhesus spinal motion segments", Spine, Vol.10, pp. 494-507

41. Biot, M.A., 1941, "General theory of three-dimensional consolidation", Journal of Applied Physics, Vol.12, pp. 155-164

42. Laible, J.P., Pflaster, D.S., Krag, M.H., et al.,1993, "A poroelastic-swelling finite element model with application to the intervertebral disc", Spine, Vol.18, pp. 659-670

43. Simon, B.R., Liable, J.P., Pflaster, D., Yuan, Y., Krag, M.H.,1996, " A poroelastic finite element formulation including transport and swelling in soft tissue structures", Journal of Biomechanical Engineering, Vol.118, pp. 1-9

44. James C.Iatridis, Jeffrey P. Laible, Martin H.Krag, 2003, "Influence of fixed charge density magnitude and distribution on the intervertebral disc: applications of a poroelastic and chemical electric (PEACE) model", Transactions of the ASME, Vol.125, pp. 12-24

45. Inoue H.,1981, "Three-dimensional architecture of lumbar intervertebral disc", Spine, Vol.6, pp. 139-146

46. White A.A., Panjabi, M.M., 1990, Clinical biomechanics of the spine,(Second ed.), Philadelphia, J.B.Lippincott Co.

47. Wainwright S.A., Biggs W.D., Currey J.D., Gosline J.M., 1976, Mechanical design in organisms. Princeton, New Jersey: Princeton University Press

48. Maroudas A., Stockwell R.A., Nachemson A., Urban J., 1975, "Factors involved in the nutrition of the human lumbar intervertebral disc: cellularity and diffusion of glucose in vitro", Journal of Anatomy, Vol.120, pp. 113-130

49. Tyrrell A.R., Reilly T., Troup J.D., 1985, "Circadian variation in stature and the effects of spinal loading", Spine, Vol. 10, pp. 161-164

50. Adams M.A., Dolan P., Hutton W.C., Porter R.W., 1990, "Diurnal changes in spinal mechanics and their clinical significance", Journal of Bone Joint Surgery, Vol. 72, pp. 266-270

51. McNally D.S., Adams M.A., 1992, "Internal intervertebral disc mechanics as revealed by stress profilometry", Spine, Vol.17, pp. 66-73

52. Kurowaski P., Kubo A., 1986, "The relationship of degeneration of the intervertebral disc to mechanical loading conditions on lumbar vertebrae", Spine, Vol.11, pp. 726-731

53. Seroussi R.E., Krag M.H., Muller D.L., Pope M.H., 1989, " Internal deformations of intact and denucleated human lumbar discs subjected to compression, flexion, and extension loads", Journal of Orthopedics Reviews, Vol.7, pp. 122-131

54. Graves, Jason Aaron, 2000, Modeling of large deformations in drying viscoelastic materials (PHD dissertation), UNIVERSITY OF MINNESOTA, pp. 62-69

55. Findley, William N., Lai, James S. and Onaran, Kasif, 1976, Creep and Relaxation of Nonlinear Viscoelastic Materials, Dover Publications, New York

56. Tanner, Roger I., 1985, Engineering Rheology, Clarendon Press, Oxford

57. Simon, B.R., Zienkiewicz, O.C., and Paul D.K., 1984, "An analytical solution for the transient response of saturated porous elastic solids", International Journal for Numerical and Analytical Methods in Geomechanics, Vol. 8, pp. 381-398

58. Chun-Yuh Huang, Van C.Mow, Gerard A.Ateshian, 2001, "The role of flow-independent viscoelasticity in the biphasic tensile and compressive response of articular cartilage", Journal of Biomechanical Engineering, Transactions of ASME, Vol.123, pp. 410-417

59. Wolfgang Ehlers, Bernd Markert, 2001, " A linear viscoelastic biphasic model for soft tissues based on the theory of porous media", Journal of Biomechanical Engineering, Transactions of the ASME, Vol.123, pp. 418-424

60. Soltz, M.A., and Ateshian, G.A., 2001, " A conewise linear elasticity mixture model for the analysis of tension-compression nonlinearity in articular cartilage", ASME Journal of Biomechanical Engineering, Vol.122, pp. 576-586

61. Simon, B.R., 1992, "Multiphase poroelastic finite element models for soft tissue structures", Applied Mechanics Reviews, Vol. 45, pp.191-218

62. Zhu, Qiliang, 2001, Biphasic poroviscoelastic simulation of brain injury under high-speed impact (PHD dissertation), University of Pittsburgh, pp. 47-48

63. Carey, G. and J.Oden, 1984, Finite elements: Mathematical aspects, Vol. IV. , Englewood Cliffs, NJ: Prentice-Hall Inc.

64. Hughes, T., 1987, The finite element method-Linear static and dynamic finite element analysis, Englewood Cliffs, NJ: Prentice-Hall Inc.

65. Zhu, Qilang, and Suh, J.K.Francis, 2001, "Dynamic biphasic poroviscoelastic model simulation of hydrated soft tissues and its potential applications for brain impact study", BED-vol., 50, Bioengineering Conference, ASME, pp.835-836

66. Suh, J.-K., Spilker, R.L., and Holmes, M.H.,1991, " A penalty finite element analysis for nonlinear mechanics of biphasic hydrated soft tissue under large deformation", International Journal for Numerical Methods in Engineering, Vol. 32, pp. 1411-1439

67. Gu, W.Y., Lai, W.M., and Mow, V.C., 1998, "A mixture theory for charged-hydrated soft tissues containing multi-electrolytes: passive transport and swelling behaviors", Journal of Biomechanical Engineering, Vol. 120, pp. 169-180

68. Loon, R.Van., Huyghe, J.M., Wijlaars, M.W., and Baaijens, F.P.T., 2003, "3D FE implementation of an incompressible quadriphasic mixture model", International Journal for Numerical Methods in Engineering, Vol. 57, pp. 1243-1258

69. Simon, B.R., Wu, J.S.S., Zienkiewicz, O.C., and Paul, D.K., 1986, "Evaluation of u-w and u-π finite element methods for the dynamic response of saturated porous media using one-dimensional models", International Journal of Numerical and Analysis Methods in Geomechanics, Vol. 10, pp. 461-482

70. Flugge, Wilhelm, 1967, Viscoelasticity, Waltham, Massachusetts, Toronto, London: Blaisdell Publishing Company.

71. Malvern, Lawrence E., 1969, Introduction to the mechanics of a continuous medium, Englewood Cliffs, New Jersey: Prentice-Hall, Inc.

72. Sun,D.N., Gu, W.Y., Guo,X.E., Lai,W.M., and Mow,V.C., 1999, "A mixed finite element formulation of Triphasic mechano-electrochemical theory for charged, hydrated biological soft tissues", International Journal of Numerical Methods in Engineering, Vol. 45, pp. 1375-1402

73. Iatridis, J.C., Setton, L.A., Weidenbaum, M., Mow, V.C., 1997, "Viscoelastic behavior of the human lumbar nucleus pulposus in shear", Journal of Biomechanics, Vol.30, pp. 1005-1013

74. Faires, J.D., Burden, R.L., 1993, Numerical methods, Boston: PWS-Kent Pub. Co.

75. Kleiven, S., Hardy, W.N., 2002, "Correlation of an FE model of the human head with local brain motion-consequences for injury predication", Stapp Car Crash Journal, Vol.46, pp. 123-144